Rational Design and Development of Dual location Dual Stimuli-Responsive Polymeric Nanocarriers for Drug Delivery

A Thesis

In the Department

Of

Chemistry and Biochemistry

Presented in Partial Fulfillment of the Requirements

For the Degree of

Master of Science (Chemistry) at

Concordia University

Montreal, Quebec, Canada

May 2020

CONCORDIA UNIVERSITY
School of Graduate Studies

This is to certify that the thesis prepared

By: Newsha Arezi

Entitled: Rational Design and Development of Dual location Dual Stimuli-Responsive Polymeric Nanocarriers for Drug Delivery

and submitted in partial fulfillment of the requirements for the degree of

Master of Science in Chemistry

complies with the regulations of the University and meets the accepted standards with respect to originality and quality.

Signed by the final examining committee:

Dr. Brandon Findlay Chair

Dr. Christopher Wilds Examiner

Dr. Louis Cuccia Examiner

Dr. John Oh Supervisor

Approved by: Dr. Yves Gélinas, Graduate Program Director

Dr. André Roy, Dean, Faculty of Arts and Science

Date: 13th May 2020

Abstract

Rational Design and Development of Dual location Dual Stimuli-Responsive Polymeric Nanocarriers for Drug Delivery

Newsha Arezi, M.Sc.

Design and development of smart nano-sized delivery devices for controlled drug release in response to endogenous stimuli (such as acidic pH and glutathione (GSH)) inherently found in tumor tissue is a promising platform in tumor-targeting nanomedicine. This platform allows for the maximization of therapeutic efficacy whilst reducing unwanted off-target side effects. Particularly, polymeric nanocarriers self-assembled from amphiphilic block copolymers (ABCP) have gained significant attention due of their size tunability and enhanced colloidal stability. Well-controlled ABCPs enable the formation of core-shell micelles in aqueous solutions having hydrophobic cores, enabling the physical entrapment of hydrophobic anticancer drugs, surrounded with hydrophilic coronas. Further, an incorporation of stimuli-responsive degradable (SRD) linkages in ABCPs allows for controlled micelle degradation and drug release at the site of action.

In this research, a dual location dual stimuli-responsive degradation (DL-DSRD) strategy is explored as a versatile platform for intracellular tumor-targeting drug delivery. Two ABCPs exhibiting dual acidic pH/reduction-responsive degradation are studied. The self-assembled ABCPs form colloidally stable nanoassemblies showing synergistically rapid release of encapsulated doxorubicin (a clinically used anticancer drug) at pH = 5.4 in 10 mM GSH solution caused by the cleavage of acid-labile and disulfide linkages. In addition, a new approach utilizing carbonylimidazole-hydroxyl coupling chemistry is explored to synthesize reduction-degradable poly(carbonate-disulfides) labeled with disulfide linkage on the backbones. They possess multi-functionalities as well as tunable and rapid reductive-degradation through main-chain degradation mechanism. Further, the versatility of the approach is demonstrated with the synthesis of an amphiphilic triblock copolymer exhibiting DL-DSRD responses.

Overall, the results obtained through this research contribute to the advancement of current understanding and helps guide the design of improved SRD-exhibiting ABCP-based drug delivery nanocarriers.

Acknowledgements

First and foremost, I would like to thank my research supervisor Dr. John Oh for his advice and support during my masters. I sincerely thank my amazing committee members, Dr. Christopher Wilds and Dr. Louis Cuccia for their support and insightful suggestions during my committee advisory meetings and for their incredibly motivating feedbacks.

My appreciation extends to members of Oh research group for their support, including Arman for his contribution. Specifically, I would like to thank Chaitra, Kamal, Twinkal and Keaton, for all their kind help and for the countless great memories during my time at Concordia University. And to Farshid, our cheerful neighbor in the lab, thank you for always offering to help and for playing extremely loud rock music that we could hear and sometimes enjoy.

I express my gratitude to Dr. Leon Wan for giving me the opportunity to be a part of his amazing team and for being the most supportive manager during my industrial internship experience. I also thank my colleagues and friends at Jazz Pharmaceuticals for their encouragement and motivation during my thesis preparation.

I also thank the following funding agencies for supporting my research: NSERC discovery grant, Canada Research Chair, and NSERC CREATE PoND program.

And last but definitely not least, I am indebted to my family, my amazing parents Marjan and Mohsen and my beautiful little sister Kimia for all their love and sacrifices that made it possible for me to peruse my dream of being a scientist. And finally, words cannot express how grateful I am to my partner, Hosein, for his endless support and encouragement throughout and for always being my guidance and ray of sunshine. This work is dedicated to the four of them.

Contribution from Authors

All research described in this thesis was conducted independently under the supervision of Dr. John Oh at Concordia University. Most of experiments and data analysis were conducted by myself, except for the design and synthesis of P1 and P2 polymers and P1 polymer CMC determination by Arman Moini Jazeni, MTT assay for cytotoxicity of P1 empty and Dox-loaded micelles by Sung Hwa Hong, and live/dead cell assay for cell viability by Chaitra Shetty in Chapter 2 as well as cytotoxicity assay by Chaitra Shetty in Chapter 3.

Table of Contents

List of Figures

List of Tables

List of Abbreviations

EPR	Enhanced Permeation and Retention
Dox	Doxorubicin
FDA	Food and Drug Administration
HPMA	*N*-(2-hydroxypropyl)methacrylamide
ABCP	Amphiphilic block copolymer
CMC	Critical micellar concentration
DMF	Dimethylformamide
SRD	Stimuli-responsive degradation
MRI	Magnetic Resonance Imaging
DTPA	Diethylenetriamine penta-acetic acid
LCST	Lower critical solution temperature
PNIPAM	Poly(N-isopropylacrylamide)
GSH	Glutathione
-SS-	Disulfide linkage
DTC	Dithiolane trimethylene carbonate
PDSM	Pyridyl disulfide ethyl methacrylate
PHMssEt	Disulfide-labeled polymethacrylate
RAFT	Reversible addition−fragmentation chain-transfer polymerization
ATRP	Atom transfer radical polymerization
PEO	Polyethylene oxide
PEG	Polyethylene glycol
LA	Lipoic acid
DCC	N,N′-Dicyclohexylcarbodiimide
ssDOH	2-Hydroxyethyl disulfide
ssCOOH	3,3′-dithiodipropionic acid
PDs	Poly(disulfide)s
PLA	Polylactic acid
PCss	Poly(carbonate-disulfide)
i.v.	Intravenous
DL-DSRD	Dual location dual stimuli-responsive degradation
DP	Degree of polymerization
GPC	Gel permeation chromatography
PTFE	Polytetrafluoroethylene
DLS	Dynamic light scattering
NMR	Nuclear magnetic resonance
UV/Vis	Ultraviolet Spectroscopy
TEM	Transmission Electron Microscopy
BSA	Bovine serum albumin
IgG	Immunoglobulin G
DTT	1,4-dithreithiol
THF	Tetrahydrofuran

PBS	Phosphate buffer saline
BCA	Bicinchoninic acid
MWCO	Molecular weight cut-off
MTT	3-(4,5-dimethylthiazol-2-yl)-2,5-diphenyltetrazolium bromide
DMSO	Dimethyl sulfoxide
DMEM	Dulbecco's modified Eagle's medium
FBS	Fetal bovine serum
OEOMA	Oligo(ethylene oxide) methacrylate
NR	Nile red
CI	Carbonylimidazole
PEss	Polyester labeled with backbone dislufide linakges
DCM	Dichloromethane
PMMA	Poly(methyl methacrylate)
CAC	Cyclic acetal

Chapter 1

Introduction

1.1 Overview of the research

My masters research is focused on the design, synthesis and characterization of smart nanometer-sized carriers for anticancer drugs. These drug delivery nanocarriers are fabricated through self-assembly of stimuli-responsive amphiphilic block copolymers and enable the encapsulation and controlled release of hydrophobic drugs on demand.

1.2 Application of nanotechnology for treatment of cancer

Cancer is a genetic disease that causes an increased and uncontrollable proliferation of cells, killing more than 8 million people worldwide per year.[1] Conventional methods for cancer therapy include surgery, radiation therapy and chemotherapy; however they all have their limitations.[2] The application of nanomedicine in cancer treatment is an emerging field offering various advantages compared to the conventional treatment options. The main advantages include 1) the improved solubility of poorly water-soluble drugs, 2) the possibility of co-delivering more than one type of drug to increase effectiveness, 3) the enhanced targetability to the site of tumor and 4) the possibility to deliver imaging agents in combination with pharmaceutical active ingredients to achieve both diagnosis and therapy (called theranostics).[3]

Due to their relatively larger sizes compared to free drug molecules, nano-formulations fall above renal clearance threshold (≈ 40 kDa) and thus show prolonged circulation times in blood following an intravenous (i.v.) injection. Further, deformities in the fast-growing tumor tissues present 1) larger fenestrations in abnormal tumor vasculatures and 2) poorly developed lymphatic drainage systems. Due to these features, the phenomenon called Enhanced Permeation and Retention (EPR) increases the extravasation of nanoparticles into tumor interstitial fluids as well as their retention in tumors, a process known as passive targeting (Figure 1.1).[4] The EPR effect could result in 10-50 folds higher concentration in solid tumors compared to healthy tissues.[5]

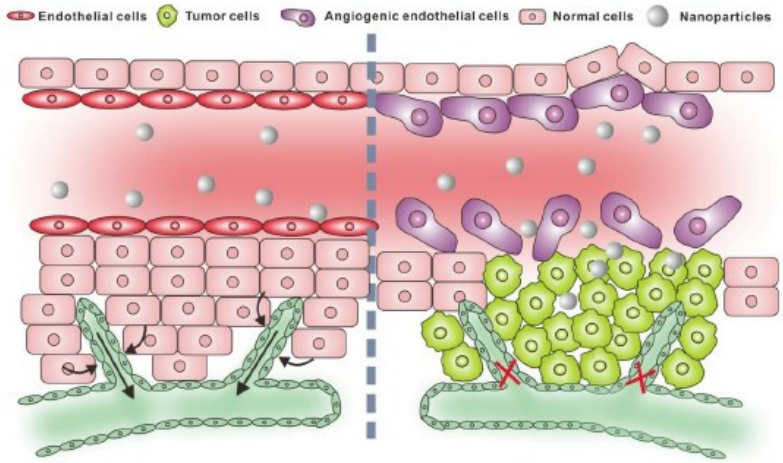

Figure 1.1 Schematic illustration of the EPR effect.[6]

After the discovery of the EPR effect by Maeda *et al*. in 1986, numerous proof-of-evidence studies have shown the effectiveness of EPR in passive targeting of nanotherapeutics, turning EPR into a ″royal gate″ for targeted antitumor therapy.[7,8] An example is the report describing a polymeric nanoconjugate based on poly(β-L-malic acid) designed to deliver oligonucleotides. The conjugate was accumulated in brain tumor following an i.v. injection which is attributed to the EPR effect.[9] O'Brien *et al.* reported that a nanoformulation of the anticancer drug doxorubicin (Dox) is accumulated selectively in breast cancer tissue, leading to a decrease in cardiac side effects of the nanoparticle formulation compared to free drug.[10] However, heterogeneity between tumors with different vasculature characteristics is an important parameter that leads to different extents of the EPR effect.[11] Recent reports claim that the EPR phenomenon is not the only mechanism responsible for the entry and accumulation of nanoparticles into tumor tissue.[12] In addition, while the initial studies on the EPR effect has shown promising results in mice and rodents, it has failed to show a significant benefit in humans in clinical trials.[13]

1.3 Types of nanocarriers for drug delivery

The year 1952 marks an important revolution in the field of drug delivery as the first sustained-release formulation was reported which enabled controlling the rate of drug release in the body.[14] Research has continued to focus on design and development of a variety of controlled-release strategies of encapsulated drugs at a specific site. The field of nanomedicines has offered

tremendous potential in the area of controlled-release delivery. After the first lipid-based nanostructure that was reported in 1964, a variety of nanoformulations were developed as promising drug delivery vehicles.[15] The timeline in Figure 1.2 summarizes the major breakthroughs in the field of cancer nanomedicine from 1964 - 2015. As depicted by this figure, the main three classes of drug delivery platforms in preclinical development include liposomes, polymer-drug conjugates and polymeric micelles. This section summarizes a brief overview of these nano delivery systems.

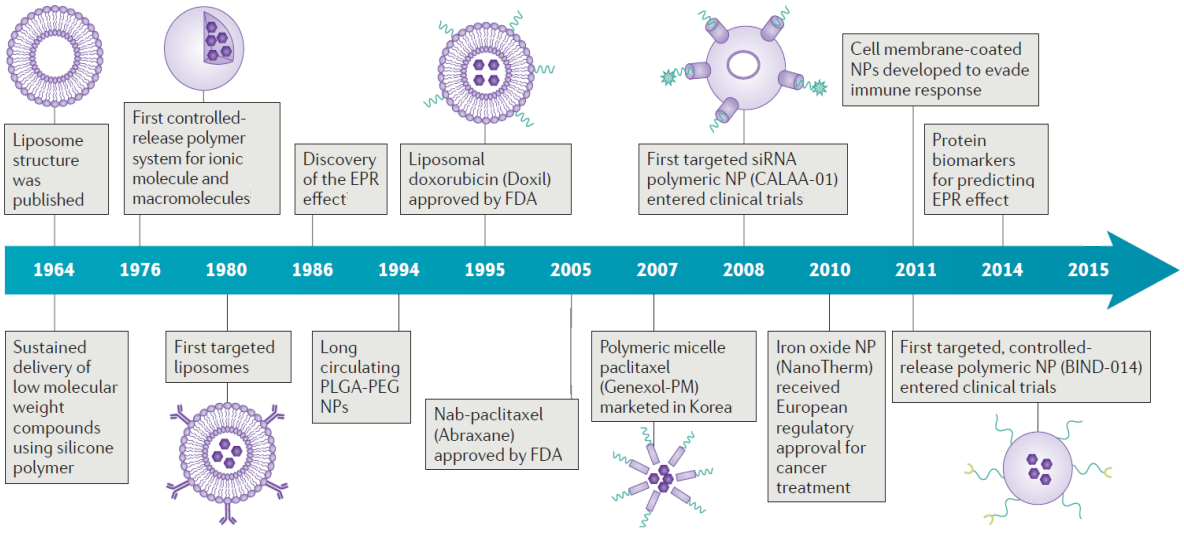

Figure 1.2 Historical timeline of major developments in cancer nanomedicine, slightly modified from original source.[15]

1.3.1 Liposomes

Liposomes are the most common nanocarrier platform for drug delivery. These spherical particles have an aqueous interior enclosed with lipid bilayer and therefore enable the encapsulation of both hydrophilic and hydrophobic drug molecules. Liposomes have large loading capacities and allow for relatively simple surface functionalization for attachment of ligands or biocompatible polymers. Doxil was the first FDA-approved nanomedicine in cancer therapeutics, a liposomal formulation of Dox. Doxil significantly increases blood circulation time of Dox by reducing the plasma clearance to 0.1 L/h compared to 45 L/h for free Dox.[16] Different types of liposomes have been designed including PEGylated liposomes with stealth properties,[9] ligand-

targeted liposomes with proteins, antibodies or small molecules on their surface for specific cell recognition[17] and theranostic liposomes containing functionalized imaging agents together with therapeutically active drugs (Figure 1.3).[18] Despite their advantages, liposomes have drawbacks including the potential to cause immunogenicity in the body, incomplete or slow release of cargo at target site and premature drug release during blood circulation.[19,20]

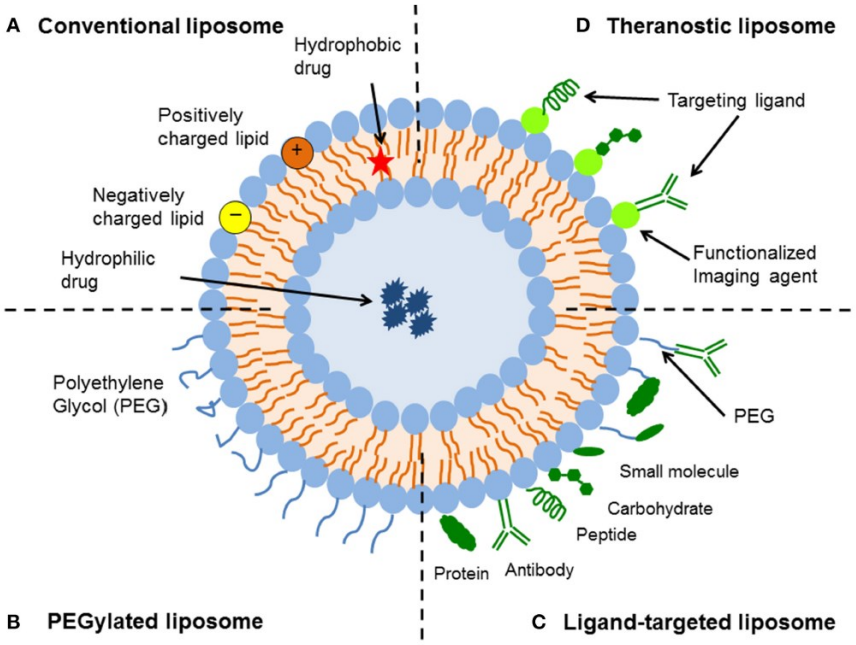

Figure 1.3 Schematic illustration of various classes of liposomes for drug delivery.[18]

1.3.2 Polymer-drug conjugates

Polymer-drug conjugates are polymer prodrugs where small drug molecules are covalently linked with water-soluble polymeric chains. Such conjugation increases the solubility and size of drug molecules, which enhances their blood circulation half-life and thus promotes accumulation into tumor tissues by EPR effect.[21] By incorporating labile linkages as cleavable spacers between drug molecules and polymers, the active form of the drug can be released in the body. Various types of cleavable linkages (either enzymatically or chemically) have been investigated in polymer prodrugs, including amide and ester bonds that could potentially cleave anywhere in the body, but also linkers that cleave in response to an endogenous trigger present specifically at the target site.

Due to the slight acidic pH present in tumor microenvironment (pH = 6.5) and low pH values found in endosomes and lysosomes inside the cells (pH = 5.0 - 5.5), acid-labile linkages are common in polymer-drug conjugates of chemotherapeutic agents. Wang *et al.* developed a polymer-Dox prodrug system using acid-labile hydrazone in the linker that released the active drug after acid treatment.[22] In another study, a HPMA copolymer-Dox conjugate was shown to have more than 10-100 folds of tumor accumulation when compared to the free drug, a factor that showed dependency to tumor size.[23] The biggest drawback of polymer-drug conjugate strategy is that the covalent attachment between the drug and the polymer, making the prodrug pharmacologically inactive. If the linker does not cleave to release the active drug after administration, the therapeutic efficiency of the drug will be heavily affected. In addition, prodrugs are considered new chemical entities, which require re-validation from regulatory bodies to ensure their safety, causing significant delays in their clinical translation.[24]

1.3.3 Polymeric micelles

Polymeric micelles are colloidal particles consisting of self-assembled amphiphilic block copolymers (ABCP). These amphiphilic molecules contain two distinct immiscible regions: a hydrophilic block and a hydrophobic block. In an aqueous environment, these amphiphiles can exist as individual polymeric chains (unimers) or as self-assembled aggregates (micelles) depending on their concentration in the solution. The concentration at which the first self-aggregate is formed is known as the critical micellar concentration (CMC). There is an inverse relationship between the CMC for an amphiphile and the stability of its micelles. The CMC of polymeric micelles (10^{-6} - 10^{-7} M) are much lower than the CMC values for smaller surfactant molecules (10^{-3} - 10^{-4} M), suggesting their higher stability in aqueous environment with a lower sensitivity to dilution.[25] In addition, advances in the field of polymer chemistry and material sciences now allows for the synthesis of more complex well-defined ABCPs with variable properties, easy incorporation of labile-linkages into the polymer structure and post-modification of polymers for the attachment of targeting ligands or imaging moieties. By fine-tuning the structure of the ABCPs, polymeric nano-assemblies with various morphologies, architecture and sizes can be fabricated.[26]

ABCPs can also be designed with pendant functional groups to allow cross-linking of the polymeric micelles after the self-assembly process. This strategy has been particularly important

in the development of anticancer drug delivery carriers with higher colloidal stability in blood circulation. Biswas *et al.* developed a core cross-linked polymeric micellar system based on redox-responsive ABA-type triblock copolymer PHMssEt-*b*-PEG-*b*-PHMssEt.[27] The stability of the cross-linking micelles compared to non-cross-linked micelles was evaluated using dynamic light scattering by diluting the micelles with DMF. Note that DMF was chosen to fully dissolve the ABCP. Upon dilution, non-cross-linked micelles dissociated while the core cross-linked micelles were intact but swollen, suggesting their higher colloidal stability. The reduction-responsive cross-links were able to cleave in the presence of a reducing agent, leading to a controlled disassembly and drug release at tumor site.

1.3.3.1 Self-assembly of amphiphilic block copolymer

The self-assembly of the ABCPs is a result of the covalent attachment of the two immiscible blocks in a selective solvent, preventing them from a macroscopic phase separation. Hence, when the ABCP is present in a solvent which can thermodynamically dissolve one of the blocks, but is a precipitant for the other block, a microscopic phase separation occurs due to the unfavorable mixing enthalpy. The self-assembly process is the attempt of the ABCP to minimize the unfavorable contact between the solvophobic block and solvent molecules. This is mainly driven by two opposing forces: an attractive force between the insoluble core-forming blocks, and a repulsive force between the soluble blocks in the shell.[26] For an amphiphilic diblock copolymer in aqueous environment, two spherical micellar structures can be formed with varying the relative lengths of the two block. As illustrated by Figure 1.4, if the length of the core-forming hydrophobic block (L_C) is longer than the shell-forming soluble hydrophilic block (L_S), the resulting micelles have a large core with a short corona and are referred to as ″crew-cut″ micelles. However, if L_S is longer than L_C, ″hairy″ micelles with small dense cores and large coronas are observed.

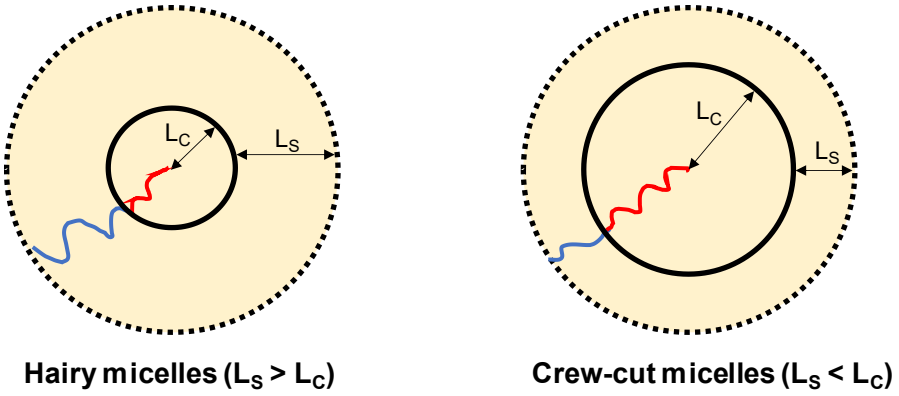

Figure 1.4 Schematic representation of AB deblock copolymer micelles, with L_C = Core thickness and L_S = Shell thickness.

ABA type triblock copolymers can also self-assemble to spherical micelles; but the structures of these micelles are more complicated. An A-selective solvent will result in ″star-like″ micelles while in the presence of a B-soluble solvent, the middle block will fold to form ″Flower-like″ micelles (Figure 1.5).

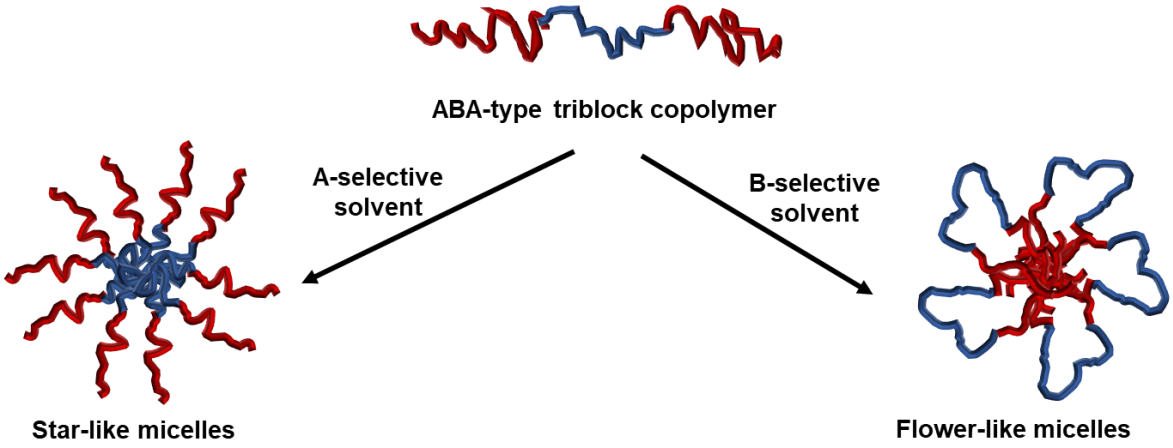

Figure 1.5 Self-assembly of ABA-type triblock copolymer under different conditions.

1.4 Stimuli-responsive polymers for drug delivery application

Stimuli-responsive polymers undergo chemical or physical changes upon exposure to external triggers. Their 'smart' behavior mimics the functions of regulatory macromolecules in living organisms that respond to their environments. This feature makes them useful in biomedical and pharmaceutical fields. Particularly in drug delivery, they offer a beneficial role in designing nanocarrier systems for controlled drug release at target tissue (such as tumor).

One class of stimuli-responsive polymers undergoes physical changes in response to an external trigger. Examples include thermo-responsive polymers exhibiting hydrophobic/ hydrophilic transition upon a change in temperature[28] and pH-responsive polymers bearing ionizable groups that undergo a phase transition in response to pH.[29] Another class of stimuli-responsive polymers involves an integration of dynamic chemical bonds that can be cleaved upon exposure to stimuli. Such stimuli-responsive degradation (SRD) utilizes chemical, physical or biological stimuli, including light, acidic pH, reduction and enzymatic reactions.

The type of stimuli triggering the polymer can be classified as exogenous or endogenous triggers. A common external stimulus for inducing drug release at the tumor site is temperature. The idea is to design thermo-sensitive nanocarriers which remain stable at normal body temperature (≈ 37 ºC) and administer them simultaneously while locally heating tumor site at temperatures ranging from 40-42 ºC.[30] Thermo-responsive Dox-loaded liposome (THERMODOX®) is in clinical trials and has demonstrated promising results of increasing the survival of primary liver cancer patients up to more than two years.[31] Tagami *et al.* reported a dual-functional thermo-sensitive liposomal formulation co-encapsulating an MRI probe (Gd-DTPA) and the anticancer drug Dox in order to achieve stimuli-responsive release and real-time release monitoring.[32] Their liposomes were shown to have a surprisingly fast release of 100% of the encapsulated Dox in only 3 minutes when heated up to 40-42 ºC and *in-vivo* studies showed very high correlation between the Dox release and the T_1-mediated response of the imaging agent (R^2 = 0.98). Thermo-responsive polymers with their lower critical solution temperature (LCST) in the physiologically relevant temperatures have also been investigated for tumor-targeted drug delivery. Poly-N-isopropylacrylamide (PNIPAM) is the most studied LCST polymer which was first used for drug delivery applications by the Okano group in 1999.[28] By studying the cell viability of their PNIPAM-based Dox-loaded polymeric micelles at two temperatures, they

demonstrated heat-responsive drug release as the micelles showed cytotoxicity at 42.5 ºC but not at 37 ºC.[33] Other reported external triggers include the use of magnetic fields,[34,35] light[36,37] or ultrasound waves.[38,39]

Internally regulated delivery systems typically respond to endogenous triggers found in the body including acidic pH, enzyme and glutathione (GSH). This strategy offers a tremendous advantage over conventional drug delivery methods because the rate and the location of drug release in the body can be tailored according to the specific physiological or chemical properties of different tissues *in-vivo.* For tumor-targeted drug delivery, the two popular and promising internal stimuli are acidic pH and reducing environment in tumor tissue and cancer cells respectively.

As summarized by Figure 1.6, several designs of block copolymers with SRD characteristics have been reported.[40,41] These classifications of micelles are based on the number and location of the SRD linkages in the polymer, and the resulting nanoparticles. Class A includes polymers with more than one labile linkage incorporated in their side chains, thus forming pendant multi-cleavable micelles. Class B are polymers with multiple SRD linkages placed repeatedly in their backbone resulting in backbone multi-cleavable micelles. Class C are cross-linked micelles formed using SRD crosslinkers. Classes D and E involve micelles with only one degradable linkage in their backbone, positioned either in the middle of the hydrophobic block or at hydrophilic/hydrophobic block junctions that self-assemble to mono-cleavable and sheddable micelles respectively.

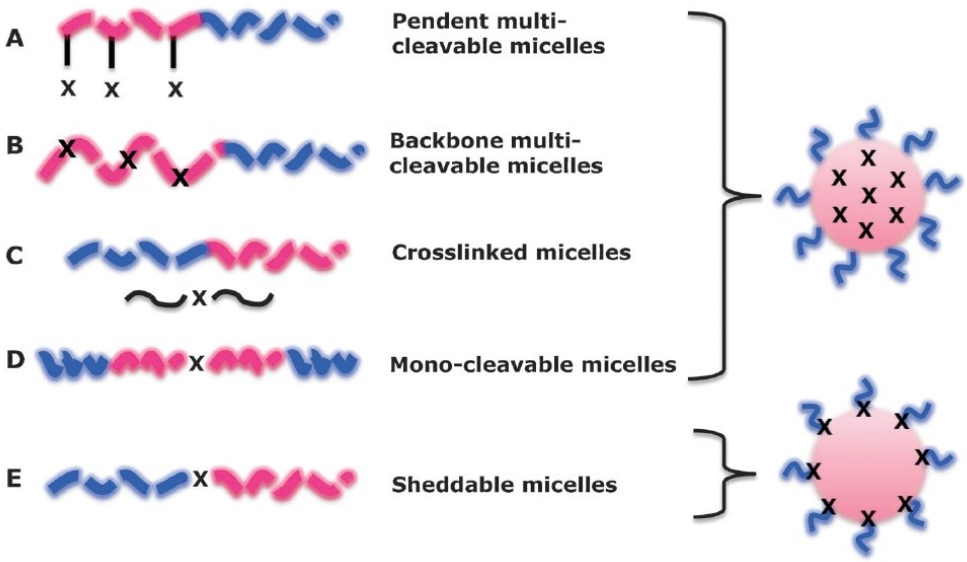

Figure 1.6 Strategies for block copolymer micelles with SRD elements with various number and locations of cleavable linkages (x).[41]

1.4.1 Reduction-responsive systems

Glutathione is a tripeptide with cysteine residue that acts as a cellular reducing agent for drug release inside cancer cells. GSH concentration is ≈ 10 μM in extracellular compartment while its concentration is 0.1-10 mM in intracellular environment and is known to be 4-7 times higher in cancer cells.[42] Disulfide (-SS-) linkages are labile covalent bonds that can be cleaved to the corresponding thiols in a reducing environment, potentially in the presence of GSH. This section reviews two types of GSH-responsive block copolymer designs for drug delivery, named as pendant multi-cleavable and backbone multi-cleavable systems.

1.4.1.1 Pendant multi-cleavable reduction-degradable systems

Figure 1.7 illustrates a schematic diagram of the self-assembly of a block copolymer having pendant -SS- placed in the side chain of the hydrophobic block to from a pendant multi-cleavable reduction-degradable nanoassemblies. The disulfide pendants are located in the hydrophobic core which can be cleaved in the presence of a reducing agent through a solubility change of the hydrophobic block to a more hydrophilic block. This change of hydrophobic/hydrophilic balance causes the disintegration and destabilizing of micelles, leading to the enhanced release of encapsulated cargo. Further, this system is attractive as to allow the formation of core-cross-linked

micelles through disulfide-thiol exchange chemistry in the presence of a small catalytic amount of a reducing agent. Core cross-linked nanoassemblies improve colloidal stability during blood circulation compared to non cross-linked particles.

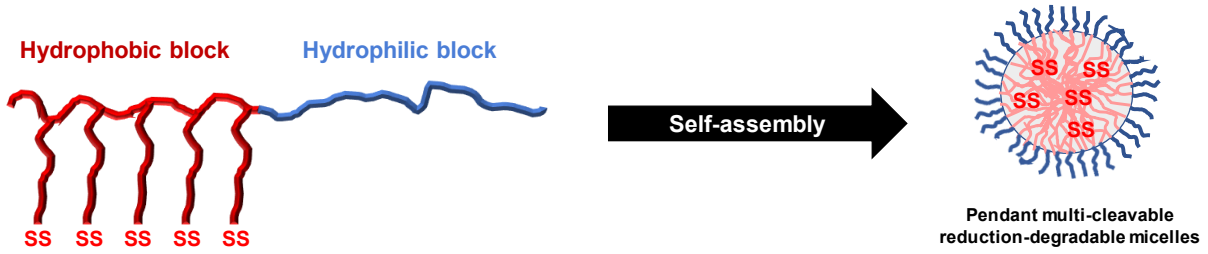

Figure 1.7 Schematic representation of pendant multi-cleavable reduction-responsive amphiphilic polymers and their self-assembled micelle.

A popular approach to the synthesis of pendant multi-cleavable reduction-responsive polymers utilizes the direct polymerization of disulfide-bearing monomers. Figure 1.8 shows the monomers reported in the literature. Dithiolane trimethylene carbonate (DTC) was synthesized for use in ring opening polymerization (ROP) while the rest of the monomers shown contain vinyl groups that can participate in various free radical polymerizations. Wong *et al.* reported the synthesis of versatile pyridyl disulfide ethyl methacrylate (PDSM)-based polymers with -SS- in pendant chains via RAFT polymerization.[43] The same group also developed Dox-conjugated cross-linked micelles based on reductive-sensitive PDSM polymers for potential anti-tumor drug delivery applications.[44]

Disulfide-bearing HMssEt was designed and synthetized in Dr Oh's laboratory. The methacrylate has been incorporated into the design of various amphiphilic block copolymers.[27,45–48] Khorsand *et al.* reported the synthesis of the amphiphilic block copolymer PEO-b-PHMssEt via atom transfer radical polymerization (ATRP) which could self-assemble into reduction-responsive micelles.[45] Dox was encapsulated in the micelles and upon exposure to GSH, the -SS- bonds in the core were cleaved resulting in disintegration of the particles and a significant increase in Dox release. A dual acid/reduction-responsive polymer was also synthesized containing a thermo-sensitive block with pendant PEO and -SS- conjugated to PEG via an acid-labile acetal linkage.[47]

The temperature-driven self-assembly of this double-hydrophilic polymer followed by the *in-situ* cross-linking process formed stimuli-responsive cross-linked nanogels with low toxicity and high colloidal stability for biomedical applications.

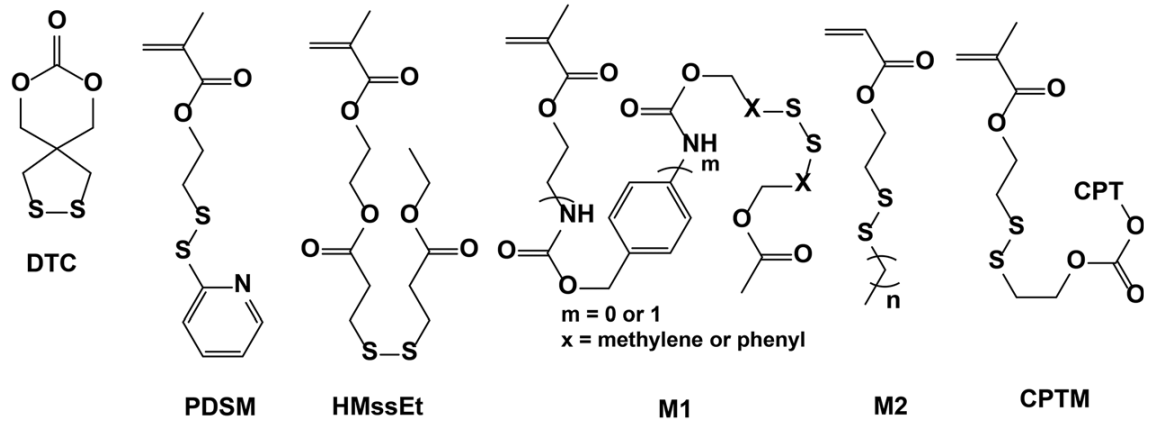

Figure 1.8 Typical monomers bearing pendant -SS- linkages reported for the synthesis of pendant multi-cleavable block copolymers by direct polymerization approach.[49]

Disulfide groups have also been incorporated into the side chains of polymers by post-conjugation, through well-established conjugation chemistries such as carbodiimide coupling reactions or click chemistries. Various reports describe the conjugation of lipoic acid (LA) to various OH-bearing polymers, such as the conjugation of LA to poly(N-2-hydroxypropyl methacrylamide) via DCC coupling[50] and the conjugation of lipoic acid anhydride to poly(L-tyrosine) by esterification.[51]

1.4.1.2 Backbone multi-cleavable reduction-responsive systems

These polymers contain more than one -SS- linkages in their backbones (Figure 1.9). They have been commonly synthesized by step-growth polymerization techniques including polycondensation and polyaddition. Numerous reports describe reduction-responsive polyphosphates,[52,53] polyurethanes,[54,55] polypeptide,[56] polycarbonate[57] and polyesters.[58] An example published by Dr. Oh's laboratory involves step-growth polymerization of a disulfide-bearing diol (ssDOH) and a disulfide-bearing dicarboxylic acid (ssCOOH) to yield a backbone cleavable reduction-responsive polyester.[59] After esterification to introduce a bromine end-group,

the formed bromine-functionalized polyester was used as a macroinitiator for ATRP. The formed block copolymer degraded in reducing environment.[60] Another example includes thiol-disulfide exchange reaction to synthesize poly(disulfide)s (PDs). Basak *et al*. developed triblock copolymers containing PDs to study the effect of the hydrophobicity of the core-forming block on the reduction-responsiveness of their micelles.[61] Their approach for the PD synthesis involved a direct disulfide-thiol exchange reaction between di-thiols and dipyridyl disulfide. Subsequent functionalization of the chain-ends allowed for bromination of HO-PD-OH to the ATRP macroinitiator Br-PD-Br and chain extension by ATRP. The results of their GSH-induced release study indicated a significantly faster release of NR from the micelles made of polymer with a more hydrophilic PD attributed to the relatively faster diffusion of polar GSH towards the more hydrophilic PD core. In addition to step-growth polymerization, chain growth polymerization techniques including ROP[52,53] and RAFT[62] have also been reported for synthesis of hyperbranched polymers with multiple -SS- linkages incorporated in their backbone.

Backbone multi-cleavable polymers have also been synthesized for the development of polymeric prodrugs. Fan *et al.* designed graft co-polymers based on disulfide-containing poly(amido amine) with alkyne side chains, that were conjugated to either camptothecin-azide or azide-terminated poly(ethylene glycol) methyl ether via click chemistry.[63]

Figure 1.9 Schematic representation of backbone multi-cleavable reduction-responsive amphiphilic polymers and their self-assembled micelle.

1.4.2 Acidic pH-responsive systems

pH-responsive drug delivery systems have been designed to achieve target-specific drug release by taking advantage of the various pH levels found in the human body. Figure 1.10 illustrates that pH values in human body can vary at organ level such as the drastic pH variation

between various organs within the gastrointestinal tract. It could also vary at tissue level whereby pathological changes cause a change in pH in tissues such as the tumor or inflamed tissue compared to normal tissue. pH variations are also observed at cellular level for different organelles within a cell. Due to the lower pH of tumor tissue compared to healthy tissue (pH = 6.7 - 6.9) and acidic environment of the endosomes and lysosomes (pH = 5.0 -6.0) inside the cancer cells, acidic pH-responsive polymers are promising in the design of tumor-targeted drug delivery systems.

Acidic pH-responsive polymers used in drug delivery can be classified into acid-ionizable polymers and acid-cleavable polymers. The first class are polymers with ionizable functional groups undergoing protonation/deprotonation depending on environmental pH, thus leading to a change in hydrophobic/hydrophilic balance of the polymeric system. Examples of widely used functional groups in this category are tertiary amine and carboxylic acid. Amines with pKa values lower than physiological pH are protonated in acidic conditions and become hydrophilic and water-soluble. Ko *et al*. reported the synthesis of an acid-responsive block copolymer based on PEG and poly(β-amino ester) which self-assembled into micelles demonstrating pH-dependent destabilization under weak acidic environment.[64] Their *in-vitro* Dox release profile demonstrated an enhanced drug release of ≈ 80% in 6 hours at pH = 6.4, compared to 30% release in 24 hours at pH = 7.4.

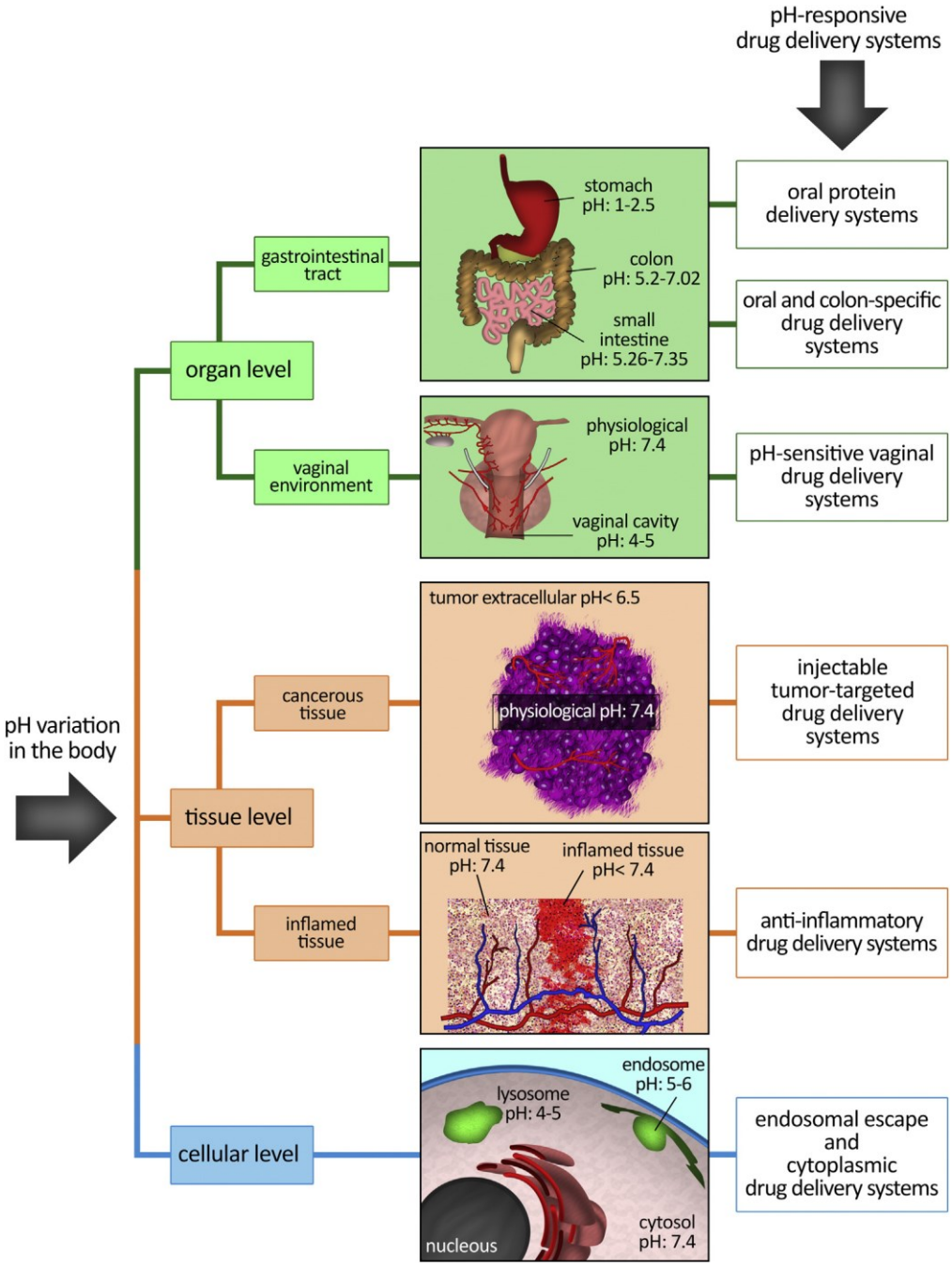

Figure 1.10 pH Variation in the body, in the organism, tissue, and cellular levels.[65]

Acid-cleavable polymers are designed with dynamic covalent bonds that can break in the presence of acidic pH, leading to the chemical degradation of the polymer into smaller fragments. Table 1.1 summarizes common acid-degradable linkages with references reported in the design of acid-responsive polymers for drug delivery.

Functional group	Structure	Ref
Acetal	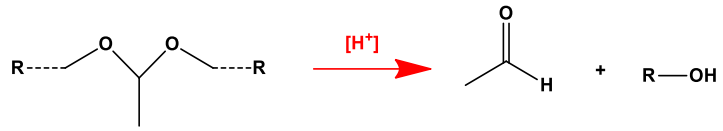	66,67
Ketal	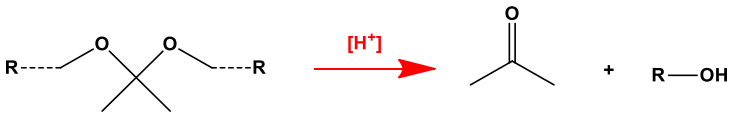	68,69
Imine		70,71
Hydrazone		72,73
Oxime		74

Table 1.1 Acidic pH-cleavable linkages commonly used in polymer-based drug delivery systems.

Acid-labile shell-sheddable nanoassemblies have been particularly popular as they can address the long-debated phenomenon known as ″PEG dilemma″ in tumor-targeted drug delivery.[75] This term refers to the unfavorable poor cell-internalization caused by covering nanoparticles with PEG chains despite the enhanced prolonged blood circulation time offered by PEGylation. By incorporating an acid-labile linkage at core/corona interfaces, nanoparticles can benefit from favorable stealth properties offered by PEG coating during blood circulation, followed by a pH-induced shell-shedding at tumor interstitial fluid to enhance cellular uptake by cancer cells.[76,77] This strategy can be achieved by carefully selecting acid-labile linkages which can undergo cleavage at slightly acidic pH environment (pH = 6.5 - 6.8). This rational design approach has been used to develop nanocarriers based on silica nanoparticles and targeting peptides coated with PEG, with acid-labile benzoimine linkages positioned between PEG chains and peptides to achieve PEG shedding and exposure of peptide ligands at tumor tissue.[78] Based on a similar approach, Sun *et al.* reported PEG-PLA-based nanoparticles with an acid-cleavable 2-propionic-3-methylmaleic bridge between the two blocks.[79] Release of PEG chains in slightly acidic tumors improved cellular uptake and *in-vivo* tumor inhibition rate by 30%.

1.4.3 Dual acidic pH/reduction-responsive systems

Recent advances in designing environment-sensitive materials shows a noticeable shift to design and synthesis of macromolecules constructed with multiple stimuli-responsive components responding to more than one type of triggers. These types of responses are found in biological processes whereby multiple changes in the environment can be sensed and responded to. For tumor-targeted therapy, combining acid and reduction responsiveness has been particularly popular with various designs and locations of incorporating acid-responsive linkages as well as disulfides in polymer structures. These include acid/reduction-responsive nanoassemblies developed by incorporating acid-sensitive and -SS- linkages as pendant chains in the hydrophobic block,[80,81] polymer backbone,[82] or cross-linkers.[83,84]

Polymeric prodrugs have also been developed with dual acid/reduction-responsive properties, including a poly(Dox) with acid-labile hydrazone and -SS- linkages placed repeatedly in the backbone demonstrating complete drug release in 1.5 days at pH = 5.0 and 10 mM GSH concentration.[85] Recently, a polymeric prodrug consisting of covalent conjugation of two anticancer drugs in a single system was reported.[86] Polymer chains were conjugated to camptothecin drug molecules through -SS- linkage and to Dox drug molecules through hydrazone bonds, hence forming a dual acid/reduction-degradable delivery system. *In-vitro* drug release assay showed enhanced release of camptothecin with increasing concentration of the reducing agent GSH in the medium in 80 hrs, as well as 50% increased Dox release at acidic pH = 5.0 compared to pH = 7.4 as control.

The blooming field of stimuli-responsive materials contributes to a significantly large proportion of research in material science and polymer chemistry fields. While responding to the environmental cues is a long-known behavior observed in plants and animals, design of intelligent synthetic material is a relatively new concept, and yet, with the vast majority of applications for such materials, research from fundamental understanding of stimuli-responsiveness to design and synthesis of functional environmentally-sensitive polymers continues to be a hot topic. The examples of SRD systems reviewed in this chapter are only a small proportion of the broad literature in the field of stimuli-responsive polymers. And yet, they demonstrate the versatility and broad application for synthetic stimuli-responsive polymers and intelligent materials.

1.5 Scope of the thesis

The main objective of my MSc research is to explore dual location dual acid/reduction-degradation strategy towards tumor-targeting intracellular drug delivery. With my focus on the synthesis, characterization, and *in-vitro* evaluation of three novel block copolymers, my research results are outlined in two research chapters. Chapter 2 describes the development of two tumor-targeting intracellular polymer-based drug delivery carriers based on dual location dual acid/reduction-degradable strategy. Chapter 3 is devoted to the synthesis and characterization of reductively degradable poly(carbonate-disulfide)s (PCss) with multifunctionality. A novel synthetic approach based on carbonylimidazole-hydroxyl chemistry was explored for the synthesis of a series of various PCss polymers including a block copolymer for potential applications in the biomedical and pharmaceutical industries. Lastly, the summary and future suggestions for the projects are discussed in Chapter 4.

Chapter 2

Development of tumor-targeting intracellular drug delivery carriers based on dual location dual acid/reduction-degradable nanoassemblies

2.1 Introduction

The development of smart nanoassemblies based on well-controlled block copolymers undergoing a chemical transition through stimuli-responsive degradation (SRD) has attracted significant attention as a promising platform for tumor-targeted drug delivery with control over drug release profile.[41,87,88] Such controlled/enhanced drug release not only improves the biodistribution of anticancer drugs but also ensures their minimal dosage, thus improving drug efficacy and minimizing undesired cytotoxicity to normal tissues common to small molecule drugs. Well-designed SRD-exhibiting nanoassemblies enable the encapsulation of hydrophobic anticancer drugs inside cores, surrounded with hydrophilic coronas endowing biocompatibility.[89–91] After being administered through intravenous (i.v.) injection to the blood, drug-loaded nanoassemblies are targeted to tumor tissues through Enhanced Permeability and Retention (EPR) effect during blood circulation.[92–95] Following endocytosis into cancer cells, they are exposed to endogenous stimuli found in tumor tissues or cancer cells. This SRD process causes the degradation (or disintegration) of the nanoassemblies, leading to controlled release of encapsulated drugs.[96–98]

Acidic pH and glutathione are typical endogenous stimuli found in cancer cells and tumor tissue. Tumor tissues are slightly acidic (pH = 6.5-6.9) and further endosomes and lysosomes are more acidic (pH = 4.5-5.5).[99] Ketal, acetal, orthoester, and imine are typical acid-labile linkages that can be cleaved through acid-catalyzed hydrolysis in a mild acidic condition.[100,101] Glutathione (a tripeptide with cysteine, GSH) is found at concentration as high as 40-60 mM and further has a large difference in redox potential between intracellular and extracellular compartments.[102] In the presence of cellular glutathione, disulfide bonds are cleaved to the corresponding thiols for reductive degradation of nanoassemblies.[40,103–106]

Dr. Oh's research group has recently explored a new strategy called dual location dual stimuli-responsive degradation (DL-DSRD).[107] This strategy offers the versatility in that response to each stimulus can independently regulate the release of encapsulated molecules and can facilitate synergistic/accelerated release at dual locations. To explore this approach, several reports have explored the synthesis of polycarprolactone-based grafted copolymers bearing pendant acetal junction and single disulfide linkages on the hydrophobic backbone[108–110] and a poly(ethylene glycol) (PEG)-based linear polyurethane with benzoic imine[111] or hydrazine[112] junction and disulfide hydrophobic backbones. These copolymers synthesized by controlled polymerization techniques self-assembled to form dual acid/reduction-degradable nanoassemblies with acid-labile interfaces and disulfide cores. In addition, a report describes the synthesis of a PEG-based polypeptide bearing dimethylmaleic anhydride junction and thiol cores by ring opening polymerization, which formed disulfide-core-crosslinked nanogels with dimethyl maleic anhydride at interfaces.[112] Despite the advances, most systems have one or more drawbacks such as the inefficiency of reductive degradation because of only single disulfide incorporation on the hydrophobic backbone or the difficulty in control of disulfide-crosslink formation through uncontrolled oxidation of pendant thiols.

This chapter describes my research projects to investigate the versatility of dual location dual acid/reduction-degradable block copolymer nanoassemblies toward tumor-targeting drug delivery. Figure 2.1 shows the chemical structure of two novel copolymers synthesized by Dr. Oh's research group (Arman Moeini Jazeni, PhD candidate).

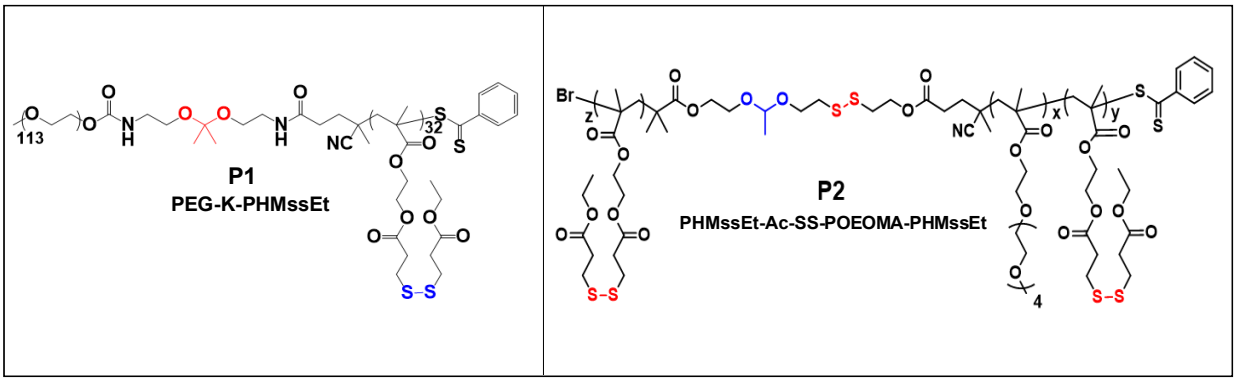

Figure 2.1 Design and chemical structures of P1 and P2 polymers.

2.2 Part I: P1 diblock copolymer

These works have been described in our publication *Polym. Chem.*, ***2019**,10, 2840-2853,* adapted from the original source material.

2.2.1 P1 Polymer design

The P1 diblock polymer was synthesized through reversible addition-fragmentation chain transfer (RAFT) polymerization using a PEG-labeled macro-RAFT agent and HMssEt as hydrophobic monomer. ^{1}H-NMR analysis showed the degree of polymerization (DP) for the HMssEt blocks to be 32, with M_n = 24.6 kg/mol. This novel block copolymer is designed with a ketal linkage at block junction and multiple disulfide pendants in the hydrophobic block. Further, the ketal linkage is sensitive to acidic pH in a mild range (< 6.8) and its acid-catalyzed hydrolysis rate can be tuned with its chemical structure.

As illustrated in Figure 2.2, the formed PEG-K-PHMssEt polymer (labelled as P1 in this chapter) self-assembles to form dual acid/reduction-degradable nanoassemblies with ketal linkages at interfaces and disulfide pendants in micellar cores. Given dual acid/reduction responses at dual core and interface locations, they exhibit synergistic and excellent release of encapsulated anticancer drugs, compared with their single response counterparts.

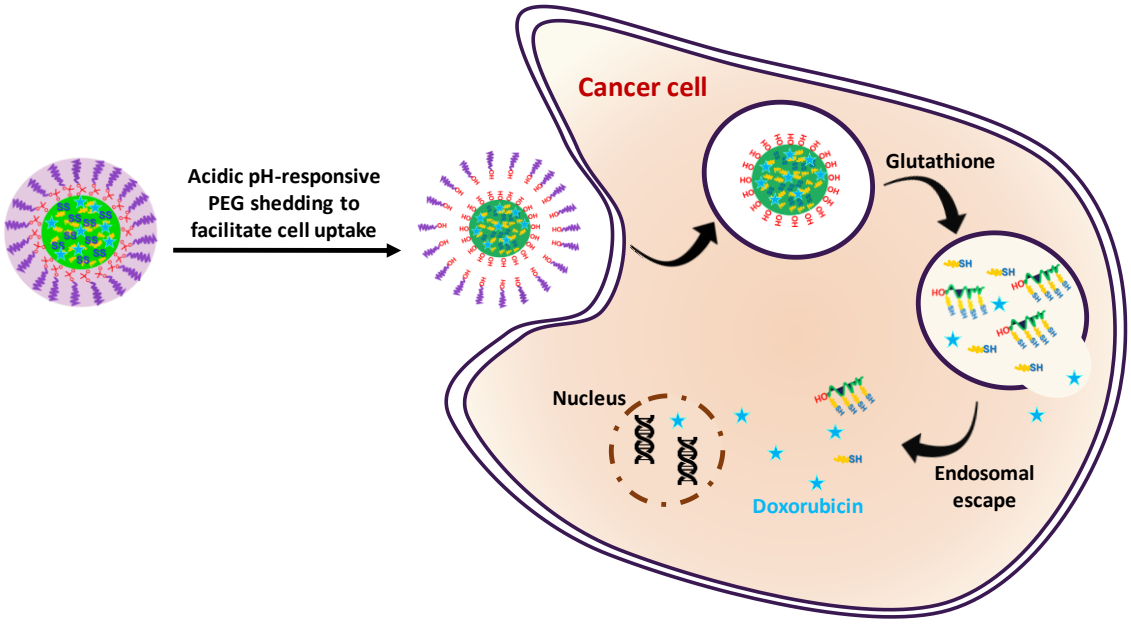

Figure 2.2 Schematic diagram of stimuli-responsive degradation and drug release of P1 nanoassemblies in tumor tissue.

2.2.2 Experimental section

2.2.2.1 Instrumentation

^{1}H-NMR spectra were recorded using a 500 MHz Varian spectrometer. The $CDCl_3$ singlet at 7.26 ppm was selected as the reference standard. Molecular weight and molecular weight distribution were determined by gel permeation chromatography (GPC). An Agilent GPC was equipped with a 1260 Infinity Isocratic Pump and a RI detector. Two Agilent PLgel mixed-C and mixed-D columns were used with DMF containing 0.1 mol% LiBr at 50 °C at a flow rate of 1.0 mL/min. Linear poly(methyl methacrylate) standards from Fluka were used for calibration. Aliquots of the polymer samples were dissolved in DMF/LiBr. The clear solutions were filtered using a 0.40 mm PTFE filter to remove any DMF-insoluble species. A drop of anisole was added as a flow rate marker. The size of micelles in hydrodynamic diameter by volume was measured by dynamic light scattering (DLS) at a fixed scattering angle of 175° at 25 °C with a Malvern Instruments Nano S ZEN1600 equipped with a 633 nm He-Ne gas laser. Fluorescence spectra on a Varian Cary Eclipse fluorescence spectrometer and UV/vis spectra on an Agilent Cary 60 UV/vis spectrometer were recorded using a 1 cm wide quartz cuvette.

Transmission Electron Microscopy (TEM) images were obtained using a Philips Tecnai 12 TEM, operated at 80kV and equipped with a thermionic LaB6 filament. An AMT V601 DVC camera with point to point resolution and line resolution of 0.34 nm and 0.20 nm respectively was used to capture images at 2048 by 2048 pixels. To prepare specimens, aqueous Dox-loaded NP dispersion was dropped onto copper TEM grids (400 mesh, carbon coated), blotted and allowed to air dry at room temperature. Subsequently, uranyl acetate (1%) was applied on the TEM grids and then dried again at room temperature.

2.2.2.2 Materials

Bovine serum albumin (BSA), immunoglobulin G from human serum (IgG, reagent grade, > 5%, essentially salt-free, lyophilized powder), glutathione (GSH), doxorubicin (Dox, $-NH_3^+Cl^-$ forms, >98%), and 1,4-dithreithiol (DTT) were purchased from Sigma Aldrich and used as received.

2.2.2.3 Aqueous micellization by dialysis method

PBS (pH = 7.4, 10 mL) was added dropwise to an organic solution of P1 dissolved in THF (2 mL) using a syringe pump equipped with a plastic syringe (20 mL volume, 20 mm diameter) at an addition rate of 0.2 mL/min. The resulting dispersion was dialyzed against phosphate buffer saline (PBS) solution (1 L) changed twice in 24 h, yielding aqueous micellar dispersion at 0.9 mg/mL concentration.

2.2.2.4 Colloidal stability in the presence of proteins

Aliquots of the formed micellar dispersion (1 mL, 0.6 mg/mL) were mixed with aliquots of aqueous PBS solutions of BSA (1 mL, 80 mg/mL) and IgG (1 mL, 16 mg/mL). Being incubated at 37 °C for 48 hrs, the resulting mixtures, along with controls (without micelles), were first analyzed with DLS to observe the occurrence of undesired protein-micelle aggregation. Then, they were subjected to centrifugation (10,000 rpm × 20 min, room temperature) to remove any aggregates. The absorbance of the resultant supernatants was recorded at λ = 562 nm using a Powerwave HT Microplate Reader (Bio-Tek) in triplicates. Quantitative analysis was conducted to estimate the concentration of proteins remaining in supernatants using a bicinchoninic acid (BCA) assay (Pierce BCA Assay Kit), according to the protocol reported in our report,[50] based on the manufacturer's instructions.

2.2.2.5 Investigation of dual acidic pH/reduction-responsive degradation

For aqueous micelles of P1 (1 mg/mL), their aliquot (1 mL) was mixed with 10 mM aqueous stock solution of GSH (3 mL) in PBS (pH = 7.4) for GSH response. Separately, their aliquots (1 mL) were mixed with aqueous acetate buffer solution at pH = 5.4 (3 mL) for acidic pH response, and aqueous acetate buffer solution containing GSH (10 mM) at pH = 5.4 (3 mL) for dual acidic pH/GSH responses. DLS was used to follow any changes in sizes and size distributions of the micelles.

2.2.2.6 Preparation of aqueous Dox-loaded micellar dispersions (Dox-NPs)

An organic solution consisting of Dox (2 mg), Et_3N (5 μL), and P1 (20 mg) dissolved in DMF (1.6 mL) was mixed with PBS at pH = 7.4 (10 mL) under magnetic stirring. The resulting mixture was placed in a dialysis tubing (MWCO = 12000 g/mol) for dialysis over PBS (1 L) for 24 hrs.

The formed dispersion was passed through 0.45 μm PES filter, yielding aqueous Dox-loaded micellar dispersion at 1.6 mg/mL.

To determine the loading level of Dox using UV/vis spectroscopy, an aliquot of aqueous Dox-loaded micellar dispersion (1 mL) was mixed with DMF (5 mL) to form a clear solution. After being passed through 0.25 μm PTFE filter, its UV/vis spectrum was recorded. The loading level was determined by the weight ratio of loaded Dox to P1.

2.2.2.7 Dual acidic pH/reduction-responsive Dox release from aqueous Dox-loaded micelles

Aliquots of Dox-loaded micellar dispersion (1.6 mg/mL, 2 mL) were transferred into dialysis tubing (MWCO = 12,000 g/mol) and immersed in outer buffer solutions (40 mL) prepared under various conditions: aqueous PBS at pH = 7.4 and aqueous acetate buffer solution at pH = 5.3 with and without 10 mM GSH. Aliquots of the outer buffer solutions (3.5 mL) were taken and their fluorescence spectra were recorded at λ_{ex} = 470 nm. The equal volume of fresh buffer was added to keep the same volume of outer buffer.

For quantitative analysis, aqueous Dox solutions (10 mL) were prepared as Dox (46 μg) being dissolved in PBS at pH = 7.4, Dox (50 μg) in acetate buffer solution at pH = 5.3, and Dox (47 μg) in aqueous PBS at pH = 7.4 with 10 mM GSH. The resultant solutions were diluted to prepare a series of solutions at various concentrations of Dox. Their fluorescence spectra were recorded at λ_{ex} = 470 nm to construct the calibration curves.

2.2.2.8 Cell viability using MTT assay

HeLa cervical cancer cells were cultured in DMEM (Dulbecco's modified Eagle's medium) containing 10% fetal bovine serum (FBS) and 1% antibiotics (50 units/mL penicillin and 50 units/mL streptomycin) at 37 °C in a humidified atmosphere containing 5% CO_2. HeLa cells were plated at 5 x 10^5 cells per well into a 96-well plate and incubated for 24 h in DMEM (100 μL) containing 10 % FBS and 1 % antibiotics. Then, they were incubated with various concentrations of empty (Dox-free), free Dox, and Dox-NPs for 48 hrs. Blank controls without nanoparticles (cells only) were run simultaneously as control. Cell viability was measured using the CellTiter 96 Non-Radioactive Cell Proliferation Assay kit (MTT, Promega) according to the manufacturer's protocol. Briefly, 3-(4,5-dimethylthiazol-2-yl)-2,5-diphenyltetrazolium bromide (MTT) solution (15 μL) was added to each well. After 4 hrs of incubation, the medium containing unreacted MTT

was carefully removed. DMSO (100 μL) was added to each well to dissolve the formed formazan purple crystals, and then the absorbance at λ = 570 nm was recorded using a Powerwave HT Microplate Reader (Bio-Tek). Cell viability was calculated as the percent ratio of absorbance of mixtures with micelles to control (cells only without NPs).

In another set, HeLa cells were incubated with Dox-NPs in DMEM without (control pH = 7.4) and containing 10 mM GSH and 15 mM HEPES buffer (pH = 6.8). Blank samples without nanoparticles were run simultaneously as controls. After 48 hr incubation at 37°C, treated cells and controls were treated with DMEM containing MTT dye at a final concentration of 10%. After further incubation at 37 °C for 4 hrs, the media was carefully removed and the standard procedure was followed.

2.2.3 Results and discussion

2.2.3.1 Aqueous micellization and colloidal stability

My project started with investigating the self-assembly behavior of the polymer previously synthesized in our lab. Due to its amphiphilic nature, P1 polymer self-assembles in aqueous solution to form micellar aggregates at concentrations above CMC. Its CMC was found by Arman Moeini Jazeni (PhD candidate) to be 8.2 μg/mL. To confirm the self-assembly behavior, nanoprecipitation method followed by dialysis was examined with THF as the organic solvent to form aqueous micellar aggregates at 1 mg/mL. DLS analysis indicates the average hydrodynamic diameter is 84.5 nm, along with the negligible presence of large aggregates (<1%) (Figure 2.3).

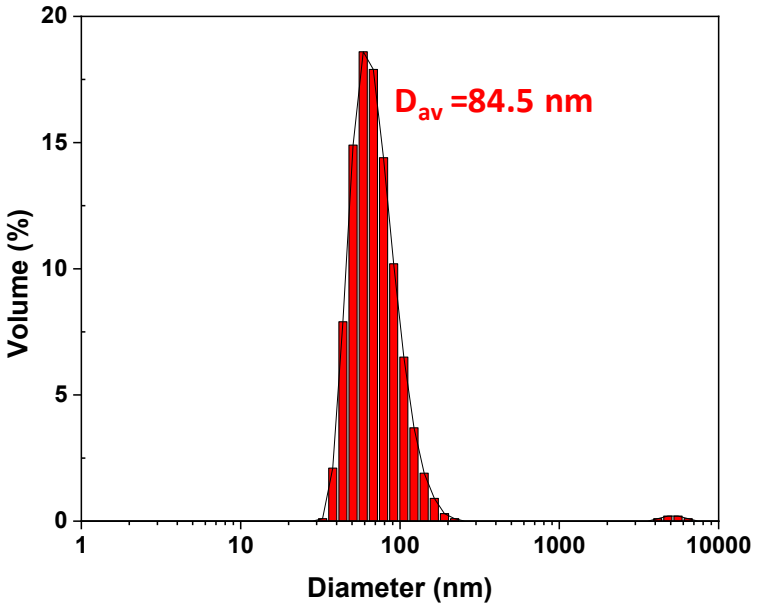

Figure 2.3 DLS diagram of P1 empty micelles in water.

Next, the formed micellar aggregates were examined for colloidal stability in physiological conditions. Serum (plasma) proteins are known to form highly undesired ″protein corona″ on nanoparticles in the blood, which results in their rapid elimination from blood circulation.[51, 52] Albumin (35−50 g/L) and IgG (7−16 g/L) are typical serum proteins found in the blood. Here, to examine the stability of P1-based nanoassemblies against serum proteins, aliquots of empty micelles were incubated with BSA (40 mg/mL) and human IgG (8 mg/mL) in PBS (pH = 7.4) at 37 °C for 48 hrs. DLS analysis shows the distinct size distributions of individual proteins and micelles, suggesting no occurrence of significant aggregation (Figure 2.5). Further, ≈100% of both proteins (BSA and IgG) remained in the supernatants of the mixtures after centrifugation, confirmed by quantitative analysis using BCA assay (Figure 2.4). These results suggest that the P1 micelles do not significantly interact with serum proteins. This could be attributed to the presence of hydrophilic PEG coronas, offering excellent stealth effect and thus excellent colloidal stability in the presence of serum proteins.

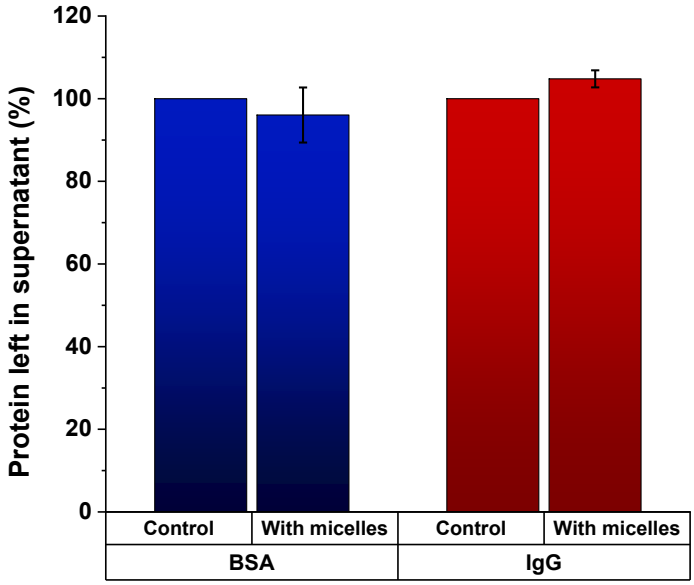

Figure 2.4 Percentage of free BSA and IgG in supernatants of mixtures of P1-micelles with physiological concentration of BSA and IgG after 48 h of incubation determined by BCA assay.

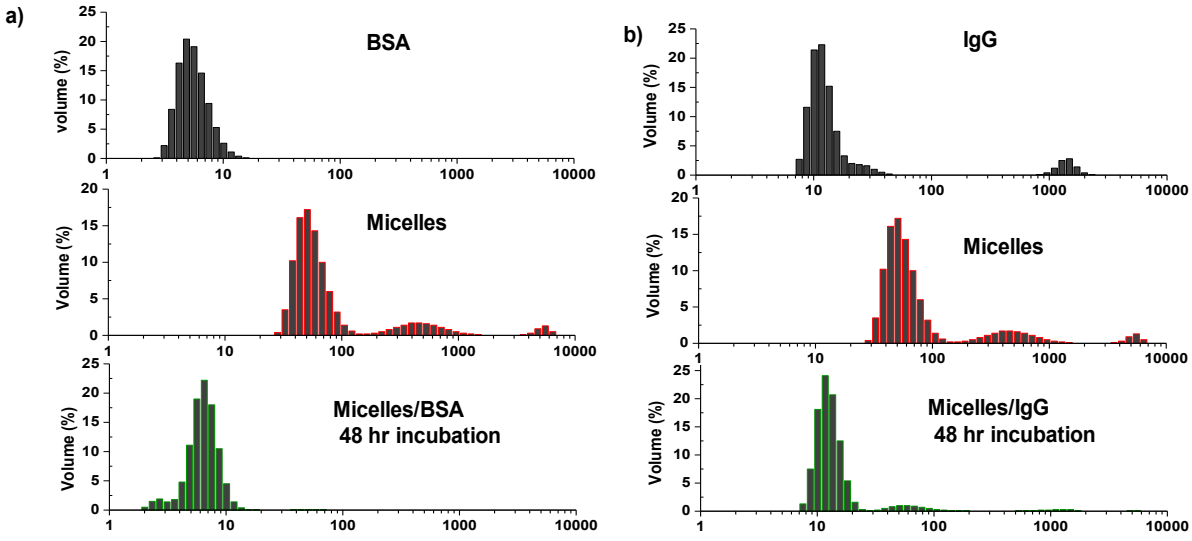

Figure 2.5 DLS diagrams to show colloidal stability of P1-micelles in the presence of serum proteins.

2.2.3.2 Investigation of dual acidic pH/reduction-responsive degradation of micelles

The next part was to study the degradation in response to stimuli in aqueous micelles (a heterogeneous system). Figure 2.6a shows the schematic illustration of micelle degradation as a consequence of the cleavage of the ketal linkages at core/corona interfaces and the cleavage of disulfide pendants in micellar cores. Figure 2.6b shows a typical DLS diagrams of micelles incubated at acidic pH = 5.4 as well as physiological pH = 7.4 with and without 10 mM GSH for 6 hrs. Note that pH = 7.4 without GSH was included as a control of no stimuli. Upon trigger with various stimuli, the change in the diameter of the micelles were monitored with Z-average diameter (by light scattering intensity) over incubation time (Figure 2.6c). When the micelles were exposed to acidic pH = 5.4, the size distribution became multimodal with the occurrence of large aggregation. Such change in size distribution at pH = 5.4 could be indicated by abrupt increase in their Z-average diameter within 12 hrs. In the presence of 10 mM GSH, the size distribution became bimodal with the appearance of a significant population of large aggregates. This is attributed to the destabilization of the micelles through polarity change of PHMssEt chains to the more hydrophilic PHMSH chains in micelle cores upon the cleavage of pendant disulfide groups, a mechanism known as solubility switch. As shown in Figure 2.6c, The Z-average diameter gradually increased over incubation time for 20 hrs, indicating destabilization of the micelles due to change in hydrophobic/hydrophilic balance upon the cleavage of pendant disulfides to corresponding hydrophilic thiols. When being incubated with 10 mM GSH at pH = 5.4 (with dual stimuli present simultaneously), the Z-average diameter increased more rapidly up to 8 hrs, compared with single stimulus; however, upon further incubation, it decreased gradually over incubation time. After 24 hrs, the DLS diagram shows a significant population of small species with diameter < 1 nm. This observation which was different from the response observed for single stimulus, is in fact very promising because it can suggest that the degraded products in dual stimuli could exist at molecular level as being soluble in aqueous environment.

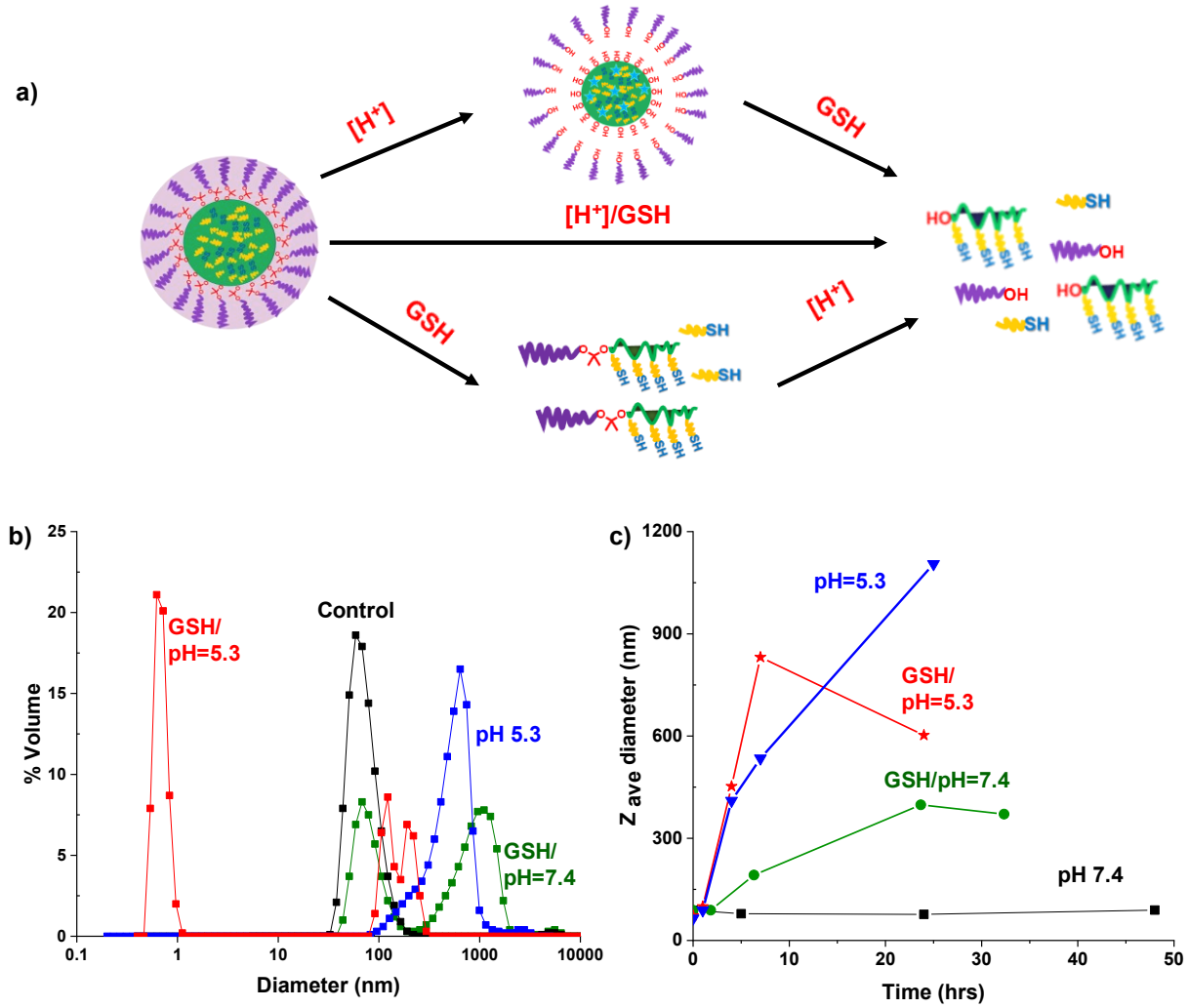

Figure 2.6 Schematic illustration of dual acidic pH/reduction-responsive degradation of P1-micelles (a); typical examples of DLS diagrams after 6 hrs (b) and evolution of z-average diameter of micelles over time (c) incubated at acidic pH= 5.4 and physiological pH = 7.4 with and without 10 mM GSH.

2.2.3.3 Preparation and characterization of Dox-loaded micelles

Doxorubicin was selected for this study as a clinically used anticancer drug. To encapsulate Dox in micelles, an organic solution of Dox treated with Et_3N in DMF was mixed with PBS (pH = 7.4) under stirring. The base treatment step of the Dox solution was important to neutralize the HCl present in commercially available Dox, to avoid cleavage of the acid-responsive ketal linkage during drug-loaded micelle preparation. The resulting mixture was subjected to intensive dialysis

over PBS to remove free (not encapsulated) Dox and Et_3N, yielding Dox-loaded micelles (Dox-NPs) at 1.6 mg/mL. After filtration to remove any formed aggregates, the UV/Vis spectrum of the dispersion was recorded (Figure 2.7). Using the pre-determined extinction coefficient of Dox (12,400 $M^{-1}cm^{-1}$) in DMF/water = 5/1 (v/v),[113] the loading level of Dox was determined to be 2.5 wt%.

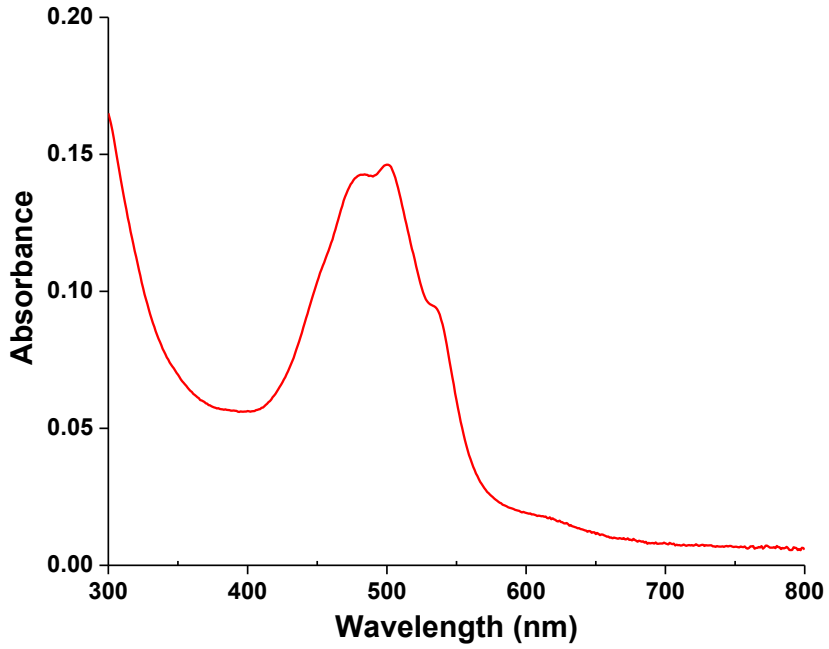

Figure 2.7 UV/Vis spectrum of a mixture of aqueous P1 Dox-micelles (1 mL) with DMF (5 mL).

Next, the size and morphology of Dox-NPs were characterized using DLS and TEM techniques. The average diameter was determined to be 116.4 ± 4.0 nm for the micelles in dispersed form by DLS (Figure 2.8a). TEM analysis indicates spherical micelles with diameter = 79 ± 30 nm in dried state (Figure 2.8b and c). Note that the size by TEM is smaller than that by DLS one, which is attributed to the dehydrated state of micelles on TEM grids, therefore showing only the hydrophobic cores.

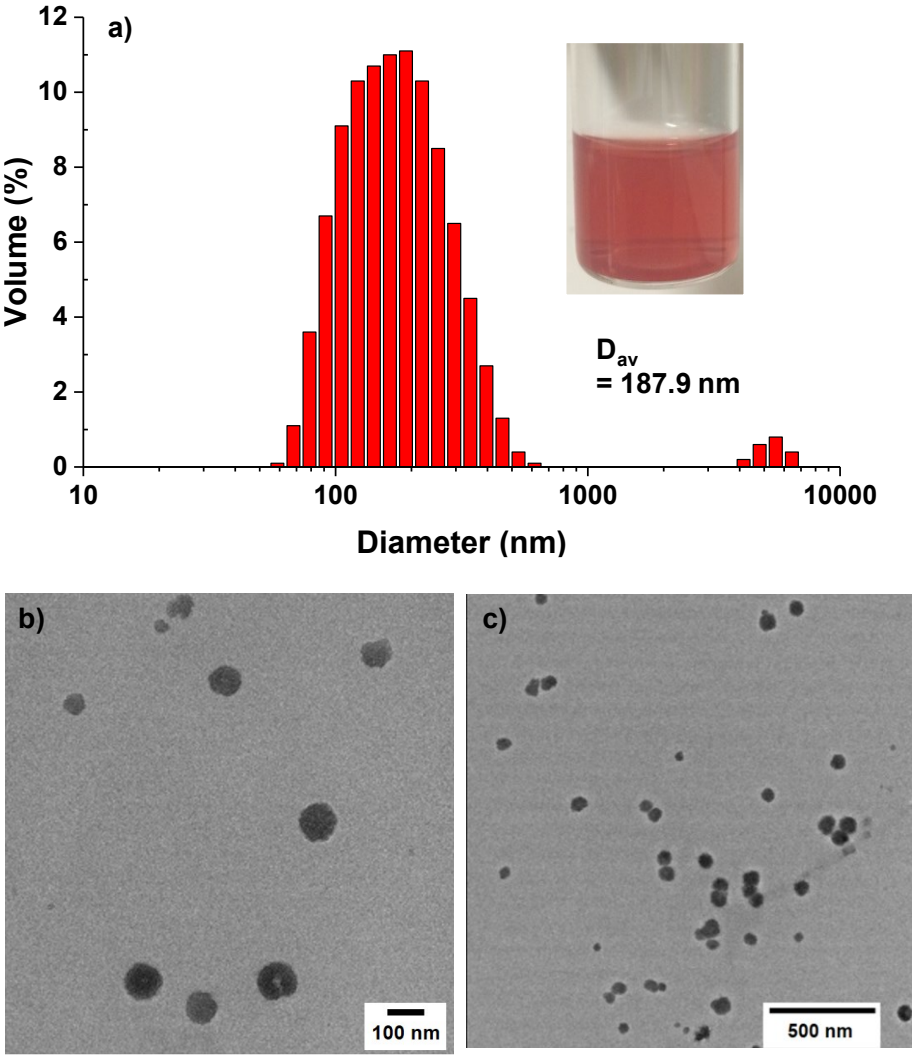

Figure 2.8 DLS diagram and digital image (inset) (a) and TEM images at high (b) and low (c) magnifications of P1 Dox-NPs. For TEM analysis, >80 micelles were selected randomly to manually calculate the average diameter.

2.2.3.4 In vitro stimuli-responsive release of encapsulated Dox

In-vitro release of Dox from Dox-NPs was examined by following the fluorescence intensity of Dox using fluorescence spectroscopy. For this study, aliquots of Dox-NPs were placed in a dialysis tubing (MWCO = 12 kDa) and submerged in outer buffer solutions under different conditions. Upon stimuli-responsive degradation of the micelles, Dox could be released from micelles and diffused out of dialysis bag into outer buffer. Aliquots (3 mL) of outer buffer were removed at given times to record their fluorescence spectra upon excitation at λ_{ex} = 470 nm. An

important underlying assumption in *in-vitro* release assay is that the rate of drug release is not limited by the solubility of the drug in the medium. Therefore, it is necessary to ensure that sink conditions are met during the study.[114] To keep a sink condition, the same volume of fresh outer buffer was added to keep the total volume of outer buffer solution constant and to prevent saturation solution of the drug. The fluorescence intensity at λ_{max}= 593 nm was used to determine the cumulative %Dox release. For the quantitative analysis, the correlation curves of fluorescence intensity at λ_{max}= 593 nm over various concentration of free Dox was constructed at pH = 7.4 and 5.4 with and without 10 mM GSH. Their slopes estimated from linear progression were similar (Figure 2.9a), suggesting that Dox fluorescence could not be affected under these conditions. Furthermore, %Dox release at pH = 7.4 (control with no stimuli) was examined in triplicate as an example to show the validity of our %Dox release data (Figure 2.9b).

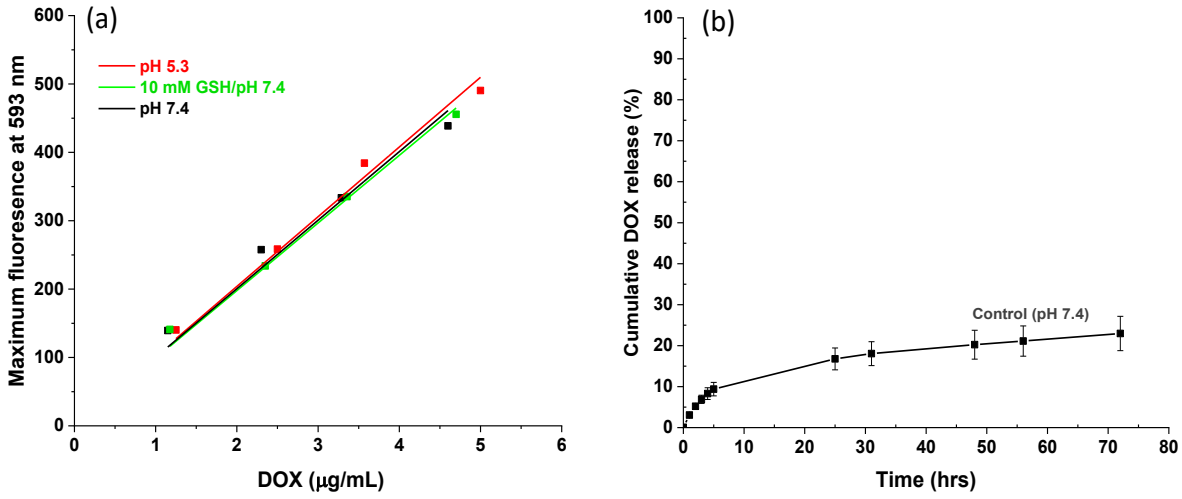

Figure 2.9 Calibration curves constructed with maximum fluorescence intensity at 593 nm over Dox concentration in buffer solutions at pH = 5.4 and pH = 7.4 with and without 10 mL GSH (a); %Dox release from Dox-NPs in triplicate being incubated at pH 7.4 (control with no stimuli) (b).

Figure 2.10 shows the %Dox release over incubation time in the presence of dual pH = 5.4/10 mM GSH, compared with single stimuli (pH = 5.4 or 10 mM GSH) as well as a control (pH = 7.4). In the absence of stimuli (i.e. pH = 7.4), the release of Dox was slow as %Dox release reached a plateau to be ≈ 25% after 24 hrs. In the presence of single stimulus (i.e. acidic pH = 5.4 and 10 mL GSH), the Dox release was enhanced. For example, %Dox release reached ≈ 50% when Dox-NPs were incubated at pH = 5.4. Such enhanced Dox release could be attributed to acid-responsive

degradation upon the cleavage of block junction ketal linkages. Interestingly, %Dox release also reached ≈ 50% in the presence of 10 mM GSH as a consequence of the cleavage of disulfide pendants. Promising Dox-release was found when Dox-NPs were incubated with 10 mM GSH at pH = 5.4 buffer solution, in the presence of both stimuli simultaneously. Dox release was synergistically accelerated under this condition, as %Dox release reached >85%. Such excellent Dox release could be attributed to the degradation of Dox-NPs upon the cleavage of both ketal junction and disulfide pendants located in both interfaces and cores. These results show the faster release kinetics with GSH in acidic pH, compared with not only single stimuli but also neutral pH, suggesting the clear benefits for dual location dual acid/reduction degradation systems exhibiting accelerated and synergistic release kinetics.

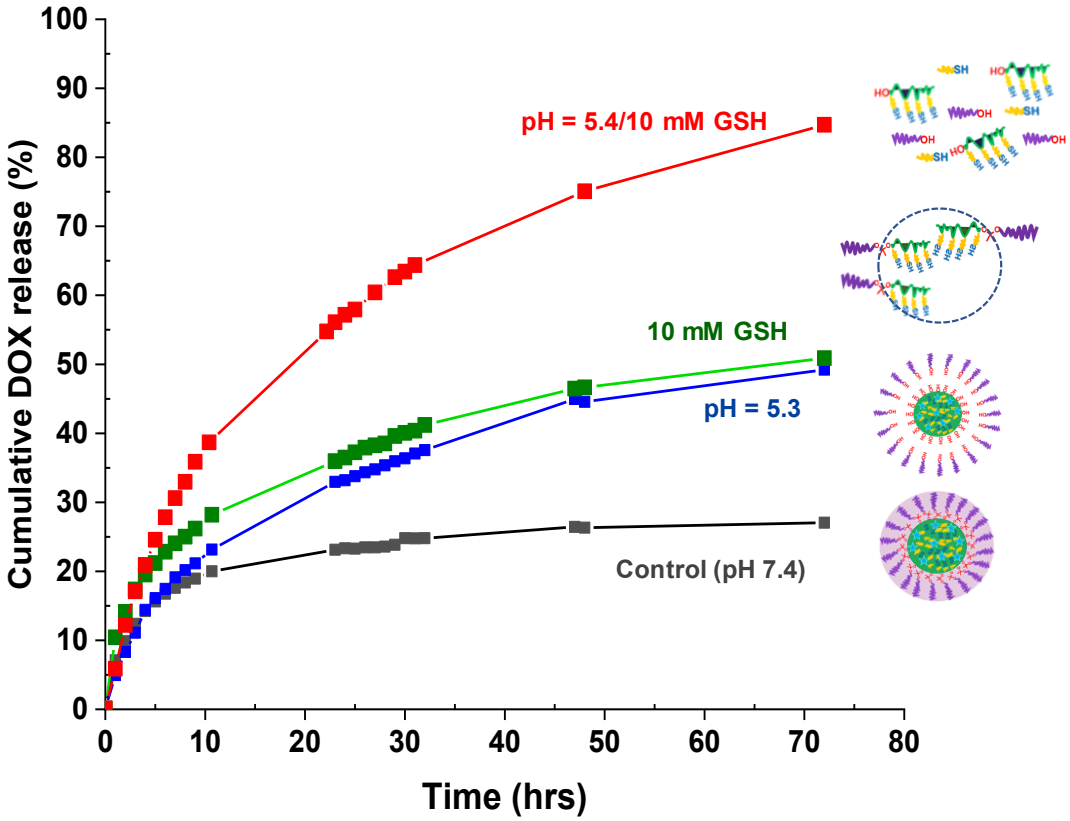

Figure 2.10 Cumulative %Dox release from P1 Dox-NPs being incubated at pH = 5.3 and 7.4 with and without 10 mM GSH.

2.2.3.5 Anticancer activity and intracellular trafficking of Dox-NPs

To ensure the biocompatibility of these micelles, the cytotoxicity of P1 micelles was evaluated by Sung Hwa Hong (MSc) in our lab on HeLa cervical cancer cells using an MTT colorimetric assay. As seen in Figure 2.11a, the viability of HeLa cells was >80% in the presence of empty micelles up to 300 µg/mL, suggesting non-toxicity of empty micelles to HeLa cells. When being incubated with Dox-NPs, their viability decreased. For example, it decreased to 70% with the presence of Dox-NPs equivalent to 1 µg/mL of Dox and further to 50% with 2.6 µg/mL of Dox (Figure 2.11b). Given that empty micelles were biocompatible, this result suggests that the inhibition of HeLa cell proliferation is presumably due to the release of Dox from Dox-NPs. However, the viability of HeLa cells was lower for free Dox at similar concentrations, compared with Dox-NPs. IC_{50} value was determined to be 0.64 µg/mL for free Dox vs 2.86 µg/mL for Dox-NPs. Such difference in cell viability could be possibly due to the time required for cleavage of ketal and disulfide linkages to release Dox from Dox-NPs whereas free Dox intercalate with DNA followed by internalization. In another set to see the significance of dual acid/reduction response to cell toxicity, we then designed an experiment where HeLa cells were incubated with Dox-NPs (i.e. Dox) in the presence of 10 mM GSH as GSH-OEt at pH = 6.8 for 48 hrs. This experiment was carried out by Chaitra Shetty (MSc Candidate) in our lab. Figure 11c reveals the lower HeLa viability with dual stimuli, compared with pH = 7.4 (control with no stimuli). This preliminary result suggests the versatility of our dual location dual-responsive NP strategy toward effective drug delivery.

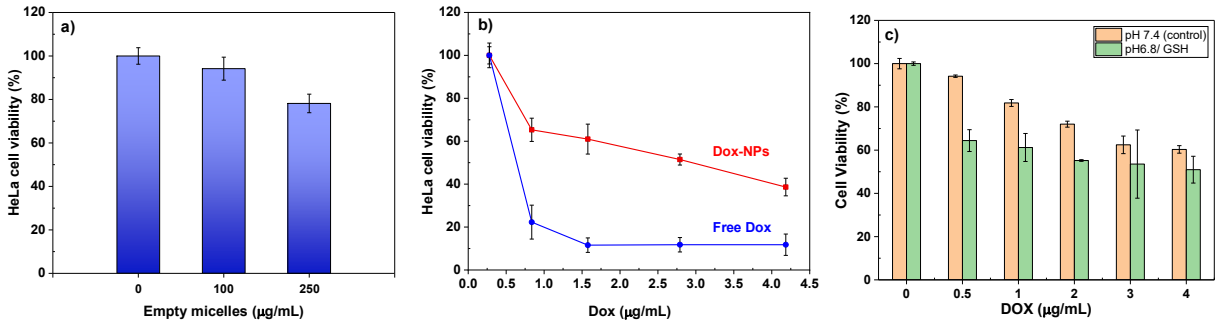

Figure 2.11 Viability of HeLa cells incubated with empty P1 micelles(a); P1 Dox-NPs and free Dox at physiological pH = 7.4 (b) and P1 Dox-NPs at pH = 6.8 with 10 mM GSH and at pH = 7.4 (no stimuli) (c).

2.3 Part II: P2 triblock copolymer

2.3.1 P2 Polymer design

The polymer was synthesized through a combination of two controlled radical polymerization techniques, namely the atom transfers radical polymerization (ATRP) and reversible addition-fragmentation chain transfer (RAFT) polymerization using OEOMA as hydrophilic monomer and HMssEt as hydrophobic monomer. ^{1}H-NMR analysis showed the DP was 21 for POEOMA and 26 for HMssEt block. The copolymer had the Mn = 16.0 kg/mol, determined by GPC.

The P2 ABA-triblock copolymer consists of poly(oligo(ethylene oxide) methacrylate) (POEOMA) having pendant OEO groups as the B block and two polymethacrylate blocks having multiple disulfide pendants (PHMssEt) as the A blocks. Both acid-labile acetal and reduction-responsive disulfide linkages are positioned in only one block junction, thus attaining asymmetric block junctions, which according to our anticipation can demonstrate unique aqueous micellization, compared with conventional triblock copolymers.

2.3.2 Experimental section

2.3.2.1 Materials

Nile red (NR), glutathione (GSH), doxorubicin (Dox, $-NH_3^+Cl^-$ forms, >98%), and 1,4-dithreithiol (DTT) were purchased from Sigma Aldrich and used as received.

2.3.2.2 Determination of critical micellar concentration (CMC) using a NR probe

A stock solution of NR in THF at 1 mg/mL and stock solutions of P2 in THF at 1 mg/mL. Water (10 mL) was then added dropwise into mixtures consisting of the same amount of the stock solution of NR (0.5 mL, 0.5 mg NR) and various amounts of the stock solution of P2. The resulting dispersions were stirred for 40 hrs to remove THF, and then were subjected to filtration using 0.45 μm PES filter to remove excess NR. A series of NR-loaded micelles at various concentrations of P2 ranging from 10^{-5} to 0.1 mg/mL were formed. From their fluorescence spectra recorded with λ_{ex}= 480 nm, the fluorescence intensity at maximum λ_{em} = 620 nm was recorded.

2.3.2.3 Aqueous micellization by dialysis method

PBS buffer (pH = 7.4, 10 mL) was added dropwise to an organic solution of P2 dissolved in THF (2 mL) using a syringe pump equipped with a plastic syringe (20 mL volume, 20 mm

diameter) at an addition rate of 0.2 mL/min. The resulting dispersion was dialyzed against PBS (1 L) twice for 24 h, yielding aqueous micellar dispersion at 0.9 mg/mL concentration.

2.3.2.4 Acidic pH-responsive degradation

A solution of polymer (10 mg) dissolved in DMF (3 mL) was mixed with HCl (20 μL, 0.24 mmol) for 72 hrs. The degraded mixture was characterized using GPC to follow any changes in molecular weight and its distribution. For ^{1}H-NMR analysis, a solution of polymer (10 mg) dissolved in $CDCl_3$ (1 mL) was mixed with DCl for 24 hrs.

2.3.2.5 Reduction-responsive degradation

A solution of polymer (10 mg) dissolved in DMF (2.5 mL) was mixed with DTT (5 mole equivalents to disulfide linkages in the polymer) for 72 hrs. The degraded mixture was characterized using GPC to follow any change in molecular weight and its distribution.

2.3.2.6 Dual acidic pH/reduction-responsive degradation of aqueous micellar aggregates

For GSH-induced response, an aliquot of aqueous micelles (1 mg/mL, 0.2 mL) was mixed with 10 mM aqueous stock solution GSH (2 mL) in PBS (pH = 7.4). Aliquots of aqueous micelles (1 mg/mL, 1 mL) were mixed with aqueous acetate buffer solution at pH = 5.4 (3 mL) for acidic pH response and mixed with 10 mM aqueous acetate buffer solution of 10 mM GSH at pH = 5.4 (3 mL) for dual acidic pH/GSH responses. DLS was used to follow any changes in sizes and size distributions of the micelles.

2.3.2.7 Preparation of aqueous Dox-loaded micellar dispersions (Dox-NPs)

An organic solution consisting of Dox (2 mg), Et_3N (5 μL), and P2 (20 mg) dissolved in DMF (1.6 mL) was mixed with PBS at pH = 7.4 (10 mL) under magnetic stirring. The resulting mixture was placed in a dialysis tubing (MWCO = 12000 g/mol) for dialysis over PBS (1 L) for 24 hrs. The formed dispersion was passed through 0.45 μm PES filter, yielding aqueous Dox-loaded micellar dispersion at 0.8 mg/mL.

To determine the loading level of Dox using UV/vis spectroscopy, an aliquot of aqueous Dox-loaded micellar dispersion (1 mL) was mixed with DMF (5 mL) to form a clear solution. After being passed through 0.25 μm PTFE filter, its UV/vis spectrum was recorded. The loading level was determined by the weight ratio of loaded Dox to P2.

2.3.2.8 Dual acidic pH/reduction-responsive Dox release from aqueous Dox-loaded micelles

Aliquots of Dox-loaded micellar dispersion (0.8 mg/mL, 2 mL) were transferred into dialysis tubing (MWCO = 12,000 g/mol) and immersed in outer buffer solutions (40 mL) prepared under various conditions: aqueous PBS at pH = 7.4 and aqueous acetate buffer solution at pH = 5.3 with and without 10 mM GSH. Aliquots of the outer buffer solutions (3.5 mL) were taken and their fluorescence spectra were recorded at λ_{ex} = 470 nm. The equal volume of fresh buffer was added to keep the same volume of outer buffer.

2.3.3 Results and discussion

2.3.3.1 Stimuli-responsive degradation of P2 polymer

After the synthesis of P2 copolymer by Arman, I then studied the acid/reduction-responsive degradation of the polymer and as well as structural investigation. This block copolymer bears acid-labile acetal linkage at the junction between the hydrophobic and the hydrophilic block, as well as reduction-cleavable disulfide bonds placed at the junction and as pendant groups in the hydrophobic block. To get an insight into its degradation, the P2 polymer dissolved in DMF was incubated with hydrogen chloride (an acid) and 1,4-dithiothreitol (DTT, a reducing agent) and GPC and ^{1}H-NMR analysis were used to follow any changes in molecular weight and its distributions upon the cleavage of acetal and disulfide linkages at the block junction and hydrophobic pendants. The degradation products upon stimuli-responsive cleavage of the labile bond are shown in Figure 2.12.

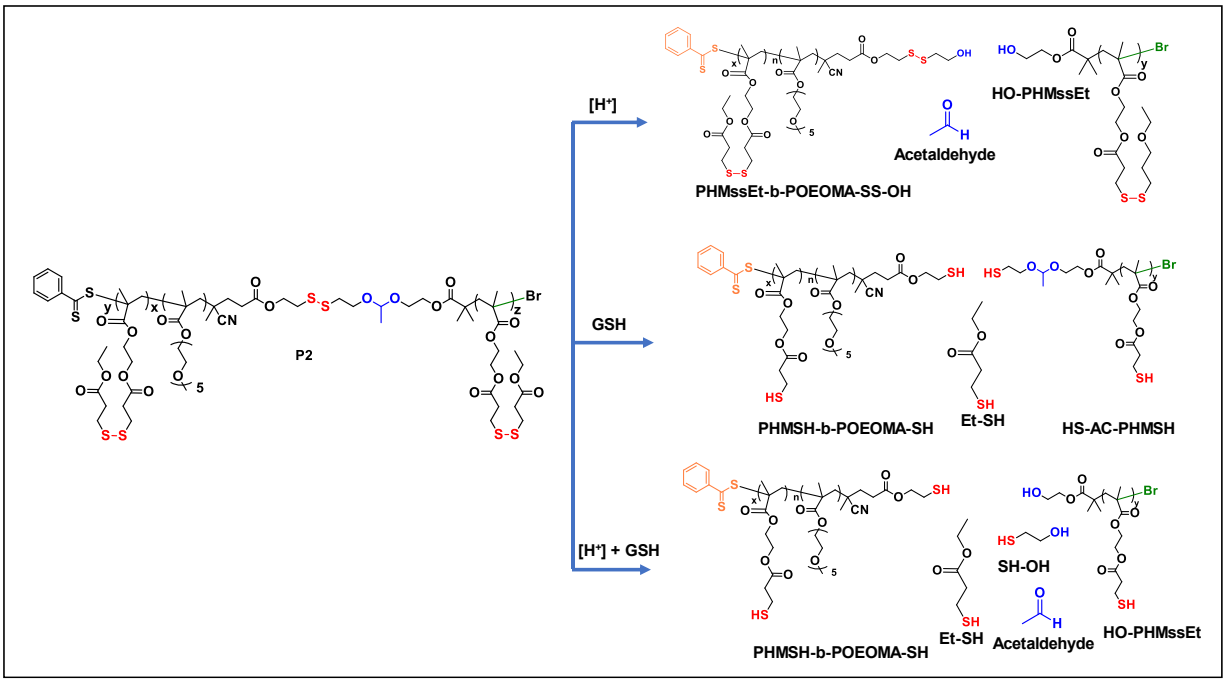

Figure 2.12 Stimuli-responsive degradation of P2 polymer and the structure of degradation products, courtesy of Arman Moini Jazeni.

In acidic pH, the junction acetal linkage was cleaved to generate PHMssEt-b-POEOMA-SS-OH and HO-PHMssEt as degraded products. As a consequence, the GPC trace was shifted to lower molecular weight region and their M_n = 13.1 kg/mol decreased from that (M_n =17.6 kg/mol) of P2 (Figure 2.13). It was observed that the GPC trace of degraded products did not overlap with the $\mathbf{P_o}$ POEOMA precursor. When being incubated with DTT, the disulfide linkages at the block junction and hydrophobic PHMssEt blocks were cleaved to generate PHMSH-b-POEOMA-SH and HS-AC-PHMSH as degraded products. Their GPC trace did not overlap with the POEOMA precursor. Their M_n also decreased to 10.4 kg/mol, which is smaller than that of acid-responsive degraded products. Such decrease is attributed to the cleavage of pendant disulfide groups in the response to DTT. The results from GPC analysis was able to successfully confirm the dual acid/reduction-responsive degradation of P2, while also providing evidence for the asymmetric structure of the triblock copolymer PHMssEt-AC-SS-POEOMA-b-PHMssEt having acetal and disulfide linkages at one block junction.

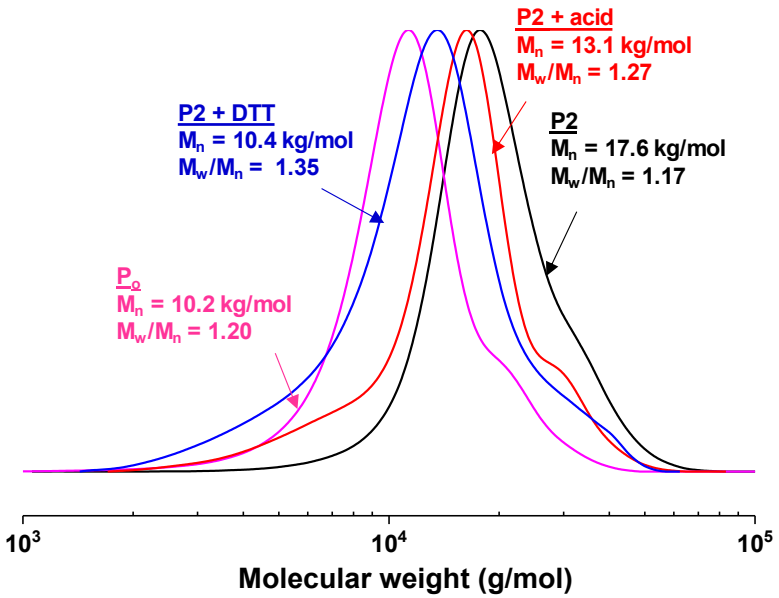

Figure 2.13 GPC traces of P2 before and after treatment with each stimulus in DMF, compared with that of P_o macro-RAFT agent precursor.

The acid-responsive cleavage of the acetal linkage was also confirmed through NMR spectroscopy. After the incubation of the P2 polymer with HCl, an aldehyde peak at 9.75 ppm was seen in the ^{1}H-NMR spectrum, which provided further evidence for the acid-responsive nature of the polymer (Figure 2.14)

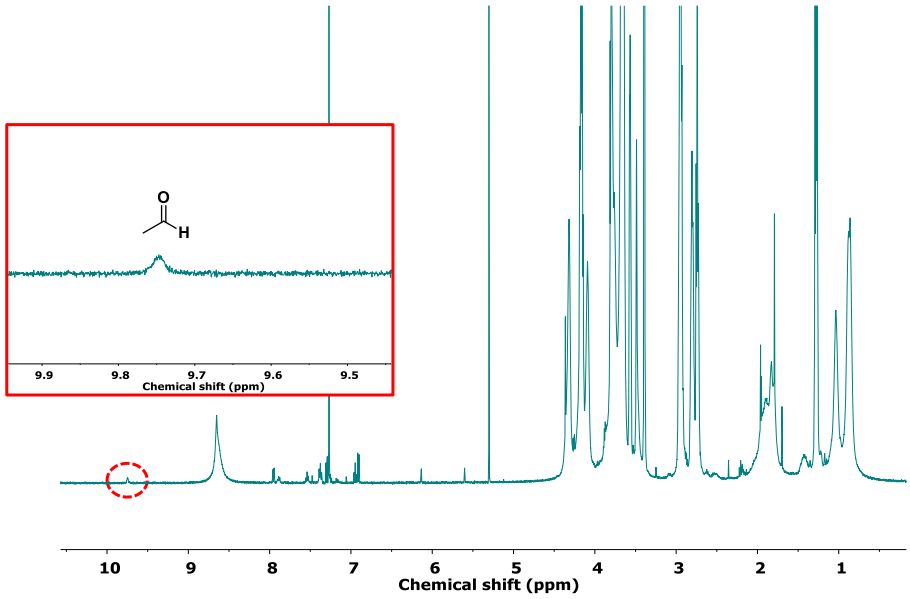

Figure 2.14 ^{1}H-NMR spectrum of P2 after treatment with HCl.

2.3.3.2 CMC determination by fluorescence spectroscopy

The CMC of P2 was determined using fluorescence spectroscopy with NR as a probe. This method utilizes the low fluorescence of NR in aqueous environment because of its low solubility in water. However, the NR fluorescence becomes intense when NR is surrounded by hydrophobic environment. Figure 2.15 (inset) shows the overlaid fluorescence spectra of NR over an increasing concentration of P2. At its lower concentration, the NR fluorescence intensity was low because of the existence of most NR molecules in aqueous solution. Upon increasing concentration of P2, the intensity increased, indicating the encapsulation of NR in micellar cores. As shown in Figure 2.15, two linear progressions of maximum fluorescence intensity allow for the determination of CMC to be 15.9 µg/mL, suggesting P2 is an amphiphilic polymer.

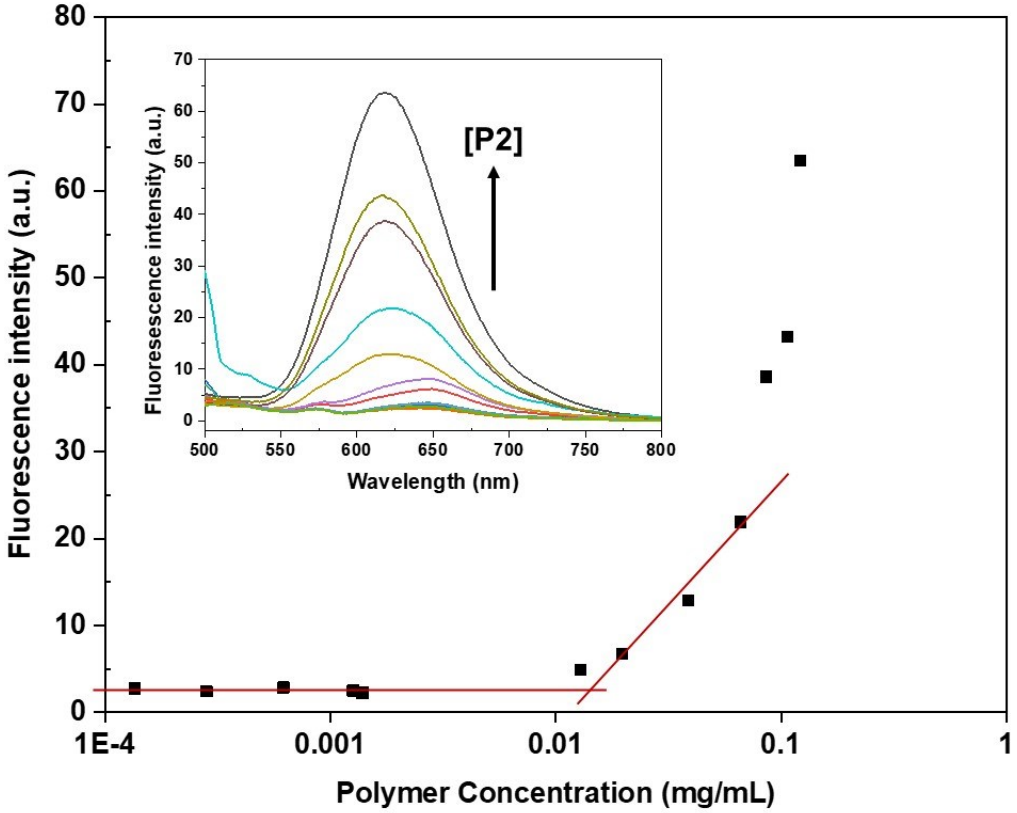

Figure 2.15 Overlaid fluorescence spectra (inset) and fluorescence intensity at maximum wavelength for aqueous mixtures consisting of NR with various amounts of P2 to determine CMC.

2.3.3.3 Aqueous micellization

Aqueous micellization through self-assembly of P2 at concentration above its CMC was investigated through a nanoprecipitation method with THF, followed by dialysis against PBS buffer. The formed micelles had hydrodynamic diameters of 61 ± 2.4 nm by DLS (Figure 2.16a). Their TEM image shows the micelles are spheres in the dehydrated state, with their average diameter of 27 ± 4.6 nm (Figure 2.16b).

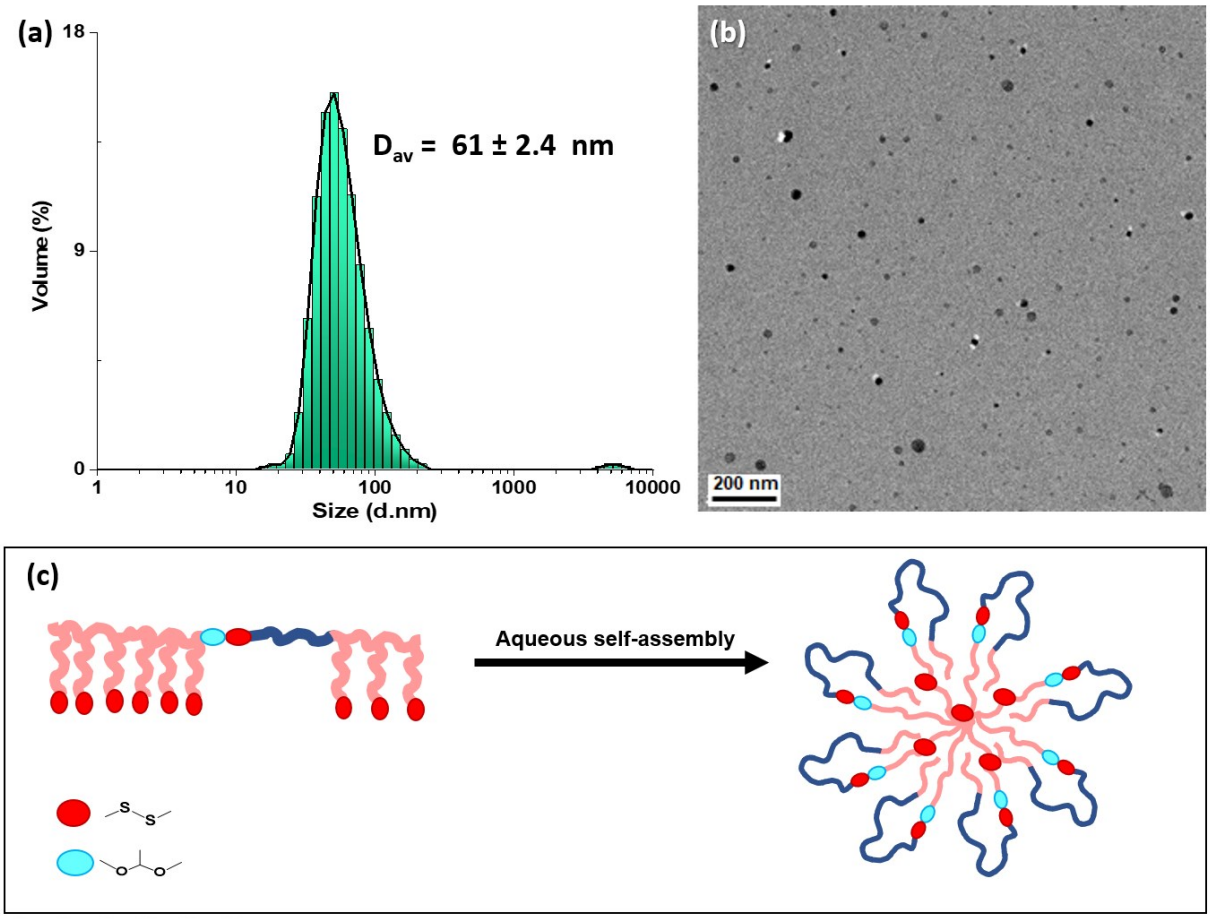

Figure 2.16 DLS diagram(a); TEM image of P2 empty micelles in water(b); schematic diagram showing the self-assembly of P2 into flower-like micelles, showing the location of stimuli-responsive linkage within the micelles(c).

2.3.3.4 Dual acidic pH/reduction-responsive degradation of the micelles

Aliquots of micelles were incubated with various buffer solutions under different conditions of stimuli and their degradation was followed with DLS technique (Figure 2.17 and 2.18). At pH = 7.4 (control), the size distribution of micelles kept unchanged within 24 hrs, suggesting great colloidal stability in physiological conditions. When being incubated in buffer solutions with single or dual stimuli, their size distribution became bimodal and eventually turned to be aggregates within 24 hrs. These changes in size distributions could be the consequence of destabilization or disintegration of micelles upon the cleavage of acetal and disulfide linkages in response to acidic pH and glutathione.

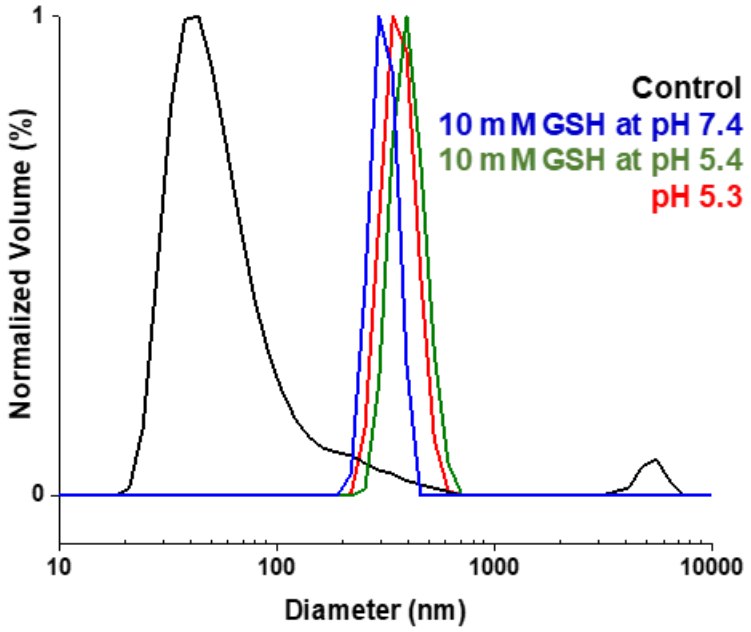

Figure 2.17 Summary of DLS diagrams of P2 micelles in the presence of various buffer solutions, after 24 hrs.

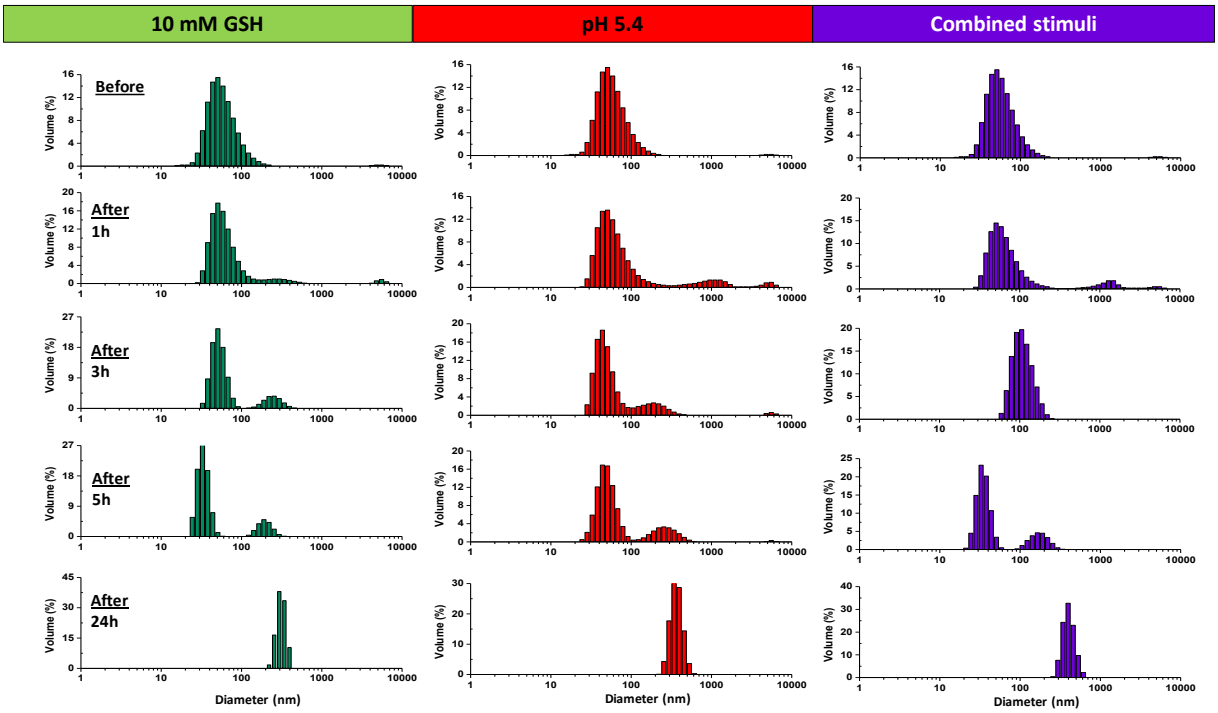

Figure 2.18 DLS diagrams of P2 micelles showing the progression of the stimuli-responsive degradation at various time points.

2.3.3.5 Preparation and characterization of Dox-loaded micelles

The similar procedure described in section **2.2.2.6** was used in an attempt to fabricate well-defined Dox-loaded nanoparticles in the desired range of 50-150 nm. After the dialysis of Dox-micelles over PBS to remove free Dox, the resulting dispersion of Dox-loaded NPs were cloudy with large aggregates present. DLS analysis showed a bimodal distribution with 70% of large particles (> 1 μm) (Figure 2.19a). Filtration through a PES filter (0.2 μm) enabled the removal of large aggregates confirmed by DLS. The resulting Dox-loaded NPs after filtration had hydrodynamic diameter D_{av} = 35 ± 6 nm (Figure 2.19b).

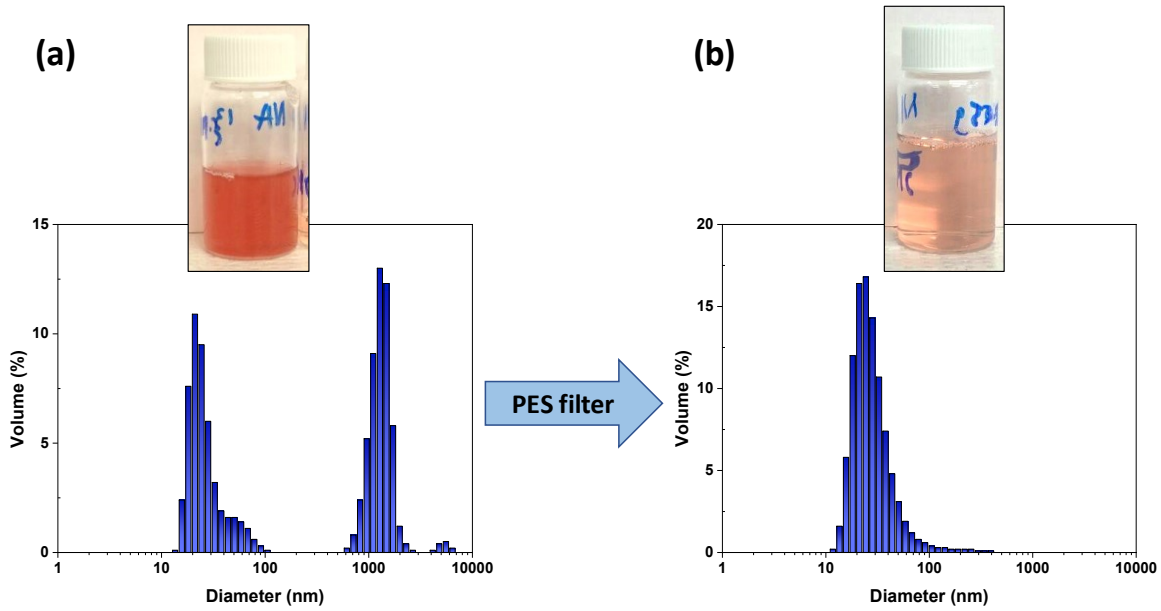

Figure 2.19 Digital image and DLS diagram of the P2 Dox-NPs before PES filtration with 0.2 μm pore size(a); digital image and DLS diagram of the P2 Dox-NPs after PES filtration (b).

For the filtered solution, the loading level of Dox was determined to be 0.94 wt% by UV/Vis spectroscopy with the pre-determined extinction coefficient of Dox (12,400 M^{-1} cm^{-1})[113] in DMF/water = 5/1 (v/v) (see Figure 2.20 for UV/VIS spectrum).

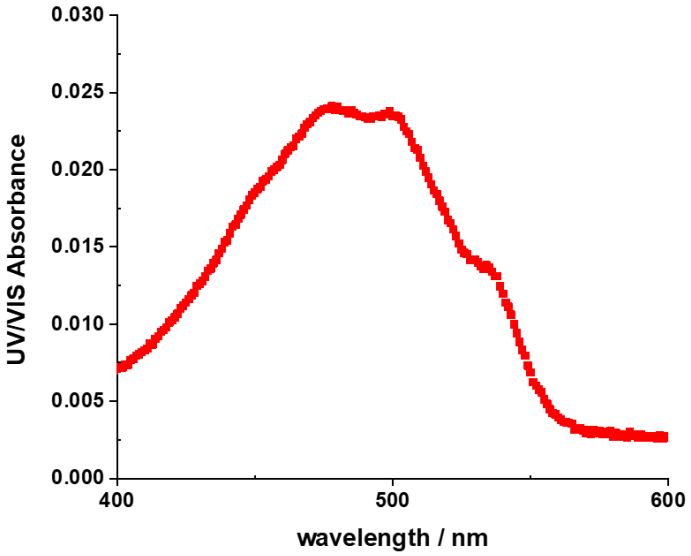

Figure 2.20 UV/Vis spectrum of a mixture of aqueous P2 Dox-micelles (1 mL) with DMF (5 mL).

2.3.3.6 In-vitro stimuli-responsive release of encapsulated Dox

In-vitro release of Dox was investigated using fluorescence spectroscopy. Here, Dox-NPs were placed in a dialysis tubing (MWCO = 12 kDa) and submerged in various buffer solutions. Upon stimuli-responsive degradation of the micelles, the encapsulated drug molecules released and diffused out of dialysis bag into an outer buffer kept at sink conditions. The fluorescence intensity at λ_{max}= 593 nm was used to determine the cumulative %Dox release. For the quantitative analysis, the slope of the concentration-fluorescence intensity correlation curve in Figure 2.9a was used.

As seen in Figure 2.21, drug release was abruptly increased within 10 hrs to reach 60% regardless of the presence or absence of any stimuli. This unexpected could be attributed to the incomplete encapsulation of Dox molecules in micellar cores. After 10 hrs, the drug release became faster in the presence of stimuli compared to our control (pH = 7.4, mimicking the normal physiological pH). As expected, it appeared to be faster in 10 mM GSH solution of pH = 5.4 (dual stimuli) than at pH = 5.4 (single stimulus).

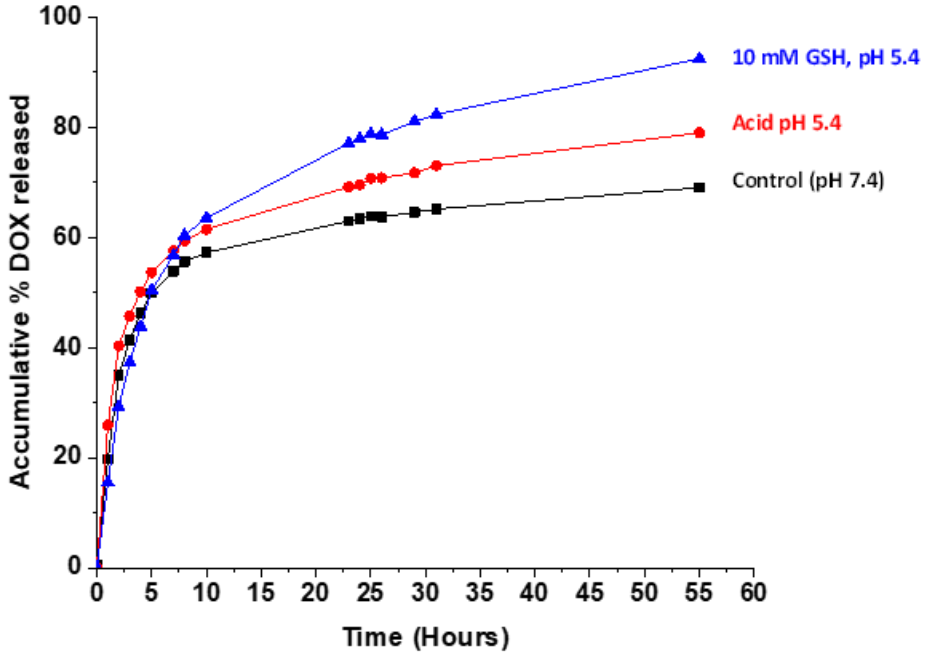

Figure 2.21 *In-vitro* Dox release profile of P2 Dox-NPs.

2.4 Conclusion

This chapter describes our investigation on the value for a new strategy called dual location dual stimuli-responsive degradation (DL-DSRD) by studying two types of acidic pH/glutathione-degradable amphiphilic polymers. **P1** is an amphiphilic diblock copolymer with acid-labile ketal linkage at the block junction and reduction-cleavable disulfide pendants in the hydrophobic block. **P2** is an amphiphilic ABA triblock copolymer with acid-labile acetal linkage and a disulfide linkage positioned at one of the block junctions, as well as disulfide pendants in two hydrophobic blocks. These two polymers were comprehensively characterized for tumor-targeting drug delivery application. Both successfully self-assembled into nano-sized micelles with spherical morphology.

Their core-shell structure allowed for the interaction and encapsulation of Dox, a hydrophobic anticancer drug. The formed Dox-loaded micelles responded to cellular glutathione, acidic pH, and their combination at different locations (micellar cores and core/corona interfaces). These results obtained from our comprehensive characterization suggests the versatility of DL-DSRD strategy and its benefits in terms of enhanced drug release in the presence of dual stimuli for advanced drug delivery and cancer therapy. Further, in order to get an insight into the structure-property relations of the two polymers, we point out their significant differences in drug loading and release profile.

The first significant difference between the **P1** and **P2** micelles was their drug loading capacity, which was 2.5% and 0.94% respectively. The higher loading capacity of the P1 is in part due to the larger size of the hydrophobic block, also known as the DP for the HMssEt which was 32 for P1 and 26 (distributed between two blocks) for P2. This suggests a larger core of the P1 micelles, potentially allowing for the encapsulation of more hydrophobic cargo. This finding is consistent with the factors that has been reported to affect drug encapsulation efficiency in polymeric micelles, including the nature of the hydrophobic core-forming block and the hydrophobic block length.[115] Another distinction between the two micellar systems lies in their fundamentally different self-assembly process. As discussed in Chapter 1, the process of self-assembly of the diblock copolymers and triblock copolymers are very different, with the assembly of triblock copolymers being more complicated. Figure 2.22 compares and contrasts P1 ″crew-cut″ micelles and P2 ″flower-like″ micelles. Based on my analysis reported in this chapter, although the

CMC for both the polymeric systems studied were relatively low compared to low molecular weight surfactants, but the value for CMC of the asymmetric triblock copolymer P2 (15.9 µg/mL) was almost double the CMC of diblock copolymer P1 (8.2 µg/mL). This interesting finding suggests that more of P2 polymer chains are needed to come together to form stable core-shell micellar assemblies, which is likely to be attributed to the smaller hydrophobic tails of P2 compared to one long hydrophobic tail of P1.

My results in this chapter suggest a lower drug loading capacity for flower-like micelles made from asymmetric triblock copolymers compared to diblock copolymers micelles. A plausible explanation could be due to the presence of aqueous pockets in the core of the P2 micelles caused by the asymmetric nature of the sizes of the two hydrophobic blocks creating more space for solvent penetration. This in turn will cause a lower hydrophobicity of the core, and therefore less favorable interactions with hydrophobic drugs leading to lower loading capacity. The lower hydrophobicity also suggests a weaker interaction between the drugs and the hydrophobic core, which can explain easy leakage of the drugs shown by the "burst-release" phenomenon of P2 micelles in the *in-vitro* release assay (see Figure 2.21)

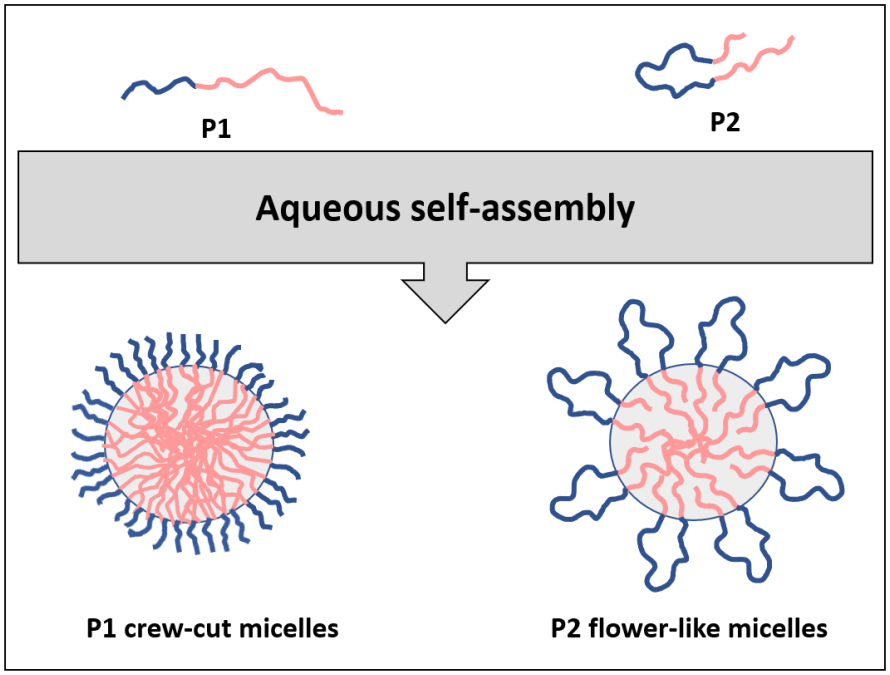

Figure 2.22 Schematic diagram of structure of P1 and P2 self-assembled micelles.

Chapter 3

Synthesis and block copolymerization of fully bio-reducible poly(carbonate-disulfide)s through carbonylimidazole-hydroxyl coupling chemistry

3.1 Introduction

In recent years the development of stimuli-responsive polymers which can degrade through a change in their chemical characteristics in response to environments has been extensively explored in material science, biotechnology, tissue engineering and biosensing.[116–118] Inspired by complex responses to dynamic environments occurred naturally in biological systems, smart polymers have proven as effective building blocks for constructing advanced delivery platforms for various biomedical and pharmaceutical applications exhibiting controlled drug/gene delivery. Reduction-responsive degradable polymers are of special interest because they can be degraded in tumor tissues as a consequence of high concentration of cellular glutathione (GSH) found in cancer cells, compared with that in extracellular environments and healthy normal cells. Disulfide bond is a typical labile linkage that undergoes the cleavage to the corresponding thiols triggered by endogenous GSH under physiological conditions. Further, polydisulfides have been reported to enhance cellular uptake.[119]

Numerous approaches have been explored to synthesize GSH-degradable polymers and block copolymers for anticancer drug delivery. However, a major challenge still remains, which is polymer backbones staying unaffected after disulfide cleavage.[120–122] This has risen a major concern on their biocompatibility and ultimately the fate of their degraded products in biological systems after drug release. In this context, there is an immediate need for design and synthesis of GSH-responsive polymers that are fully biodegraded. Polydisulfides with disulfide linkages positioned repeatedly on their backbone have been previously synthesized by mainly step-growth polymerization techniques through esterification,[58,60] Michael addition,[123] and thiol-disulfide exchange.[61,124]

This chapter describes a novel approach to synthesize robust reduction-responsive degradable poly(carbonate-disulfide)s (PCss) constructed with both carbonate and disulfide bonds repeatedly

on the backbones. Our approach explores a robust carbonylimidazole-hydroxyl (CI-OH) coupling chemistry for step-growth polymerization through polycondensation, which to our best knowledge, has never been reported for applications in polymer synthesis. A novel bifunctional ssDCI monomer was synthesized and reacted with various commercially available/synthesized diols to build a variety of functional PCss copolymers for biomedical applications. In the presence of a reducing agent, these responsive copolymers underwent a two-step degradation whereby the entire polymer chains were disintegrated into small degradation products. Using this novel approach, we developed and characterized a library of PCss polymers with various molecular weights and degradation properties. As a proof-of-concept demonstration, a dual acid and reduction-responsive PCss-based amphiphilic block copolymer was synthesized and self-assembled to form nanoassemblies for potential applications in controlled release drug delivery.

3.2 Experimental

3.2.1 Materials

2-Hydroxyethyl disulfide (ssDOH, 99%), 1′-carbonyldiimidazole (CDI, ≥90%), 1,1,1-tris(hydroxymethyl)ethane (THME, 99%), terephthalaldehyde (TPA, 99%), phosphate buffered saline (PBS) tablets, 1,12-dodecanediol (C12-DOH, 99%), polycaprolactone diol (PCL-DOH, M_n = 2000 g/mol), poly(ethylene glycol) (PEG-DOH, average M_n = 1305-1595 g/mol), triethylamine (Et_3N, >99%), 1,8-diazabicyclo[5.4.0]undec-7-ene (DBU, 98%), 1,4-dithreithiol (DTT), poly(ethylene oxide) monomethyl ether (mPEG-OH, M_w = 5000 g/mol, #EO unit =113), 4-(dimethylamino)pyridine (DMAP, 99%), and vanillin (99%) from Sigma-Aldrich; succinic anhydride (SA, 99%) from Acros; and 1-ethyl-3-(3-dimethylaminopropyl)carbodiimide-HCl salt (EDC) from Matrix Innovation were purchased and used as received.

A reduction-degradable polyester labeled with backbone dislufide linakges (PEss) with M_n = 1,800 g/mol and M_w/M_n = 1.56 was synthesized and purified as described in our previous publication.[60] Briefly, 3,3′ -dithiodipropionic acid (5.0 g, 23.8 mmol) reacted with ssDOH (3.7 g, 24.3 mmol) in the presence of DCC (10.0 g, 48.5 mmol) and a catalytic amount of DMAP (0.3 g, 2.4 mmol) in THF (70 mL) at 0 °C.

3.2.2 Instrumentation

^{1}H-NMR spectra were recorded using a 500 MHz Varian spectrometer. The $CDCl_3$ singlet at 7.3 ppm, DMSO-d_6 quintet at 2.5 ppm, and DMF-d_7 singlet at 8.03 were selected as the reference standard. Spectral features are tabulated in the following order: chemical shift (ppm); multiplicity (s - singlet, d - doublet, t – triplet, m - complex multiplet); number of protons; position of protons. Molecular weight and molecular weight distribution of (co)polymers were determined by gel permeation chromatography (GPC). An Agilent GPC was equipped with a 1260 Infinity Isocratic Pump and a refractive index (RI) detector. Two Agilent PLgel mixed-C and mixed-D columns were used with DMF containing 0.1 mol% LiBr at 50 °C at a flow rate of 1.0 mL/min. Linear poly(methyl methacrylate) (PMMA) standards from Fluka were used for calibration. Aliquots of the polymer samples were dissolved in DMF/LiBr. The clear solutions were filtered using a 0.40 mm PTFE filter to remove any DMF-insoluble species. A drop of anisole was added as a flow rate marker. A Viscotek GPC was equipped with a VE1122 pump and a RI detector with onePolyAnalytik column (PAS-103L) running THF as an eluent at 30 °C at a flow rate of 1.0 mL/min. With PMMA standards from Fluka, samples were prepared using the similar procedure.

The size and size distribution of nanoassemblies in hydrodynamic diameter was measured by dynamic light scattering (DLS) at a fixed scattering angle of 175° at 25 °C with a Malvern Instruments Nano S ZEN1600 equipped with a 633 nm He-Ne gas laser.

Transmission electron microscopy (TEM) images were obtained using a FEI Tecnai G2 F20 200 kV Cryo-STEM with Gatan Ultrascan 4000 4kx4k CCD Camera System Model 895. To prepare the specimens, a drop of the aqueous NP dispersion was added onto copper TEM grids (300 mesh, carbon coated), blotted and allowed to air dry at room temperature.

3.2.3 Synthesis of a disulfide-bearing ssDCI

ssDOH (2.6g, 16.7 mmol) was mixed with CDI (10.8 g, 66.7 mmol) in anhydrous acetonitrile (200 mL) under stirring for 3 hours at room temperature. The reaction was quenched with water (250 mL) and the product was extracted from chloroform. The chloroform was washed with water twice and aqueous brine solution once. After being dried over sodium sulfate, chloroform was removed by rotary evaporation. The product was dried in a vacuum oven at room temperature for 18 hrs to white powder: Yield = 5.0 g (87%).

3.2.4 Synthesis of a cyclic acetal-bearing diol (CAC-DOH)

THME (3 g, 25 mmol) was mixed with TPA (0.42 g, 3 mmol) in a CEM Discover SP microwave reactor at 140 °C for 15 min. The reaction mixture was dissolved in DMF (10 mL) at 120 °C, and then precipitated from cold PBS buffer solution (10 mM, pH = 7.4). The product was isolated by vacuum filtration and dried in a vacuum oven at room temperature for 18 h. Yield = 0.7 g (72%).

3.2.5 General procedure for step-growth polymerization to synthesize PCss polymers

The purified, dried ssDCI was mixed with diols in the presence of a base catalyst (Et_3N or DBU) in an organic solvent including anhydrous THF or DMF (5 mL) under stirring for 18 hrs. The formed products were precipitated from cold diethyl ether (400 mL), isolated by vacuum filtration, and dried in a vacuum oven at room temperature for 18 h.

The similar process was applied to synthesize functional PCss polymers with the use of ssDCI (0.20 g, 0.58 mmol), ssDOH (94.4 mg, 0.58 mmol) and DBU (11 μL) in anhydrous THF (3 mL) at room temperature for **PCss-E**; ssDCI (0.30 g, 0.89 mmol), C12DOH (0.19 g, 0.89 mmol) and DBU (20 μL) in anhydrous THF (5 mL) at room temperature for **PCss-G;** ssDCI (0.20 g, 0.58 mmol), PCL-DOH (1.18 g, 0.58 mmol) and DBU (11 μL) in anhydrous THF (6 mL) at room temperature for **PCss-H;** ssDCI (0.27 g, 0.78 mmol), PEG-DOH (1.12 g, 0.78 mmol) and DBU (14.5 μL) in a 1/1 THF/DCM v/v (6 mL in total) at room temperature for **PCss-I;** and ssDCI (0.20 g, 0.58 mmol), CAC-DOH (0.18 g, 0.58 mmol), DBU (11 μL) in anhydrous DMF (6 mL) at 130 ° C for **PCss-J**.

3.2.6 Reductive degradation of PCss

Aliquots of the purified, dried PCss (10 mg) were dissolved in THF (2 mL) and then mixed with DTT (3.1 mg, 0.02 mmol) to retain 10 mM DTT for GPC analysis. ^{1}H-NMR analysis was conducted on PCss-F (10 mg) dissolved in DMF-d_7 (1 mL) mixed with DTT (8.5 mg, 0.06 mmol).

3.2.7 Synthesis of mPEG-cyclic acetal-OH (mPEG-CAC-OH)

mPEG-COOH: An organic solution consisting of mPEG-OH (2.0 g, 0.4 mmol), Et_3N (0.17 μL, 1.2 mmol), and DMAP (50 mg, 0.4 mmol) dissolved in DCM (15 mL) was mixed with a solution of SA (0.12 g, 1.2 mmol) dissolved in DCM (7 mL) under stirring for 48 hrs. The resulting

mixture was precipitated from diethyl ether twice and dried in a vacuum oven at room temperature for 24 hrs to yield white powder: 1.8 g (88%).

mPEG-benzaldehyde (mPEG-BA): The purified, dried PEG-COOH (0.8 g, 0.16 mmol) was mixed with vanillin (0.24 g, 1.6 mmol), EDC (0.24 g, 1.2 mmol), and a catalytic amount of DMAP in a 1/1 DCM/THF v/v (50 mL in total) under stirring for 24 hrs. After the removal of solvent by rotary evaporation the product was dissolved in DCM (25 mL), washed with water twice and with aqueous brine solution once, and then dried over sodium sulfate. The product was precipitated from cold diethyl ether to remove impurities and dried in a vacuum oven at room temperature for 24 hrs: Yield 0.64 g (79%).

mPEG-CAC-OH: The purified, dried PEG-BA (0.16 g, 0.03 mmol) was mixed with THME (2.5 g, 21.1 mmol) and HCl (2.5 μ) in THF (15 mL) under stirring at 60 ° C for 30 min. The reaction mixture was quenched with Et_3N (1 μL). After the removal of solvent by rotary evaporation, the residue was dissolved in chloroform (10 mL) and passed through PTFE filter (0.25 μm) to remove excess and unreacted THME. The product was precipitated from cold diethyl ether to remove impurities and dried in a vacuum oven at room temperature for 24 hrs: Yield = 0.12 g (75%).

3.2.8 Block copolymerization of PCss

The purified, dried **PCss-F** (synthesized with mole equivalent ratio of CI/OH = 1.2/1 (0.3 g) was mixed with mPEG-CSC-OH (30 mg) and DBU (0.01 mmol) in anhydrous DCM (2 mL) under stirring for 18 hrs at room temperature. The block copolymers were precipitated from cold diethyl ether (600 mL), isolated by vacuum filtration, and dried in a vacuum oven at room temperature for 12 hrs.

3.2.9 Aqueous micellization by nanoprecipitation

The block copolymer (10 mg) dissolved in a mixture of THF (1 mL) and DMF (200 μL) was mixed dropwise with deionized water (10 mL) under stirring. After THF was removed, the mixture was dialyzed against water using a dialysis tubing with MWCO = 12 kg/mol for 6 hrs to form an aqueous dispersion of nanoassemblies at 1.4 mg/mL.

3.2.10 Cell viability using Alamar Blue assay

HeLa cells (8000 cells) were seeded into a 96-well plate and incubated at 37 °C for 24 hr. The existing media was replaced with DMEM containing varying concentrations of mPEG-CAC-PCss-CAC-mPEG micelles and incubated at 37 °C for 48 hr. The media was replaced with media containing Alamar blue dye. After 4 hrs incubation, the absorbance was recorded at 570 nm and 600 nm.

3.3 Results and discussion

3.3.1 Synthesis of a disulfide-bearing ssDCI

Figure 3.1a depicts our approach to synthesize a disulfide-bearing difunctional monomer with terminal carbonyl imidazole groups (ssDCI). The approach utilizes a facile coupling reaction of ssDOH with CDI in acetonitrile. No catalysts were required for the reaction to achieve a yield as high as 88% after purification. ^{1}H-NMR in Figure 3.1b shows the presence of methylene groups adjacent to terminal CI groups at 4.7 ppm and CI moieties at 7.1, 7.4, and 8.2 ppm (see Figure A.1 in Appendix A for its ^{1}H-NMR spectrum overlaid with its precursors of ssDOH and CDI). This result, combined with ^{13}C-NMR of ssDCI (Figure A.2), confirms the synthesis of ssDCI with >98% conjugation efficiency.

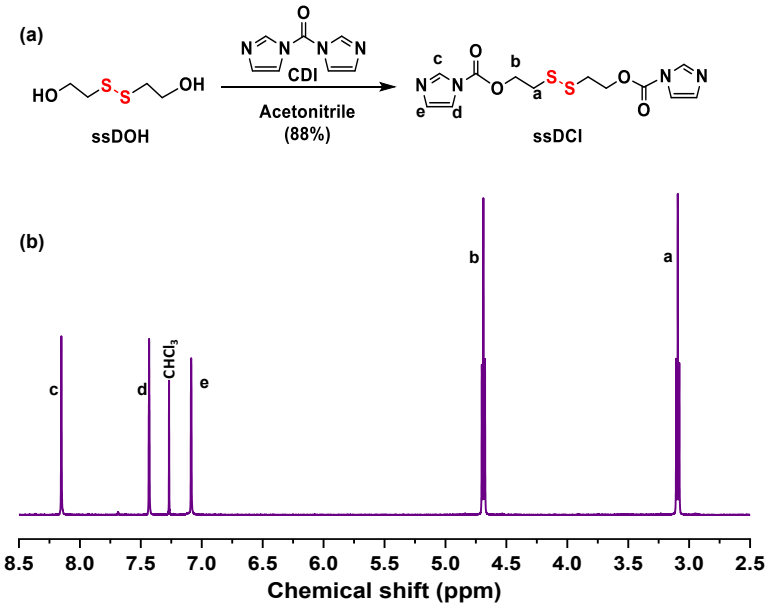

Figure 3.1 Synthetic route (a) and ^{1}H-NMR spectrum in $CDCl_3$ of ssDCI (b).

3.3.2 Investigation of step-growth polymerization to synthesize reduction-degradable PCss

As illustrated in Figure 3.2, our approach to synthesize PCss explores a carbonylimidazole (CI)-mediated step-growth polymerization of the formed ssDCI with various diols. This polycondensation undergoes a facile coupling reaction of a CI group with an OH group in the presence of a base catalyst at a given temperature. Table 3.1 summarizes our results.

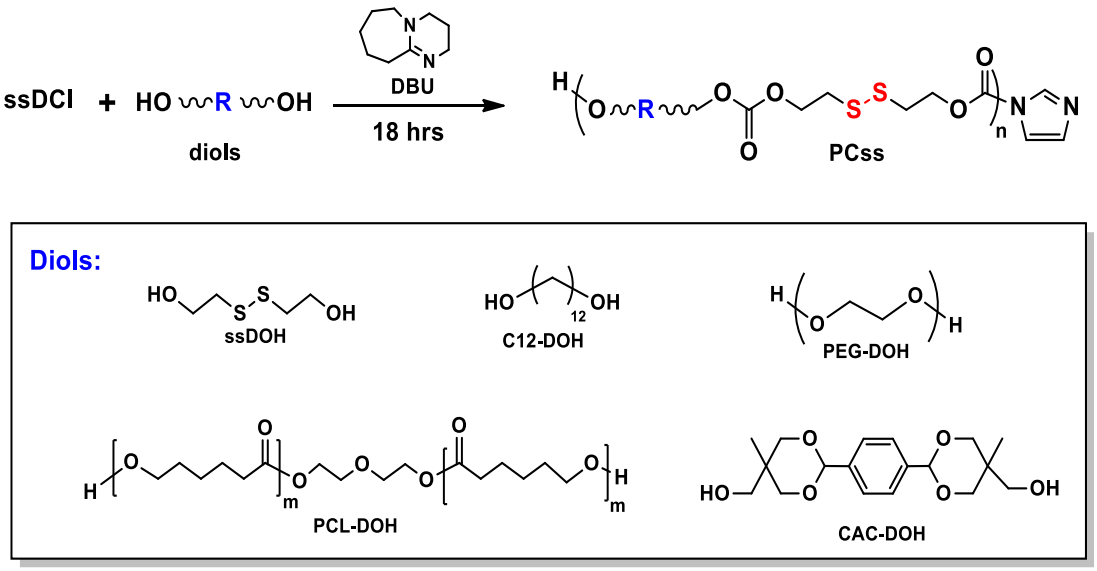

Figure 3.2 Schematic illustration of our approach to synthesize a variety of functional PCss polymers with various diols.

Table 3.1 Characteristics and molecular weight data of various PCss polymers synthesized by step-growth polymerization of ssDCI with various diols. a) Conditions for step-growth polymerization: 18 h at room temperature; b) Based on OH mole equivalent; c) Temp = 120 °C; d) By GPC calibrated with PMMA standards.

PCss [a]	Diol	CI/OH mole equivalent	DBU[b] (mol eq%)	Polymerization solvent	M_n[d] (g/mol)	M_w/M_n[d]
A	C12-DOH	1/1	6.3	THF	8600	1.25
B	C12-DOH	1/1	12.5	THF	6700	1.98
C	C12-DOH	1/1	25	THF	12700	1.50
D	C12-DOH	1/1	37.5	THF	9100	1.26
E	ssDOH	1.2/1	12.5	THF	3,300	2.00
F	ssDOH	1/1	12.5	THF	21,000	1.40
G	PCL-DOH	1/1	6.3	THF	13,000	1.38
H	PEG-DOH	1/1	6.3	THF/DCM	50,300	1.46
I[c]	CAC-DOH	1/1	6.3	DMF	5,300	1.46

We investigated the important parameters that can significantly influence the final properties of the polymers, particularly molecular weights (or the average number of disulfide linkages on the backbones) and CI functionalities of PCss copolymers. First, the nature and amount of base catalysts were examined at a stoichiometric balance of CI to OH groups at 1/1 mole equivalent ratio. C12-DOH was chosen as a source of OH for this experiment. In the absence of catalysts and with Et_3N as a base catalyst used up to 55 mol eq% (which is much greater than DBU used later) to OH groups, no polymerization was observed. A plausible reason could be due to the lower basicity of Et_3N. DBU is known to be a stronger base than Et_3N. Under similar conditions, the amount of DBU was varied to examine its effect on molecular weight and CI functionality of the formed PCss polymers (PCss-A to D). As summarized in Table 3.1, they had relatively high molecular weights as their number average molecular weight (M_n) ranging at 6.7-12 kg/mol with relatively broad dispersity (Đ) of 1.3 - 2.0 by GPC analysis (Figure A.3). Interestingly, no trend of molecular weight over the amount of DBU is noticed. Further to GPC analysis, the polymers were characterized for chemical structure using ^{1}H-NMR spectroscopy. Figure 3.3 shows ^{1}H-NMR spectrum of PCss-A as a typical example, which shows the peaks presenting ssDCI and C12-OH

moieties on the backbones. Their integral ratio was estimated to be 1/1, which is in good agreement with that in the feed.

An interesting observation was the dependence of the CI functionality in the formed PCss chains over the amount of DBU. When a 1/1 mole equivalent ratio of CI/OH group is designed, the major PCss polymers could be expected to have both OH and CI groups at their chain ends, thus the formation of HO-PCss-CI. Although the quantification of terminal CI groups by end group analysis using ^{1}H-NMR was not straightforward, Figure A.4 shows the clear decrease in the peaks corresponding to CI protons with an increasing amount of DBU used (PCss-A to C). Ultimately, no CI peaks appeared in ^{1}H-NMR spectra of PCss-D prepared with 37.5 mole eq% of DBU. A plausible reason is the over-reaction of DBU with CI groups.

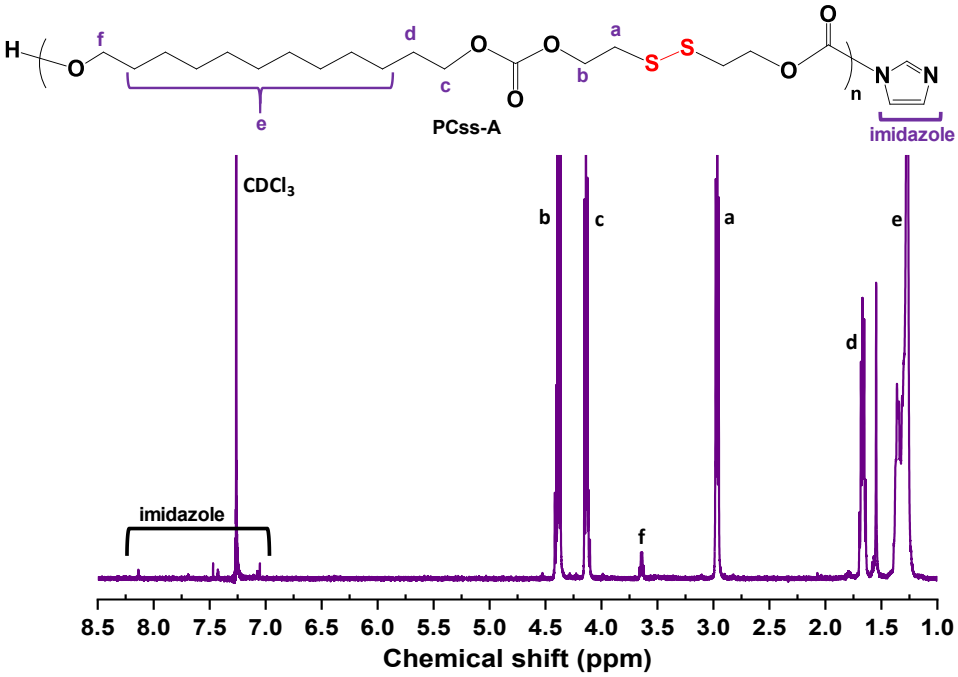

Figure 3.3 ^{1}H-NMR spectrum in $CDCl_3$ of PCss-A composed of ssDCI and C12-DOH as a typical example.

Given our investigation of step-growth polymerization with DBU catalyst, an excess CI mole equivalent was examined with the choice of ssDOH. Under stoichiometric imbalance condition, the major product is expected to be a PCss functionalized with CI groups at both ends, thus the formation of CI-PCss-CI. To test this, two PCss polymers were synthesized: PCss-E with the mole eq ratio of CI/OH = 1.2/1, while PCss-F with CI/OH mole eq = 1/1 for comparison. As shown in

Figure 3.4, ^{1}H-NMR spectrum of PCss-E shows the peaks at 4.4 and 3.0 ppm corresponding to two types of backbone methylene protons. These peaks are also seen in ^{1}H-NMR of PCss-F (Figure A.5). However, the peaks at 7.1, 7.4, and 8.2 ppm corresponding to imidazole protons appeared only in PCss-E NMR spectrum. In addition, the peak at 4.7 ppm (b′) corresponds to methylene protons adjacent to terminal CI group and the peak at 4.1 ppm (b″) is equivalent to methylene protons adjacent to a terminal OH group (which is not functionalized with a CI group). Using the integral ratio of the peaks (b′ and b″), the CI functionality could be estimated to be 91%. Furthermore, the integral ratio of the peaks (b′ and b) allow for the estimation of the DP of the repeating unit whose molecular weight = 360.5 g/mol to be 17, in the assumption that CI-PCss-CI is a major population along with small and negligible portion of CI-PCss-OH and HO-PCss-OH. This end group analysis allows for the estimation of theoretical M_n = 6.13 kg/mol of PCss-E.

Given our NMR analysis, PCss-E and PCss-F polymers were further characterized by GPC (Figure A.6). PCss-E (prepared with excess CI) had the M_n = 3.3 kg/mol, which is much smaller than that (M_n = 21 kg/mol) of PCss-F (prepared under the stoichiometric balance). Such difference could be predicted by Carothers' theory for step-growth polymerization under stoichiometric imbalance. Based on the results above, our approach allows for the synthesis of PCss with higher functionality of terminal CI groups with scarifying molecular weight at stoichiometric imbalance.

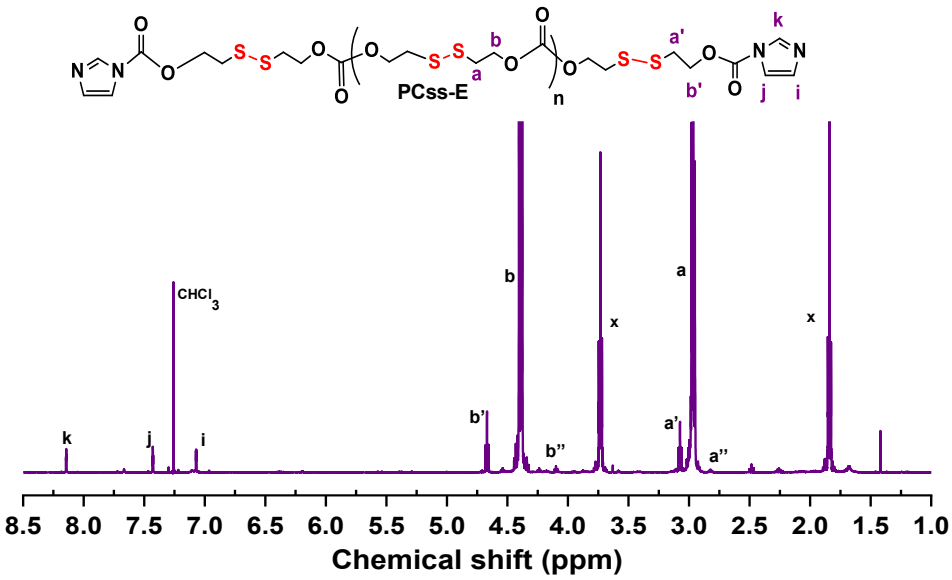

Figure 3.4 ^{1}H-NMR spectrum in $CDCl_3$ of PCss-E synthesized under stoichiometric imbalance. X denotes residual THF.

3.3.3 Synthesis of functional PCss

Our approach utilizing step-growth polymerization through CI-induced OH-activation was further investigated with various diols to synthesize reductively degradable functional PCss polymers. The chemical structures of various diols used in our experiments are depicted in Figure 3.2. The formed polymers were characterized by ^{1}H-NMR (Figure A.7-A.9) and GPC (Figure A10). As described above, the polymerization with ssDOH yielded PCss-F with a higher density of disulfide linkages on the backbone. Compared with other PCss prepared with diols with no disulfide, this polymer could degrade faster, because the reductive degradation greatly depends on the backbone disulfide density.[59] Polycarprolactone (PCL) is known to be biocompatible and crystalline as well as exhibit crystallinity-driven shape memory upon heating.[125,126] A PCL diol (PCL-DOH) with M_w = 2000 g/mol reacted ssDCI to form PCss-G with the M_n = 13,000 kg/mol and Đ = 1.38. Its ^{1}H-NMR spectrum shows the characteristic peaks for both ssDCI and PCL segments. With PEG-DOH with M_w = 1450 g/mol, the formed PCss-H had its molecular weight as high as M_n = 51 kg/mol, compared with other diols. It is composed of alternating units of PEG with ssDOH on the main chain (see Figure A.8 for ^{1}H-NMR). This polymer is amphiphilic to form self-assembled nanoassemblies with the diameter =12 nm in aqueous solution (Figure A.11).

Further to the commercially available diols, a diol labeled with cyclic acetal group (CAC-DOH) was examined to synthesize PCss-I exhibiting dual acid and reduction-responsive degradation. As illustrated in Figure A.12a, CAC-DOH was synthesized by the reaction of TPA with THME through a microwave-assisted process. The procedure was slightly modified as described in literature.[127] This process is advantageous because of no requirements for catalysis for the reaction and extra purification steps such as column chromatography. The chemical structure of the synthesized CAC-DOH was confirmed by ^{1}H-NMR analysis (Figure A.12b). Then, CAC-DOH was subjected to step-growth polymerization with ssDCI under similar conditions, yielding PCss-I with M_n = 5300 g/mol and Đ = 1.46. Overall, our results suggest that our approach exploring a CI-OH coupling-mediated step-growth polymerization of ssDCI with various diols enables the synthesis of functional poly(carbonate-disulfide)s.

3.3.4 Reduction-responsive degradation and tunable degradation rate of PCss

PCss is designed with disulfide linkages positioned on the backbones, which can be cleaved in a reducing environment to corresponding thiols. Such reductive cleavage can lead the dissociation of PCss polymers through main-chain degradation mechanism. With a choice of PCss-F prepared by reaction of ssDCI with ssDOH, we investigated the reductive degradation in the presence of DTT (a typical reducing agent) using NMR spectroscopy. Figure 3.5a schematically illustrates DTT-induced reductive degradation of PCss-F. ^{1}H-NMR spectra in Figure 3.5b shows the disappearance of the peaks (a) at 4.4 ppm and (b) at 3.1 ppm representing polymer units, suggesting the cleavage of backbone disulfide linkages to the corresponding ″thiol A″ and 2-mecaptoethanol. Further, the degraded thiol A can be subjected to facile 5-membered cyclization to generate ethylene monothiolcarbonate because of the β-position of thiol to carbonate bond. This is confirmed by the appearance of new peaks (a*) at 4.9 ppm and (b*) at 3.1 ppm.

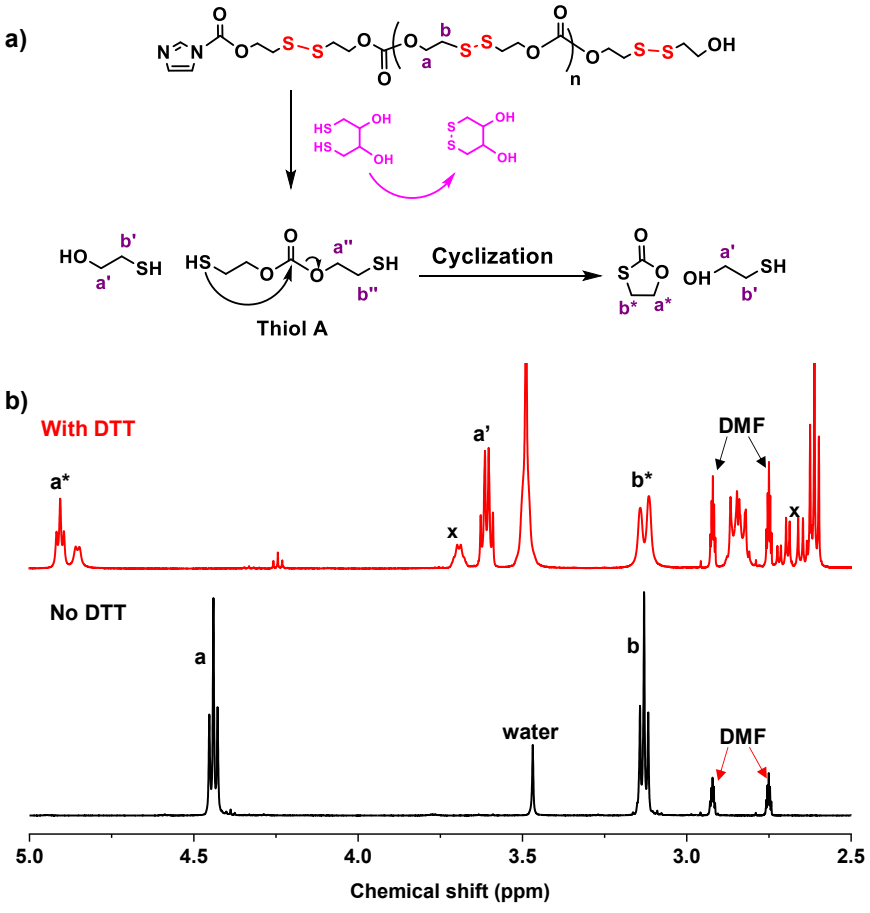

Figure 3.5 Schematic illustration of reduction-responsive degradation of PCss (a) and ^{1}H-NMR spectra of PCss-F before and 10 min after the addition of DTT (b).

Knowing the possible mechanism, the DTT-induced reductive degradation of PCss polymers were further investigated. GPC analysis was used to follows the shift of molecular weight distribution of degraded products to smaller molecular weight region with a decrease in their molecular weights upon the cleavage of the backbone disulfide linkages. Two PCss polymers with different backbone disulfide densities, PCss-F with high density and PCss-B with low density were examined and compared with a poly(ester-disulfide) (PEss) as a control. Note that intramolecular cyclization is not favorable for the degraded product of PEss.[128] For the reasonable comparison of degradation rate for three different polymers, the same amount of their aliquots were incubated in 10 mM DTT solution in THF; thus, the density of backbone disulfide linkages of PCss-E (ssDOH) is similar to PEss, however, greater than PCss-B (C12-DOH). Figure 3.6 shows the GPC traces with the characteristic peaks corresponding to polymers and DTT. For PCss-E, the polymer peak disappeared rapidly within 10 min after the treatment with DTT in THF. For PCss-G, the polymer peak was shifted to lower molecular weight region within the same time, but completely disappeared in 2.5 hrs. This result suggests that the cleavage of backbone disulfide linkages for PCss with lower disulfide density is slower than that with greater disulfide density. Further, PEss did not show no significant cleavage of backbone disulfide linkages within 30 min, although the disulfide density is similar to PCss-E. Our GPC analysis suggests that PCss with a carbonate linkage exhibits the enhanced disulfide cleavage rate compared to PEss, the counter part of PCss with an ester linkage. Further, the disulfide cleavage rate for PCss could be finely- tuned with varying disulfide densities.

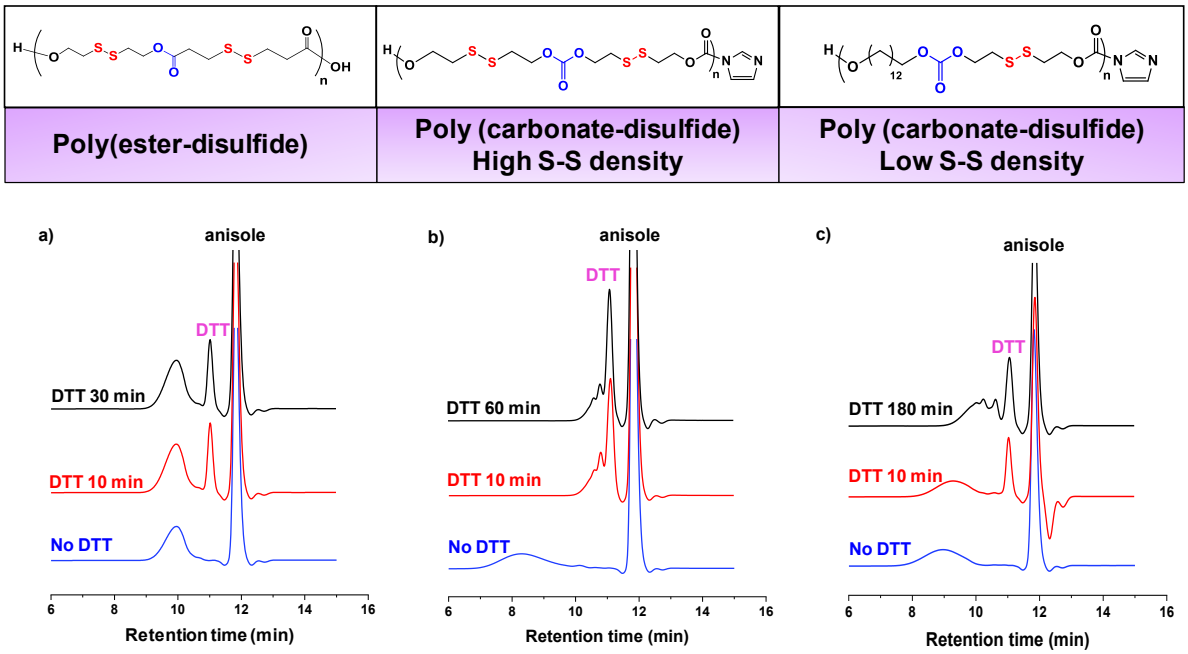

Figure 3.6 GPC traces of PCss and PEss degradation before and after addition of 10 mM DTT.

3.3.5 Synthesis of an mPEG-CAC-OH precursor

The three steps synthesis of an acid-cleavable cyclic acetal-bearing mPEG precursor (mPEG-CAC-OH) is depicted in Figure 3.7. Starting with mPEG-OH, the first step is its reaction with SA in a basic condition to synthesize a COOH-terminated mPEG (mPEG-COOH) according to the previous publications.[129] Beside the peaks at 3.4 - 3.7 ppm corresponding to EO protons, two peaks at 4.25 and 2.6 - 2.7 ppm newly appeared. Their integral ratio is quantitative as 2/4 (Figure A.13). In the second step, the formed mPEG-COOH reacted with vanillin through an EDC-medicated coupling reaction between COOH and OH groups, yielding an mPEG-benzaldehyde (mPEG-BA). ^{1}H-NMR spectrum in Figure 3.8a shows the peak at 9.9 ppm (i) corresponding to the aldehyde proton. Its integral ratio to the peak at 3.2 ppm (d) corresponding to the terminal methyl group of mPEG moiety is quantitative to be 1/3. In the last step, the formed mPEG-BA reacted with THME under acidic condition (HCl) to synthesize mPEG-CAC-OH. The peak at 5.5 ppm (i′) corresponds to the acetal proton in the cyclic acetal moiety and its integral ratio to PEG methyl peak is quantitative to be 1/3 (Figure 3.8b). These results confirm the successful synthesis of mPEG-CAC-OH precursor for our block copolymerization.

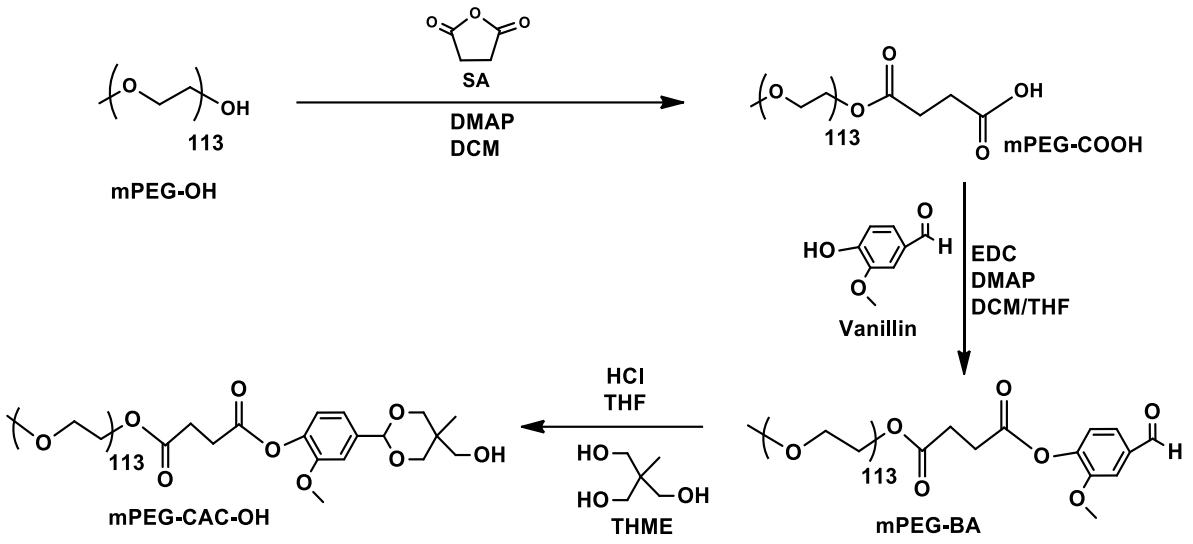

Figure 3.7 Synthetic route to mPEG-CAC-OH.

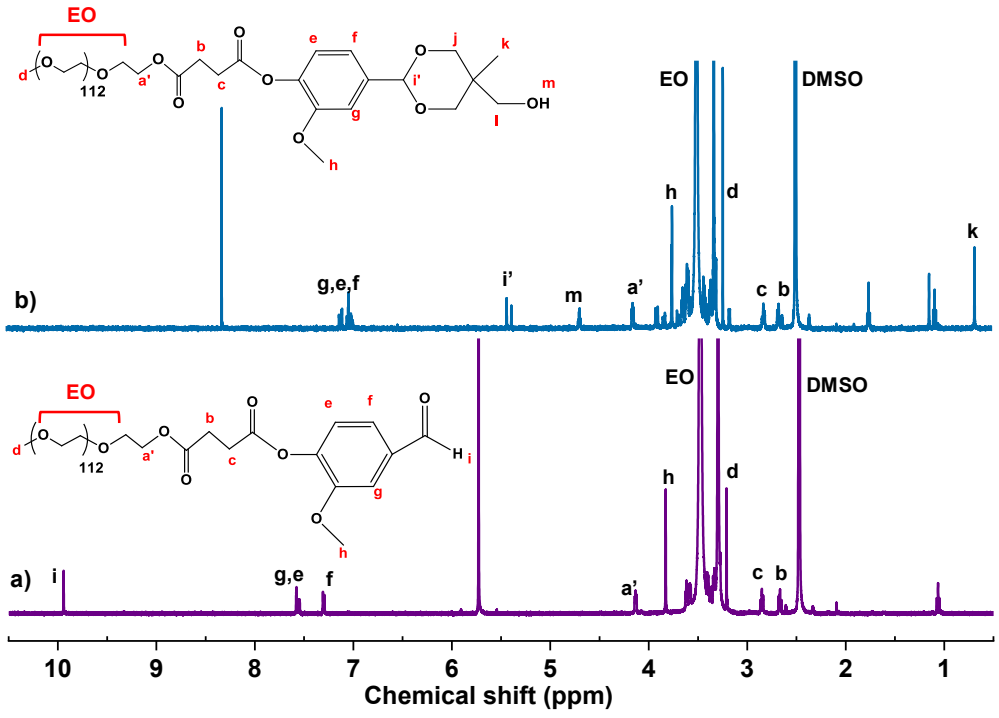

Figure 3.8 ^{1}H-NMR spectra of mPEG-BA (a) and mPEG-CAC-OH (b) in DMSO-d_6.

3.3.6 Block copolymerization and aqueous micellization of PCss

Given the promising synthesis and tunable reduction-responsive degradation, the PCss was further evaluated for block copolymerization. We investigated a post-modification approach of PCss with OH-bearing mPEG precursors through a CI-OH coupling reaction. Figure 3.9 illustrates our proof-of-concept approach to synthesize a novel PCss-based dual location dual acid/reduction-responsive amphiphilic degradable triblock copolymer for intracellular drug delivery application. The synthesized PCss bearing CI groups at both chain ends (CI-PCss-CI) with CI functionality = 90% and M_n = 4.7 kg/mol were conjugated with the synthesized mPEG-CAC-OH in the presence of DBU at room temperature, yielding mPEG-CAC-PCss-CAC-mPEG triblock copolymer. The conjugation was designed with the weight ratio of mPEG-CAC-OH/PCss-F = 0.1/1, which corresponds to 0.05/1 mole equivalent of OH/DI.

After being purified by precipitation from diethyl ether, the block copolymer was analyzed for molecular weight by GPC. As shown in figure 3.10, the molecular weight distribution appeared to be bimodal, with M_n = 11.2 kg/mol with M_w/M_n = 1.86. The peak appeared in higher molecular weight region corresponds to the block copolymer, while the peak appeared in lower molecular weight region overlapped with free PEG-CAC-OH precursor. Our GPC analysis suggests that the triblock copolymer could contain free precursor. Using deconvolution analysis, the portion of free PEG precursor is estimated to be 27% (Figure A.14).

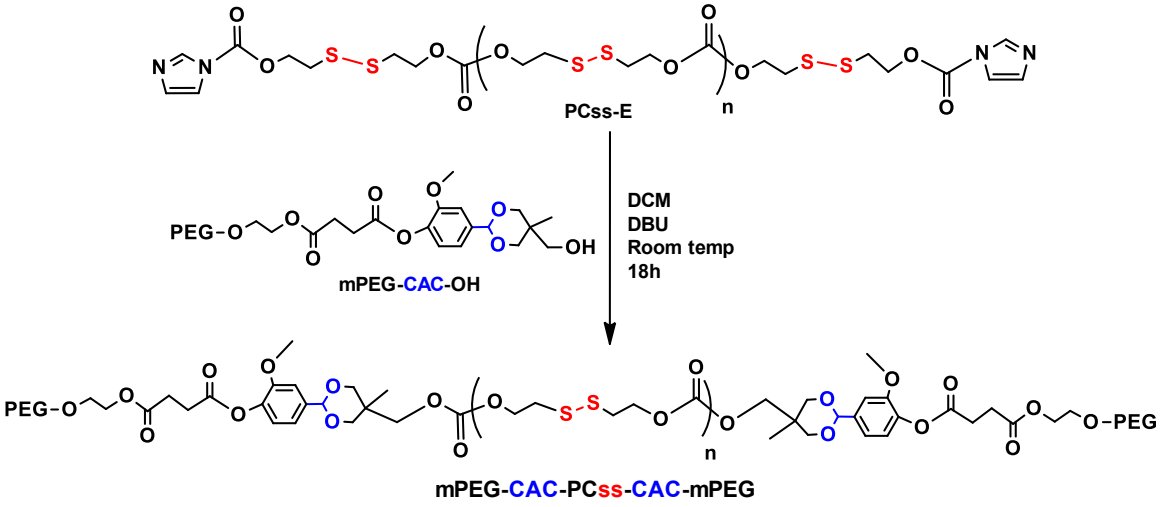

Figure 3.9 Synthetic approach to a novel PCss-based amphiphilic triblock copolymer.

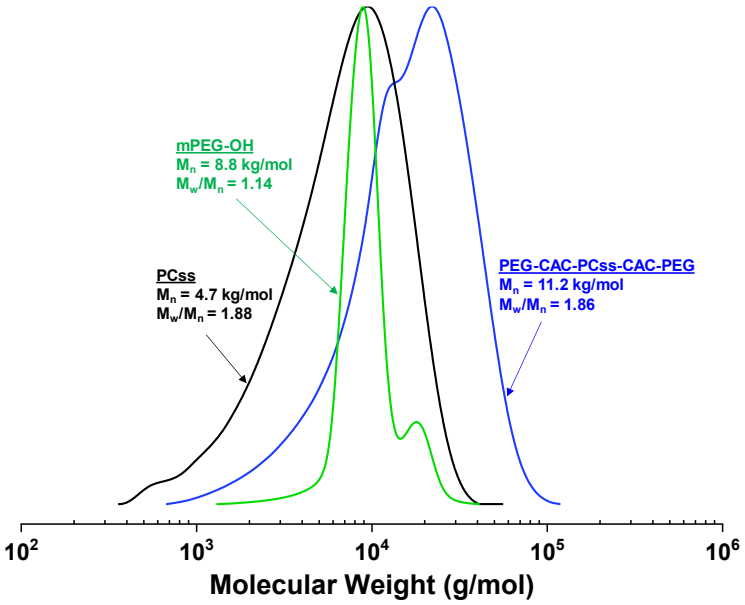

Figure 3.10 GPC diagram of mPEG-CAC-PCss-CAC-mPEG triblock copolymer compared with its two precursors: mPEG-CAC-OH and PCss.

The synthesized triblock copolymer is amphiphilic and thus its aqueous micellization through self-assembly was examined. Using the nanoprecipitation method followed by solvent-evaporation and dialysis to remove the organic solvents, aqueous nanoassemblies were formed with cyclic acetal linkages at core/corona interfaces and backbone disulfides in hydrophobic cores in dual locations. DLS analysis confirms the average diameter = 143 ± 1.4 nm (Figure 3.11b). TEM images show that the nanoparticles in a dried state is spherical with the average diameter to be of 20 ± 6 nm, which is significantly smaller than that determined by DLS because as the micelles are dehydrated on the TEM grids and their PEG shells are not visible. (Figure 3.11c and 3.11d).

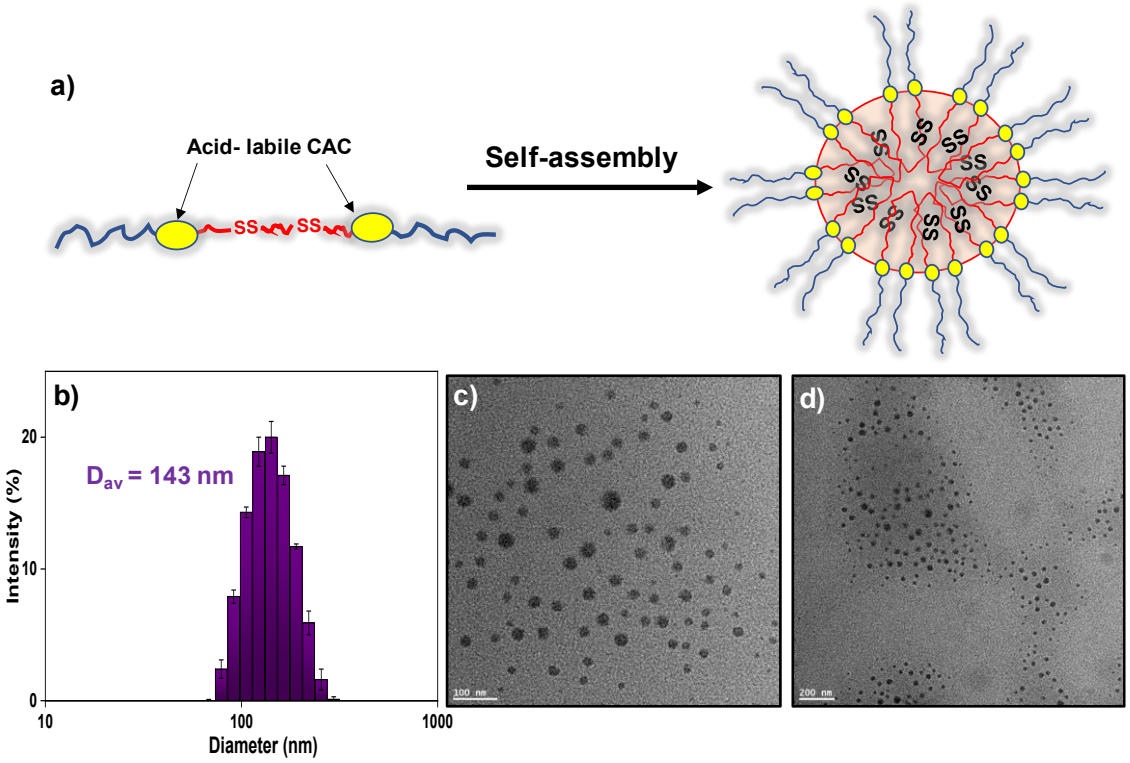

Figure 3.11 Schematic diagram of the self-assembly of mPEG-CAC-PCss-CAC-mPEG triblock copolymer (a); DLS diagram (b) and TEM images at high (c) and low (d) magnifications of the micelles. For TEM analysis, >100 micelles were selected randomly to manually calculate the average diameter.

3.3.7 Cytotoxicity evaluation

To ensure the biocompatibility of these micelles, the cytotoxicity of of mPEG-CAC-PCss-CAC-mPEG micelles was evaluated by Chaitra Shetty (MSc) in our lab on HeLa cervical cancer cells using an Alamar Blue assay. As seen in Figure 3.12, the viability of HeLa cells was >90% in the presence of empty micelles up to 200 μg/mL, suggesting non-toxicity of empty micelles to HeLa cells and an excellent biocompatibility.

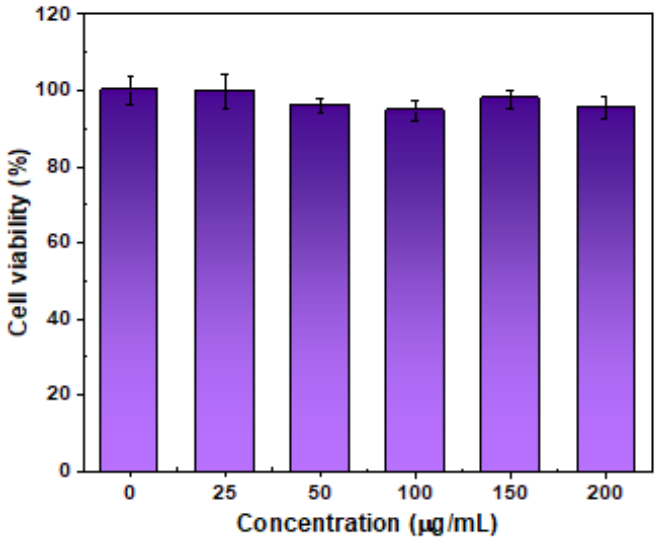

Figure 3.12 Viability of HeLa cells incubated with mPEG-CAC-PCss-CAC-mPEG micelles.

3.4 Conclusion

A new approach utilizing step-growth polymerization through CI-induced OH activation was explored for the synthesis of bio-reducible poly(carbonate-disulfide)s (PCss). Their molecular weight and chain-end functionality could be fine-tuned with variations in the amount of base catalyst and stoichiometric ratio of monomers. Use of various diols reacting with a difunctional ssDCI bearing terminal CI groups enabled the synthesis of PCss with various backbone designs exhibiting multi-functional structures such as amphiphilicity, acid-responsive degradation, and shape memory. The formed PCss exhibited tunable and rapid reductive degradation compared with counterpart of a polyester. To demonstrate the versatility of the designed PCss, a proof-of-concept block copolymerization was examined to successfully synthesize an mPEG-based triblock copolymer bearing a cyclic acetal linkage at the junction of PEG and PCss blocks. Due to its amphiphilic nature, the resulting acid/reduction- degradable block copolymer self-assembled into nanoaggregates having disulfide linkages in the hydrophobic PCss cores and acid labile linkages at core/corona interfaces. These results demonstrate that our approach can be used as a facile means to synthesize a variety of functional PCss polymers and allow for careful engineering of their backbone architecture which can widen the rang of building blocks available for the development of novel stimuli-responsive degradable polymeric nanomaterials for drug delivery and biomedical applications.

Chapter 4

Conclusion and future work

4.1 Conclusion

My MSc research investigated an effective dual-location dual stimuli-responsive degradation (DL-DSRD) strategy with three block copolymers exhibiting dual responses to endogenous acidic pH and glutathione found in tumor tissues and cancer cells for intracellular tumor-targeting drug delivery.

In Chapter 2, two amphiphilic block copolymers self-assembled to form aqueous nanoassemblies having acid-labile and/or disulfide linkages at the core/corona interfaces and disulfide pendants in the hydrophobic cores, thus attaining dual locations. They were colloidally-stable in a physiological condition, including with serum proteins. In the presence of dual stimuli (pH = 5.4 with 10 mM GSH), the formed nanoassemblies exhibited synergistically rapid release of encapsulated Dox as a result of their disassembly at both interfaces and cores caused by the cleavage of acid-labile and disulfide linkages. Furthermore, they had excellent anti-tumor activity upon cellular uptake to inhibit the proliferation of HeLa cancer cells due to the effective and rapid release of Dox.

In Chapter 3, a novel approach utilizing carbonylimidazole-hydroxyl coupling chemistry was explored to synthesize reduction-degradable PCss labeled with carbonate and disulfide bonds on the backbones exhibiting multi-functionalities as well as tunable and rapid reductive-degradation. Further, the versatility of the approach was demonstrated with the synthesis of an mPEG-based triblock copolymer bearing a cyclic acetal linkage at the junction of PEG and PCss blocks. The resulting acid/reduction-degradable block copolymer self-assembled into nanoaggregates having disulfide linkages in the hydrophobic PCss cores and acid labile linkages at core/corona interfaces.

Overall, DL-DSRD strategy with acidic pH and GSH responses is demonstrated as a robust means to design and synthesize intracellular tumor-targeting drug delivery nanocarriers based on smart amphiphilic block copolymers, exhibiting enhanced/accelerated release of encapsulated drugs at tumor site.

4.2 Future work

New designs of DL-DSRD block copolymers and their nanoassemblies with different properties can be investigated. Below are my suggested future directions for this project.

First, as described in Chapter 2, P1 and P2 copolymers were designed with different architectures (diblock vs triblock), chain lengths, and hydrophilic blocks (PEG vs POEOMA). As a result, their nanoassemblies have different properties such as CMC, size, morphology, and chain entanglement in core and corona. These differences could cause the variations in observed trend of loading capacity and stability of Dox-loaded micelles as well as burst-release of Dox. Fundamental studies on structure-property relationship could be carried out with the design of a variety of DL-DSRD block copolymers.

Second, as described in Chapter 3, an mPEG-based triblock copolymer with a GSH-responsive degradable poly(carbonate-disulfide) copolymer was synthesized through carbonylimidazole-hydroxyl coupling chemistry between a difunctional PCss labeled with terminal carbonylimdazole groups (CI-PCss-CI) and a terminal hydroxyl group of mPEG-OH. Our preliminary results suggest the possible loss of terminal carbonylimidazole groups during block copolymerization in the presence of DBU catalyst. As a consequence, the formed block copolymer contains ≈ 30% free mPEG-OH based on my deconvolution analysis. A better reaction condition is required to slow down or eliminate the loss of terminal CI groups. Another challenge is the reproducibility in a large-scale synthesis of a difunctional PCss labeled with terminal carbonylimdazole groups (CI-PCss-CI) with high conjugation efficiency (>95%). The current approach involves the use of excess carbonylimidazole (CI) functional groups over hydroxyl (OH) groups to synthesize CI-PCss-CI. As depicted in Figure 4.1, another proposed approach is to synthesize a PCss labeled with terminal OH groups, forming HO-PCss-OH, followed by the activation of OH groups with CDI , thus yielding CI-PCss-CI. This approach can avoid the possible loss of terminal CI groups during polymerization.

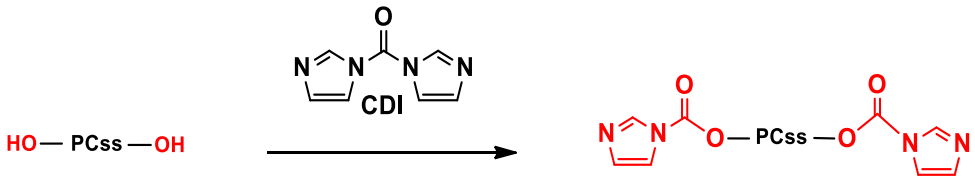

Figure 4.1 Proposed approach for synthesis of PCss with high CI end-functionality.

Third and last, the design and synthesis of the acid-labile linkages for the junction of hydrophilic and hydrophobic blocks are crucial for the synthesis of DL-DSRD copolymers.[130,131] This linkages should be stable in physiological environment (pH = 7.4), whereas be unstable to be cleaved rapidly in mild pH condition (6.5 - 6.9 in tumor extracellular compartment). Thus, one of the requirements of the linkage is to have adjustable acid-catalyzed hydrolysis (i.e. cleavage) rate (not too fast and not too slow at pH = 6.5 - 6.9). More importantly, the linkages should be stable during polymerization.[132]

In an effort to investigate this topic in my MSc research, I synthesized two novel cyclic acetal-labeled PEG precursors. The synthesis and ^{1}H-NMR analysis of mPEG-CAC-OH was described in Chapter 3 (Section 3.2.7), and mPEG-CAC-OH-T2 in Appendix B. Figure 4.2b shows the % cleavage of cyclic acetal linkages over incubation time in a pH = 4 buffer solution (see Appendix B for degradation conditions). According to my preliminary degradation kinetics study, their degradation rates were slow and are anticipated to be even slower at pH = 6.5 - 6.9 (tumor tissue pH). From literature publications,[133,134] three candidates of ketal/acetal family (L, M, and N) might meet our criteria (Figure 4.2c). These groups can be integrated to the block junctions of copolymer by various polymerization techniques and their acid hydrolysis rate can be studied.

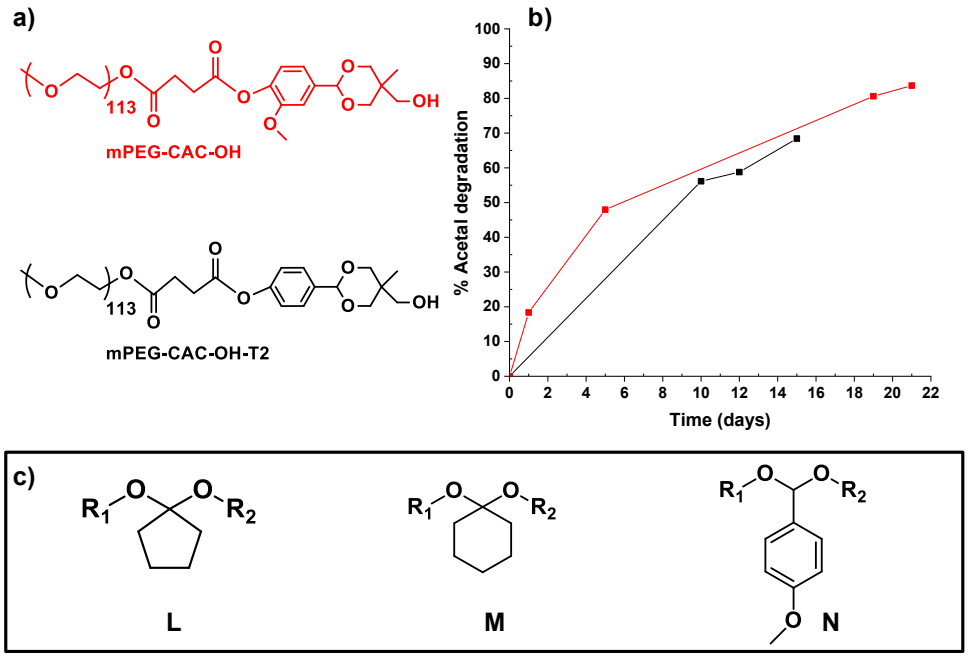

Figure 4.2 Chemical structures of two cyclic acetal-bearing PEG precursors (a), % cleavage of their acetal linkages at pH = 4 (b) and three potential candidates of ketal/acetal family (c).

References

(1) Pelengaris, S.; Khan, M. *The Molecular Biology of Cancer*; John Wiley & Sons, 2009.

(2) Singh, O. P.; Nehru, R. M. Nanotechnology and Cancer Treatment. *Asian J Exp Sci* **2008**, *22* (2), 6.

(3) Ho, B. N.; Pfeffer, C. M.; Singh, A. T. K. Update on Nanotechnology-Based Drug Delivery Systems in Cancer Treatment. *Anticancer Res.* **2017**, *37* (11), 5975–5981.

(4) Iyer, A. K.; Khaled, G.; Fang, J.; Maeda, H. Exploiting the Enhanced Permeability and Retention Effect for Tumor Targeting. *Drug Discov. Today* **2006**, *11* (17–18), 812–818.

(5) Bazak, R.; Houri, M.; Achy, S. E.; Hussein, W.; Refaat, T. Passive Targeting of Nanoparticles to Cancer: A Comprehensive Review of the Literature. *Mol. Clin. Oncol.* **2014**, *2* (6), 904–908.

(6) Xie, X.; Zhang, Y.; Li, F.; Lv, T.; Li, Z.; Chen, H.; Jia, L.; Gao, Y. Challenges and Opportunities from Basic Cancer Biology for Nanomedicine for Targeted Drug Delivery. *Curr. Cancer Drug Targets* **2019**, *19* (4), 257–276.

(7) Greish, K. Enhanced Permeability and Retention of Macromolecular Drugs in Solid Tumors: A Royal Gate for Targeted Anticancer Nanomedicines. *J. Drug Target.* **2007**, *15* (7–8), 457–464.

(8) Matsumura, Y.; Kimura, M.; Yamamoto, T.; Maeda, H. Involvement of the Kinin-Generating Cascade in Enhanced Vascular Permeability in Tumor Tissue. *Jpn. J. Cancer Res.* **1988**, *79* (12), 1327–1334.

(9) Yang, T.; Choi, M.-K.; Cui, F.-D.; Kim, J. S.; Chung, S.-J.; Shim, C.-K.; Kim, D.-D. Preparation and Evaluation of Paclitaxel-Loaded PEGylated Immunoliposome. *J. Controlled Release* **2007**, *120* (3), 169–177.

(10) O'Brien, M. E. R.; Wigler, N.; Inbar, M.; Rosso, R.; Grischke, E.; Santoro, A.; Catane, R.; Kieback, D. G.; Tomczak, P.; Ackland, S. P.; Orlandi, F.; Mellars, L.; Alland, L.; Tendler, C. Reduced Cardiotoxicity and Comparable Efficacy in a Phase IIItrial of Pegylated Liposomal Doxorubicin HCl(CAELYX^{TM}/Doxil®) versus Conventional Doxorubicin Forfirst-Line Treatment of Metastatic Breast Cancer. *Ann. Oncol.* **2004**, *15* (3), 440–449.

(11) Maeda, H. Toward a Full Understanding of the EPR Effect in Primary and Metastatic Tumors as Well as Issues Related to Its Heterogeneity. *Adv. Drug Deliv. Rev.* **2015**, *91*, 3–6.

(12) Sindhwani, S.; Syed, A. M.; Ngai, J.; Kingston, B. R.; Maiorino, L.; Rothschild, J.; MacMillan, P.; Zhang, Y.; Rajesh, N. U.; Hoang, T. The Entry of Nanoparticles into Solid Tumours. *Nat. Mater.* **2020**, 1–10.

(13) Danhier, F. To Exploit the Tumor Microenvironment: Since the EPR Effect Fails in the Clinic, What Is the Future of Nanomedicine? *J. Controlled Release* **2016**, *244*, 108–121.

(14) Wen, H.; Park, K. *Oral Controlled Release Formulation Design and Drug Delivery: Theory to Practice*; John Wiley & Sons, 2011.

(15) Shi, J.; Kantoff, P. W.; Wooster, R.; Farokhzad, O. C. Cancer Nanomedicine: Progress, Challenges and Opportunities. *Nat. Rev. Cancer* **2017**, *17* (1), 20.

(16) Gabizon, A.; Catane, R.; Uziely, B.; Kaufman, B.; Safra, T.; Cohen, R.; Martin, F.; Huang, A.; Barenholz, Y. Prolonged Circulation Time and Enhanced Accumulation in Malignant Exudates of Doxorubicin Encapsulated in Polyethylene-Glycol Coated Liposomes. *Cancer Res.* **1994**, *54* (4), 987–992.

(17) Forssen, E.; Willis, M. Ligand-Targeted Liposomes. *Adv. Drug Deliv. Rev.* **1998**, *29* (3), 249–271.
(18) Sercombe, L.; Veerati, T.; Moheimani, F.; Wu, S. Y.; Sood, A. K.; Hua, S. Advances and Challenges of Liposome Assisted Drug Delivery. *Front. Pharmacol.* **2015**, *6*.
(19) Szebeni, J.; Moghimi, S. M. Liposome Triggering of Innate Immune Responses: A Perspective on Benefits and Adverse Reactions: Biological Recognition and Interactions of Liposomes. *J. Liposome Res.* **2009**, *19* (2), 85–90.
(20) Russell, L. M.; Hultz, M.; Searson, P. C. Leakage Kinetics of the Liposomal Chemotherapeutic Agent Doxil: The Role of Dissolution, Protonation, and Passive Transport, and Implications for Mechanism of Action. *J. Controlled Release* **2018**, *269*, 171–176.
(21) Zhang, L.; Gu, F. X.; Chan, J. M.; Wang, A. Z.; Langer, R. S.; Farokhzad, O. C. Nanoparticles in Medicine: Therapeutic Applications and Developments. *Clin. Pharmacol. Ther.* **2008**, *83* (5), 761–769.
(22) Du, J.-Z.; Du, X.-J.; Mao, C.-Q.; Wang, J. Tailor-Made Dual PH-Sensitive Polymer–Doxorubicin Nanoparticles for Efficient Anticancer Drug Delivery. *J. Am. Chem. Soc.* **2011**, *133* (44), 17560–17563.
(23) Duncan, R.; Vicent, M. J.; Greco, F.; Nicholson, R. I. Polymer–Drug Conjugates: Towards a Novel Approach for the Treatment of Endrocine-Related Cancer. *Endocr. Relat. Cancer* **2005**, *12* (Supplement_1), S189–S199.
(24) Larson, N.; Ghandehari, H. Polymeric Conjugates for Drug Delivery. *Chem. Mater. Publ. Am. Chem. Soc.* **2012**, *24* (5), 840–853.
(25) Oerlemans, C.; Bult, W.; Bos, M.; Storm, G.; Nijsen, J. F. W.; Hennink, W. E. Polymeric Micelles in Anticancer Therapy: Targeting, Imaging and Triggered Release. *Pharm. Res.* **2010**, *27* (12), 2569–2589.
(26) Karayianni, M.; Pispas, S. Self-Assembly of Amphiphilic Block Copolymers in Selective Solvents. In *Fluorescence Studies of Polymer Containing Systems*; Procházka, K., Ed.; Springer International Publishing: Cham, 2016; Vol. 16, pp 27–63.
(27) Biswas, D.; An, S. Y.; Li, Y.; Wang, X.; Oh, J. K. Intracellular Delivery of Colloidally Stable Core-Cross-Linked Triblock Copolymer Micelles with Glutathione-Responsive Enhanced Drug Release for Cancer Therapy. *Mol. Pharm.* **2017**, *14* (8), 2518–2528.
(28) Chung, J. E.; Yokoyama, M.; Yamato, M.; Aoyagi, T.; Sakurai, Y.; Okano, T. Thermo-Responsive Drug Delivery from Polymeric Micelles Constructed Using Block Copolymers of Poly(N-Isopropylacrylamide) and Poly(Butylmethacrylate). *J. Controlled Release* **1999**, *62* (1–2), 115–127.
(29) Li, D.; Bu, Y.; Zhang, L.; Wang, X.; Yang, Y.; Zhuang, Y.; Yang, F.; Shen, H.; Wu, D. Facile Construction of PH-and Redox-Responsive Micelles from a Biodegradable Poly (β-Hydroxyl Amine) for Drug Delivery. *Biomacromolecules* **2016**, *17* (1), 291–300.
(30) Mura, S.; Nicolas, J.; Couvreur, P. Stimuli-Responsive Nanocarriers for Drug Delivery. *Nat. Mater.* **2013**, *12* (11), 991–1003.
(31) Celsion Announces IRB Approval to Begin a Clinical Study of ThermoDox® Plus High Intensity Focused Ultrasound in Breast Cancer Patients at University Medical Center Utrecht in the Netherlands http://investor.celsion.com/news-releases/news-release-details/celsion-announces-irb-approval-begin-clinical-study-thermodoxr (accessed Mar 2, 2020).

(32) Tagami, T.; Foltz, W. D.; Ernsting, M. J.; Lee, C. M.; Tannock, I. F.; May, J. P.; Li, S.-D. MRI Monitoring of Intratumoral Drug Delivery and Prediction of the Therapeutic Effect with a Multifunctional Thermosensitive Liposome. *Biomaterials* **2011**, *32* (27), 6570–6578.
(33) Bordat, A.; Boissenot, T.; Nicolas, J.; Tsapis, N. Thermoresponsive Polymer Nanocarriers for Biomedical Applications. *Adv. Drug Deliv. Rev.* **2019**, *138*, 167–192.
(34) Oliveira, H.; Pérez-Andrés, E.; Thevenot, J.; Sandre, O.; Berra, E.; Lecommandoux, S. Magnetic Field Triggered Drug Release from Polymersomes for Cancer Therapeutics. *J. Controlled Release* **2013**, *169* (3), 165–170.
(35) Cai, K.; Luo, Z.; Hu, Y.; Chen, X.; Liao, Y.; Yang, L.; Deng, L. Magnetically Triggered Reversible Controlled Drug Delivery from Microfabricated Polymeric Multireservoir Devices. *Adv. Mater.* **2009**, *21* (40), 4045–4049.
(36) Agasti, S. S.; Chompoosor, A.; You, C.-C.; Ghosh, P.; Kim, C. K.; Rotello, V. M. Photoregulated Release of Caged Anticancer Drugs from Gold Nanoparticles. *J. Am. Chem. Soc.* **2009**, *131* (16), 5728–5729.
(37) Azagarsamy, M. A.; Alge, D. L.; Radhakrishnan, S. J.; Tibbitt, M. W.; Anseth, K. S. Photocontrolled Nanoparticles for On-Demand Release of Proteins. *Biomacromolecules* **2012**, *13* (8), 2219–2224.
(38) Cheng, W.; Gu, L.; Ren, W.; Liu, Y. Stimuli-Responsive Polymers for Anti-Cancer Drug Delivery. *Mater. Sci. Eng. C* **2014**, *45*, 600–608.
(39) Javadi, M.; Pitt, W. G.; Belnap, D. M.; Tsosie, N. H.; Hartley, J. M. Encapsulating Nanoemulsions inside ELiposomes for Ultrasonic Drug Delivery. *Langmuir* **2012**, *28* (41), 14720–14729.
(40) Bawa, K. K.; Oh, J. K. Stimulus-Responsive Degradable Polylactide-Based Block Copolymer Nanoassemblies for Controlled/Enhanced Drug Delivery. *Mol Pharm.* **2017**, *14* (8), 2460–2474.
(41) Zhang, Q.; Ko, N. R.; Oh, J. K. Recent Advances in Stimuli-Responsive Degradable Block Copolymer Micelles: Synthesis and Controlled Drug Delivery Applications. *Chem. Commun.* **2012**, *48* (61), 7542–7552.
(42) Cheng, R.; Feng, F.; Meng, F.; Deng, C.; Feijen, J.; Zhong, Z. Glutathione-Responsive Nano-Vehicles as a Promising Platform for Targeted Intracellular Drug and Gene Delivery. *J. Controlled Release* **2011**, *152* (1), 2–12.
(43) Wong, L.; Boyer, C.; Jia, Z.; Zareie, H. M.; Davis, T. P.; Bulmus, V. Synthesis of Versatile Thiol-Reactive Polymer Scaffolds via RAFT Polymerization. *Biomacromolecules* **2008**, *9* (7), 1934–1944.
(44) Jia, Z.; Wong, L.; Davis, T. P.; Bulmus, V. One-Pot Conversion of RAFT-Generated Multifunctional Block Copolymers of HPMA to Doxorubicin Conjugated Acid-and Reductant-Sensitive Crosslinked Micelles. *Biomacromolecules* **2008**, *9* (11), 3106–3113.
(45) Khorsand, B.; Lapointe, G.; Brett, C.; Oh, J. K. Intracellular Drug Delivery Nanocarriers of Glutathione-Responsive Degradable Block Copolymers Having Pendant Disulfide Linkages. *Biomacromolecules* **2013**, *14* (6), 2103–2111.
(46) An, S. Y.; Noh, S. M.; Oh, J. K. Multiblock Copolymer-Based Dual Dynamic Disulfide and Supramolecular Crosslinked Self-Healing Networks. *Macromol. Rapid Commun.* **2017**, *38* (8), 1600777.

(47) Maruya-Li, K.; Shetty, C.; Moini Jazani, A.; Arezi, N.; Oh, J. K. Dual Reduction/Acid-Responsive Disassembly and Thermoresponsive Tunability of Degradable Double Hydrophilic Block Copolymer. *ACS Omega* **2020**.
(48) Chan, N.; Khorsand, B.; Aleksanian, S.; Oh, J. K. A Dual Location Stimuli-Responsive Degradation Strategy of Block Copolymer Nanocarriers for Accelerated Release. *Chem. Commun.* **2013**, *49* (68), 7534–7536.
(49) Oh, J. K. Disassembly and Tumor-Targeting Drug Delivery of Reduction-Responsive Degradable Block Copolymer Nanoassemblies. *Polym. Chem.* **2019**, *10* (13), 1554–1568.
(50) Wei, R.; Cheng, L.; Zheng, M.; Cheng, R.; Meng, F.; Deng, C.; Zhong, Z. Reduction-Responsive Disassemblable Core-Cross-Linked Micelles Based on Poly (Ethylene Glycol)-b-Poly (N-2-Hydroxypropyl Methacrylamide)–Lipoic Acid Conjugates for Triggered Intracellular Anticancer Drug Release. *Biomacromolecules* **2012**, *13* (8), 2429–2438.
(51) Xue, S.; Gu, X.; Zhang, J.; Sun, H.; Deng, C.; Zhong, Z. Construction of Small-Sized, Robust, and Reduction-Responsive Polypeptide Micelles for High Loading and Targeted Delivery of Chemotherapeutics. *Biomacromolecules* **2018**, *19* (8), 3586–3593.
(52) Liu, J.; Pang, Y.; Huang, W.; Zhu, Z.; Zhu, X.; Zhou, Y.; Yan, D. Redox-Responsive Polyphosphate Nanosized Assemblies: A Smart Drug Delivery Platform for Cancer Therapy. *Biomacromolecules* **2011**, *12* (6), 2407–2415.
(53) Liu, J.; Huang, W.; Pang, Y.; Huang, P.; Zhu, X.; Zhou, Y.; Yan, D. Molecular Self-Assembly of a Homopolymer: An Alternative To Fabricate Drug-Delivery Platforms for Cancer Therapy. *Angew. Chem. Int. Ed.* **2011**, *50* (39), 9162–9166.
(54) Ding, M.; Zeng, X.; He, X.; Li, J.; Tan, H.; Fu, Q. Cell Internalizable and Intracellularly Degradable Cationic Polyurethane Micelles as a Potential Platform for Efficient Imaging and Drug Delivery. *Biomacromolecules* **2014**, *15* (8), 2896–2906.
(55) de Paz, M. V.; Zamora, F.; Begines, B.; Ferris, C.; Galbis, J. A. Glutathione-Mediated Biodegradable Polyurethanes Derived from L -Arabinitol. *Biomacromolecules* **2010**, *11* (1), 269–276.
(56) Wu, J.; Zhao, L.; Xu, X.; Bertrand, N.; Choi, W. I.; Yameen, B.; Shi, J.; Shah, V.; Mulvale, M.; MacLean, J. L.; Farokhzad, O. C. Hydrophobic Cysteine Poly(Disulfide)-Based Redox-Hypersensitive Nanoparticle Platform for Cancer Theranostics. *Angew. Chem. Int. Ed.* **2015**, *54* (32), 9218–9223.
(57) Xu, Z.; Liu, S.; Kang, Y.; Wang, M. Glutathione-Responsive Polymeric Micelles Formed by a Biodegradable Amphiphilic Triblock Copolymer for Anticancer Drug Delivery and Controlled Release. *ACS Biomater. Sci. Eng.* **2015**, *1* (7), 585–592.
(58) Yameen, B.; Vilos, C.; Choi, W. I.; Whyte, A.; Huang, J.; Pollit, L.; Farokhzad, O. C. Drug Delivery Nanocarriers from a Fully Degradable PEG-Conjugated Polyester with a Reduction-Responsive Backbone. *Chem. - Eur. J.* **2015**, *21* (32), 11325–11329.
(59) Pinnel, P.; Mendez-Nelson, A.; Noh, S. M.; Nam, J. H.; Oh, J. K. Rapid and Tunable Reductive Degradation of Disulfide-Labeled Polyesters. *Macromol. Chem. Phys.* **2012**, *213* (6), 678–685.
(60) Nelson-Mendez, A.; Aleksanian, S.; Oh, M.; Lim, H.-S.; Oh, J. K. Reductively Degradable Polyester-Based Block Copolymers Prepared by Facile Polycondensation and ATRP: Synthesis, Degradation, and Aqueous Micellization. *Soft Matter* **2011**, *7* (16), 7441–7452.

(61) Basak, D.; Bej, R.; Ghosh, S. Amphiphilic Poly(Disulfide) Micelles and a Remarkable Impact of the Core Hydrophobicity on Redox Responsive Disassembly. *Polym. Chem.* **2015**, *6* (36), 6465–6474.
(62) Zhuang, Y.; Deng, H.; Su, Y.; He, L.; Wang, R.; Tong, G.; He, D.; Zhu, X. Aptamer-Functionalized and Backbone Redox-Responsive Hyperbranched Polymer for Targeted Drug Delivery in Cancer Therapy. *Biomacromolecules* **2016**, *17* (6), 2050–2062.
(63) Fan, H.; Huang, J.; Li, Y.; Yu, J.; Chen, J. Fabrication of Reduction-Degradable Micelle Based on Disulfide-Linked Graft Copolymer-Camptothecin Conjugate for Enhancing Solubility and Stability of Camptothecin. *Polymer* **2010**, *51* (22), 5107–5114.
(64) Ko, J.; Park, K.; Kim, Y.-S.; Kim, M. S.; Han, J. K.; Kim, K.; Park, R.-W.; Kim, I.-S.; Song, H. K.; Lee, D. S.; Kwon, I. C. Tumoral Acidic Extracellular PH Targeting of PH-Responsive MPEG-Poly(β-Amino Ester) Block Copolymer Micelles for Cancer Therapy. *J. Controlled Release* **2007**, *123* (2), 109–115.
(65) Bazban-Shotorbani, S.; Hasani-Sadrabadi, M. M.; Karkhaneh, A.; Serpooshan, V.; Jacob, K. I.; Moshaverinia, A.; Mahmoudi, M. Revisiting Structure-Property Relationship of PH-Responsive Polymers for Drug Delivery Applications. *J. Controlled Release* **2017**, *253*, 46–63.
(66) Samanta, S.; Bogdanowicz, D. R.; Lu, H. H.; Koberstein, J. T. Polyacetals: Water-Soluble, PH-Degradable Polymers with Extraordinary Temperature Response. *Macromolecules* **2016**, *49* (5), 1858–1864.
(67) Cao, H.; Chen, C.; Xie, D.; Chen, X.; Wang, P.; Wang, Y.; Song, H.; Wang, W. A Hyperbranched Amphiphilic Acetal Polymer for PH-Sensitive Drug Delivery. *Polym. Chem.* **2018**, *9* (2), 169–177.
(68) Shenoi, R. A.; Narayanannair, J. K.; Hamilton, J. L.; Lai, B. F. L.; Horte, S.; Kainthan, R. K.; Varghese, J. P.; Rajeev, K. G.; Manoharan, M.; Kizhakkedathu, J. N. Branched Multifunctional Polyether Polyketals: Variation of Ketal Group Structure Enables Unprecedented Control over Polymer Degradation in Solution and within Cells. *J Am Chem Soc* **2012**, *134* (36), 14945–14957.
(69) Lee, I.; Park, M.; Kim, Y.; Hwang, O.; Khang, G.; Lee, D. Ketal Containing Amphiphilic Block Copolymer Micelles as PH-Sensitive Drug Carriers. *Int. J. Pharm.* **2013**, *448* (1), 259–266.
(70) Yu, Y.; Chen, C.-K.; Law, W.-C.; Sun, H.; Prasad, P. N.; Cheng, C. A Degradable Brush Polymer–Drug Conjugate for PH-Responsive Release of Doxorubicin. *Polym. Chem.* **2015**, *6* (6), 953–961.
(71) Mao, J.; Li, Y.; Wu, T.; Yuan, C.; Zeng, B.; Xu, Y.; Dai, L. A Simple Dual-PH Responsive Prodrug-Based Polymeric Micelles for Drug Delivery. *ACS Appl. Mater. Interfaces* **2016**, *8* (27), 17109–17117.
(72) Lim, C. W.; Park, J. H.; Ahn, C.-H.; Kim, D. Self-Assembled Nanoaggregates Based on Polyaspartamide Graft Copolymers for PH-Controlled Release of Doxorubicin. *J. Mater. Chem. B* **2015**, *3* (15), 2978–2985.
(73) Liu, N.; Li, B.; Gong, C.; Liu, Y.; Wang, Y.; Wu, G. A PH-and Thermo-Responsive Poly (Amino Acid)-Based Drug Delivery System. *Colloids Surf. B Biointerfaces* **2015**, *136*, 562–569.
(74) Jin, Y.; Song, L.; Su, Y.; Zhu, L.; Pang, Y.; Qiu, F.; Tong, G.; Yan, D.; Zhu, B.; Zhu, X. Oxime Linkage: A Robust Tool for the Design of PH-Sensitive Polymeric Drug Carriers. *Biomacromolecules* **2011**, *12* (10), 3460–3468.

(75) Fang, Y.; Xue, J.; Gao, S.; Lu, A.; Yang, D.; Jiang, H.; He, Y.; Shi, K. Cleavable PEGylation: A Strategy for Overcoming the "PEG Dilemma" in Efficient Drug Delivery. *Drug Deliv.* **2017**, *24* (2), 22–32.
(76) Jin, Q.; Deng, Y.; Chen, X.; Ji, J. Rational Design of Cancer Nanomedicine for Simultaneous Stealth Surface and Enhanced Cellular Uptake. *ACS Nano* **2019**, *13* (2), 954–977.
(77) Kong, L.; Campbell, F.; Kros, A. DePEGylation Strategies to Increase Cancer Nanomedicine Efficacy. *Nanoscale Horiz.* **2019**, *4* (2), 378–387.
(78) Xiao, D.; Jia, H.-Z.; Zhang, J.; Liu, C.-W.; Zhuo, R.-X.; Zhang, X.-Z. A Dual-Responsive Mesoporous Silica Nanoparticle for Tumor-Triggered Targeting Drug Delivery. *Small* **2014**, *10* (3), 591–598.
(79) Sun, C.-Y.; Liu, Y.; Du, J.-Z.; Cao, Z.-T.; Xu, C.-F.; Wang, J. Facile Generation of Tumor-PH-Labile Linkage-Bridged Block Copolymers for Chemotherapeutic Delivery. *Angew. Chem. Int. Ed.* **2016**, *55* (3), 1010–1014.
(80) Liu, X.; Hu, D.; Jiang, Z.; Zhuang, J.; Xu, Y.; Guo, X.; Thayumanavan, S. Multi-Stimuli-Responsive Amphiphilic Assemblies through Simple Postpolymerization Modifications. *Macromolecules* **2016**, *49* (17), 6186–6192.
(81) Sun, Y.; Du, X.; He, J.; Hu, J.; Zhang, M.; Ni, P. Dual-Responsive Core-Crosslinked Polyphosphoester-Based Nanoparticles for PH/Redox-Triggered Anticancer Drug Delivery. *J. Mater. Chem. B* **2017**, *5* (20), 3771–3782.
(82) Zhang, Y.; He, J.; Cao, D.; Zhang, M.; Ni, P. Galactosylated Reduction and PH Dual-Responsive Triblock Terpolymer Gal-PEEP-a-PCL-Ss-PDMAEMA: A Multifunctional Carrier for the Targeted and Simultaneous Delivery of Doxorubicin and DNA. *Polym. Chem.* **2014**, *5* (17), 5124–5138.
(83) Xiong, D.; Yao, N.; Gu, H.; Wang, J.; Zhang, L. Stimuli-Responsive Shell Cross-Linked Micelles from Amphiphilic Four-Arm Star Copolymers as Potential Nanocarriers for "PH/Redox-Triggered" Anticancer Drug Release. *Polymer* **2017**, *114*, 161–172.
(84) Hu, X.; Li, H.; Luo, S.; Liu, T.; Jiang, Y.; Liu, S. Thiol and PH Dual-Responsive Dynamic Covalent Shell Cross-Linked Micelles for Triggered Release of Chemotherapeutic Drugs. *Polym Chem* **2013**, *4* (3), 695–706.
(85) Li, J.; Liu, P. PH/Reduction Dual-Triggered Degradable Poly(Doxorubicin) Prodrug Nanoparticles for Leakage-Free Tumor-Specific Self-Delivery. *Macromol Rapid Commun* **2018**, *39* (18), n/a.
(86) Dong, S.; Sun, Y.; Liu, J.; Li, L.; He, J.; Zhang, M.; Ni, P. Multifunctional Polymeric Prodrug with Simultaneous Conjugating Camptothecin and Doxorubicin for PH/Reduction Dual-Responsive Drug Delivery. *ACS Appl. Mater. Interfaces* **2019**, *11* (9), 8740–8748.
(87) Wei, H.; Zhuo, R.-X.; Zhang, X.-Z. Design and Development of Polymeric Micelles with Cleavable Links for Intracellular Drug Delivery. *Prog Polym Sci* **2013**, *38* (3–4), 503–535.
(88) Jackson, A. W.; Fulton, D. A. Making Polymeric Nanoparticles Stimuli-Responsive with Dynamic Covalent Bonds. *Polym Chem* **2013**, *4* (1), 31–45.
(89) Mikhail, A. S.; Allen, C. Block Copolymer Micelles for Delivery of Cancer Therapy: Transport at the Whole Body, Tissue and Cellular Levels. *J Control. Release* **2009**, *138* (3), 214–223.

(90) Allen, C.; Maysinger, D.; Eisenberg, A. Nano-Engineering Block Copolymer Aggregates for Drug Delivery. *Colloids Surf B* **1999**, *16* (1–4), 3–27.
(91) Xiong, X.-B.; Falamarzian, A.; Garg, S. M.; Lavasanifar, A. Engineering of Amphiphilic Block Copolymers for Polymeric Micellar Drug and Gene Delivery. *J Control. Release* **2011**, *155* (2), 248–261.
(92) Taurin, S.; Nehoff, H.; Greish, K. Anticancer Nanomedicine and Tumor Vascular Permeability; Where Is the Missing Link? *J. Controlled Release* **2012**, *164* (3), 265–275.
(93) Nichols, J. W.; Bae, Y. H. Odyssey of a Cancer Nanoparticle: From Injection Site to Site of Action. *Nano Today* **2012**, *7* (6), 606–618.
(94) Bae, Y. H.; Park, K. Targeted Drug Delivery to Tumors: Myths, Reality and Possibility. *J. Controlled Release* **2011**, *153* (3), 198.
(95) Farokhzad, O. C.; Langer, R. Impact of Nanotechnology on Drug Delivery. *ACS Nano* **2009**, *3* (1), 16–20.
(96) Delplace, V.; Nicolas, J. Degradable Vinyl Polymers for Biomedical Applications. *Nat Chem* **2015**, *7* (10), 771–784.
(97) Rijcken, C. J. F.; Soga, O.; Hennink, W. E.; van Nostrum, C. F. Triggered Destabilization of Polymeric Micelles and Vesicles by Changing Polymers Polarity: An Attractive Tool for Drug Delivery. *J Control. Release* **2007**, *120* (3), 131–148.
(98) Mura, S.; Nicolas, J.; Couvreur, P. Stimuli-Responsive Nanocarriers for Drug Delivery. *Nat Mater* **2013**, *12* (11), 991–1003.
(99) Tannock, I. F.; Rotin, D. Acid PH in Tumors and Its Potential for Therapeutic Exploitation. *Cancer Res* **1989**, *49* (16), 4373–4384.
(100) Binauld, S.; Stenzel, M. H. Acid-Degradable Polymers for Drug Delivery: A Decade of Innovation. *Chem Commun* **2013**, *49* (21), 2082–2102.
(101) Kocak, G.; Tuncer, C.; Butun, V. PH-Responsive Polymers. *Polym Chem* **2017**, *8* (1), 144–176.
(102) Saito, G.; Swanson, J. A.; Lee, K.-D. Drug Delivery Strategy Utilizing Conjugation via Reversible Disulfide Linkages: Role and Site of Cellular Reducing Activities. *Adv Drug Deliv. Rev* **2003**, *55* (2), 199–215.
(103) Lee, M. H.; Yang, Z.; Lim, C. W.; Lee, Y. H.; Sun, D.; Kang, C.; Kim, J. S. Disulfide-Cleavage-Triggered Chemosensors and Their Biological Applications. *Chem Rev* **2013**, *113* (7), 5071–5109.
(104) Deng, C.; Jiang, Y.; Cheng, R.; Meng, F.; Zhong, Z. Biodegradable Polymeric Micelles for Targeted and Controlled Anticancer Drug Delivery: Promises, Progress and Prospects. *Nano Today* **2012**, *7* (5), 467–480.
(105) Quinn, J. F.; Whittaker, M. R.; Davis, T. P. Glutathione Responsive Polymers and Their Application in Drug Delivery Systems. *Polym Chem* **2017**, *8* (1), 97–126.
(106) Gao, Y.; Dong, C.-M. Reduction- and Thermo-Sensitive Core-Cross-Linked Polypeptide Hybrid Micelles for Triggered and Intracellular Drug Release. *Polym Chem* **2017**, *8* (7), 1223–1232.
(107) Sun, T.; Li, P.; Oh, J. K. Dual Location Dual Reduction/Photoresponsive Block Copolymer Micelles: Disassembly and Synergistic Release. *Macromol. Rapid Commun.* **2015**, *36* (19), 1742–1748.
(108) Zhu, A.; Miao, K.; Deng, Y.; Ke, H.; He, H.; Yang, T.; Guo, M.; Li, Y.; Guo, Z.; Wang, Y.; Yang, X.; Zhao, Y.; Chen, H. Dually PH/Reduction-Responsive Vesicles for

Ultrahigh-Contrast Fluorescence Imaging and Thermo-Chemotherapy-Synergized Tumor Ablation. *ACS Nano* **2015**, *9* (8), 7874–7885.
(109) Liu, H.; Li, C.; Tang, D.; An, X.; Guo, Y.; Zhao, Y. Multi-Responsive Graft Copolymer Micelles Comprising Acetal and Disulfide Linkages for Stimuli-Triggered Drug Delivery. *J Mater Chem B* **2015**, *3* (19), 3959–3971.
(110) Miao, K.; Shao, W.; Liu, H.; Zhao, Y. Synthesis and Properties of a Dually Cleavable Graft Copolymer Comprising Pendant Acetal Linkages. *Polym Chem* **2014**, *5* (4), 1191–1201.
(111) Song, N.; Ding, M.; Pan, Z.; Li, J.; Zhou, L.; Tan, H.; Fu, Q. Construction of Targeting-Clickable and Tumor-Cleavable Polyurethane Nanomicelles for Multifunctional Intracellular Drug Delivery. *Biomacromolecules* **2013**, *14* (12), 4407–4419.
(112) Ding, Y.; Du, C.; Qian, J.; Zhou, L.; Su, Y.; Zhang, R.; Dong, C.-M. Tumor PH and Intracellular Reduction Responsive Polypeptide Nanomedicine with a Sheddable PEG Corona and a Disulfide-Cross-Linked Core. *Polym Chem* **2018**, *9* (25), 3488–3498.
(113) Chan, N.; An, S. Y.; Oh, J. K. Dual Location Disulfide Degradable Interlayer-Crosslinked Micelles with Extended Sheddable Coronas Exhibiting Enhanced Colloidal Stability and Rapid Release. *Polym. Chem.* **2014**, *5* (5), 1637–1649.
(114) Abouelmagd, S. A.; Sun, B.; Chang, A. C.; Ku, Y. J.; Yeo, Y. Release Kinetics Study of Poorly Water-Soluble Drugs from Nanoparticles: Are We Doing It Right? *Mol. Pharm.* **2015**, *12* (3), 997–1003.
(115) Sahu, A.; Kasoju, N.; Goswami, P.; Bora, U. Encapsulation of Curcumin in Pluronic Block Copolymer Micelles for Drug Delivery Applications. *J. Biomater. Appl.* **2011**, *25* (6), 619–639.
(116) Mendes, P. M. Stimuli-Responsive Surfaces for Bio-Applications. *Chem. Soc. Rev.* **2008**, *37* (11), 2512–2529.
(117) Bajpai, A. K.; Shukla, S. K.; Bhanu, S.; Kankane, S. Responsive Polymers in Controlled Drug Delivery. *Prog. Polym. Sci.* **2008**, *33* (11), 1088–1118.
(118) Alexander, C.; Shakesheff, K. M. Responsive Polymers at the Biology/Materials Science Interface. *Adv. Mater.* **2006**, *18* (24), 3321–3328.
(119) Gasparini, G.; Bang, E.-K.; Montenegro, J.; Matile, S. Cellular Uptake: Lessons from Supramolecular Organic Chemistry. *Chem. Commun.* **2015**, *51* (52), 10389–10402.
(120) Ryu, J.-H.; Chacko, R. T.; Jiwpanich, S.; Bickerton, S.; Babu, R. P.; Thayumanavan, S. Self-Cross-Linked Polymer Nanogels: A Versatile Nanoscopic Drug Delivery Platform. *J. Am. Chem. Soc.* **2010**, *132* (48), 17227–17235.
(121) Ryu, J.-H.; Jiwpanich, S.; Chacko, R.; Bickerton, S.; Thayumanavan, S. Surface-Functionalizable Polymer Nanogels with Facile Hydrophobic Guest Encapsulation Capabilities. *J. Am. Chem. Soc.* **2010**, *132* (24), 8246–8247.
(122) Chan, N.; Yee, N.; An, S. Y.; Oh, J. K. Tuning Amphiphilicity/Temperature-Induced Self-Assembly and in-Situ Disulfide Crosslinking of Reduction-Responsive Block Copolymers. *J. Polym. Sci. Part Polym. Chem.* **2014**, *52* (14), 2057–2067.
(123) Sun, Y.; Yan, X.; Yuan, T.; Liang, J.; Fan, Y.; Gu, Z.; Zhang, X. Disassemblable Micelles Based on Reduction-Degradable Amphiphilic Graft Copolymers for Intracellular Delivery of Doxorubicin. *Biomaterials* **2010**, *31* (27), 7124–7131.
(124) Ju, P.; Hu, J.; Li, F.; Cao, Y.; Li, L.; Shi, D.; Hao, Y.; Zhang, M.; He, J.; Ni, P. A Biodegradable Polyphosphoester-Functionalized Poly(Disulfide) Nanocarrier for

Reduction-Triggered Intracellular Drug Delivery. *J. Mater. Chem. B* **2018**, *6* (44), 7263–7273.
(125) Ping, P.; Wang, W.; Chen, X.; Jing, X. The Influence of Hard-Segments on Two-Phase Structure and Shape Memory Properties of PCL-Based Segmented Polyurethanes. *J. Polym. Sci. Part B Polym. Phys.* **2007**, *45* (5), 557–570.
(126) Peponi, L.; Navarro-Baena, I.; Sonseca, A.; Gimenez, E.; Marcos-Fernandez, A.; Kenny, J. M. Synthesis and Characterization of PCL–PLLA Polyurethane with Shape Memory Behavior. *Eur. Polym. J.* **2013**, *49* (4), 893–903.
(127) Pawar, R. R.; Jadhav, S. V.; Bajaj, H. C. Microwave-Assisted Rapid Valorization of Glycerol towards Acetals and Ketals. *Chem. Eng. J.* **2014**, *235*, 61–66.
(128) Riber, C. F.; Smith, A. A.; Zelikin, A. N. Self-Immolative Linkers Literally Bridge Disulfide Chemistry and the Realm of Thiol-Free Drugs. *Adv. Healthc. Mater.* **2015**, *4* (12), 1887–1890.
(129) Chan, N.; Laprise-Pelletier, M.; Chevallier, P.; Bianchi, A.; Fortin, M.-A.; Oh, J. K. Multidentate Block-Copolymer-Stabilized Ultrasmall Superparamagnetic Iron Oxide Nanoparticles with Enhanced Colloidal Stability for Magnetic Resonance Imaging. *Biomacromolecules* **2014**, *15* (6), 2146–2156.
(130) Jazani, A. M.; Arezi, N.; Shetty, C.; Hong, S. H.; Li, H.; Wang, X.; Oh, J. K. Tumor-Targeting Intracellular Drug Delivery Based on Dual Acid/Reduction-Degradable Nanoassemblies with Ketal Interface and Disulfide Core Locations. *Polym. Chem.* **2019**, *10* (22), 2840–2853.
(131) Bawa, K. K.; Jazani, A. M.; Shetty, C.; Oh, J. K. PLA-Based Triblock Copolymer Micelles Exhibiting Dual Acidic PH/Reduction Responses at Dual Core and Core/Corona Interface Locations. *Macromol. Rapid Commun.* **2018**, *39* (24), 1800477.
(132) Jazani, A. M.; Oh, J. K. Dual Location, Dual Acidic PH/Reduction-Responsive Degradable Block Copolymer: Synthesis and Investigation of Ketal Linkage Instability under ATRP Conditions. *Macromolecules* **2017**, *50* (23), 9427–9436.
(133) Liu, B.; Thayumanavan, S. Substituent Effects on the PH Sensitivity of Acetals and Ketals and Their Correlation with Encapsulation Stability in Polymeric Nanogels. *J Am Chem Soc* **2017**, *139* (6), 2306–2317.
(134) Seidi, F.; Jenjob, R.; Crespy, D. Designing Smart Polymer Conjugates for Controlled Release of Payloads. *Chem. Rev.* **2018**, *118* (7), 3965–4036.

Appendix A

Supplementary Figures for Chapter 3

Figure A.1 Overlaid ^{1}H-NMR spectra of ssDCI, ssDOH, and CDI in $CDCl_3$. *Unidentifiable impurities.

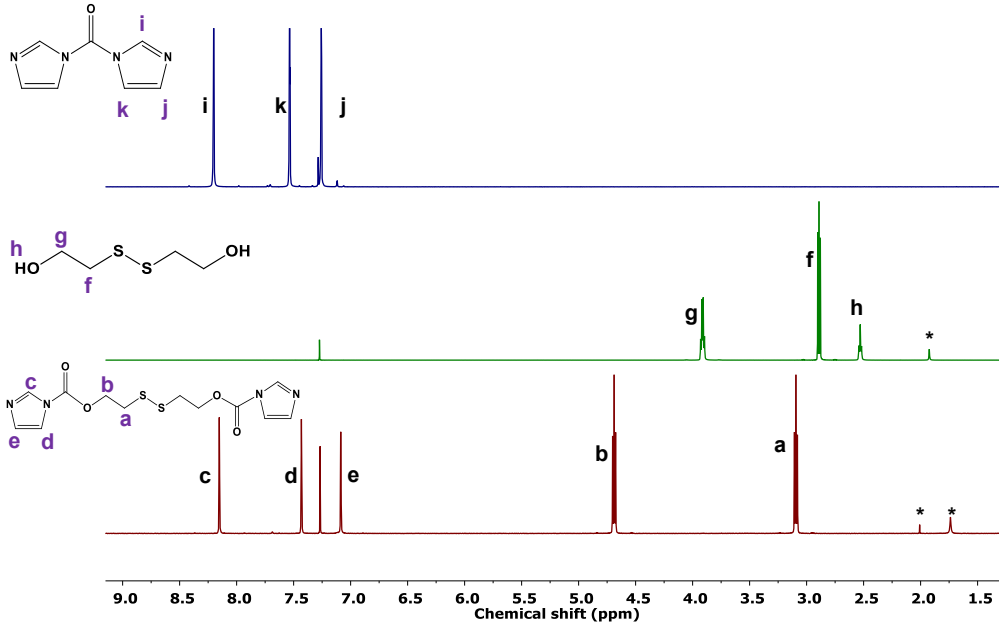

Figure A.2 ^{13}C-NMR spectrum of ssDCI in $CDCl_3$.

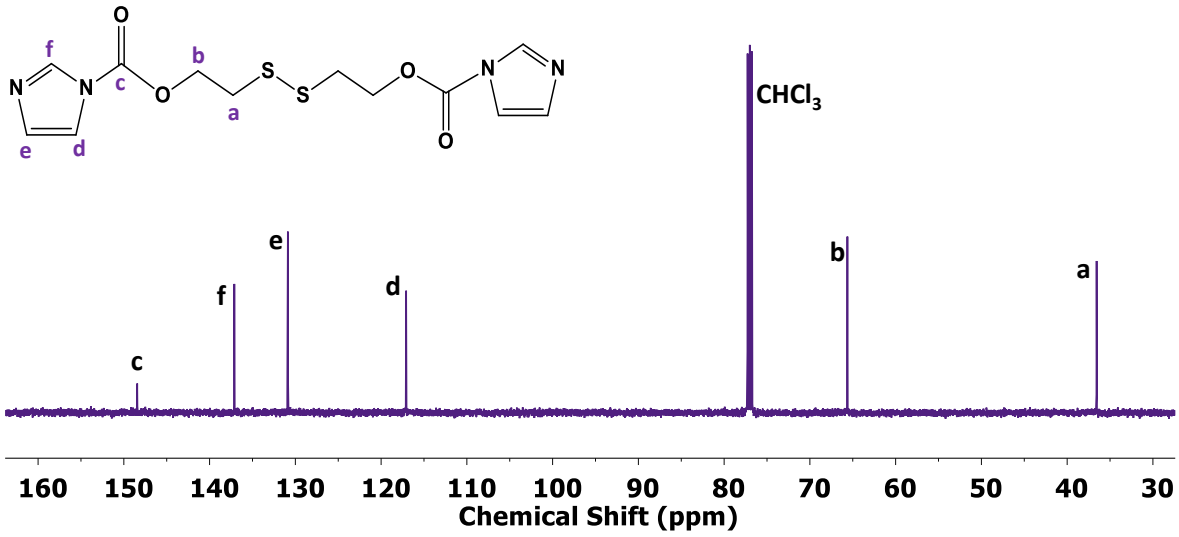

Figure A.3 GPC traces of PCss-A to PCss-D.

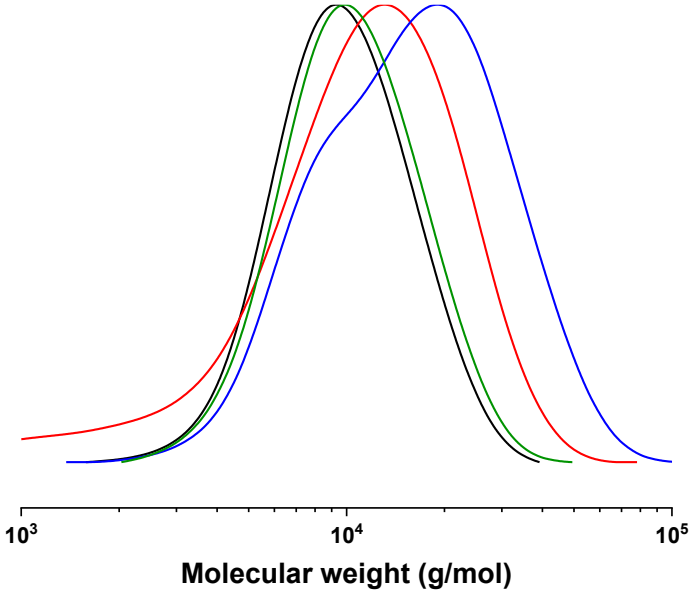

Figure A.4 ^{1}H-NMR spectrum of PCss-A to PCss-D in $CDCl_3$.

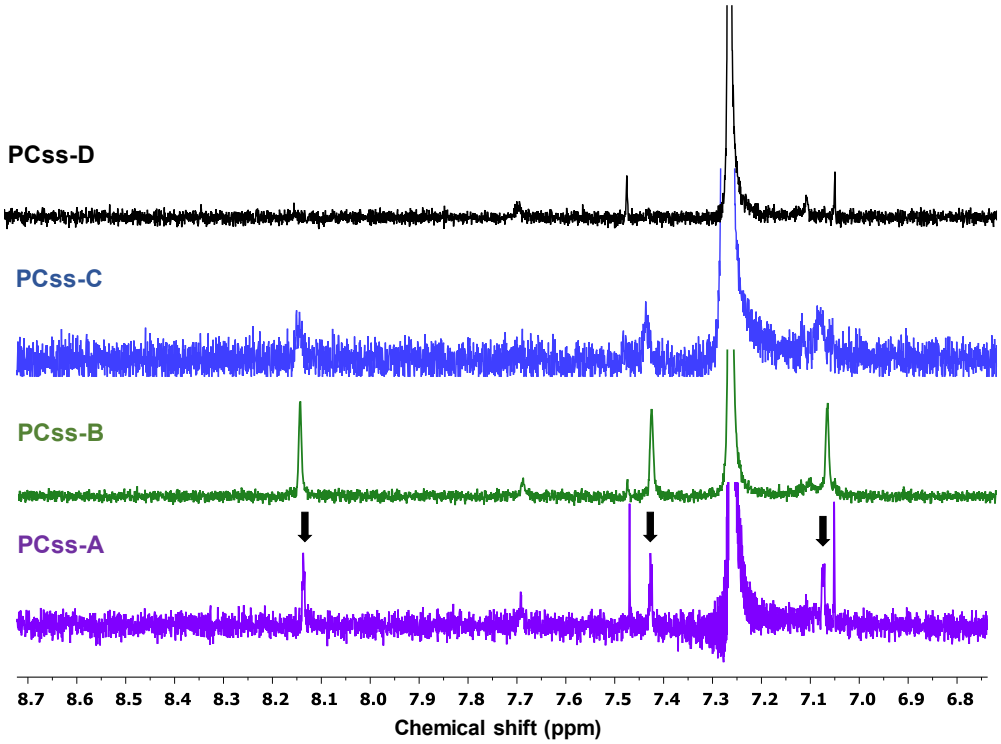

Figure A.5 ^{1}H-NMR spectrum in $CDCl_3$ of PCss-F synthesized under stoichiometric balance.

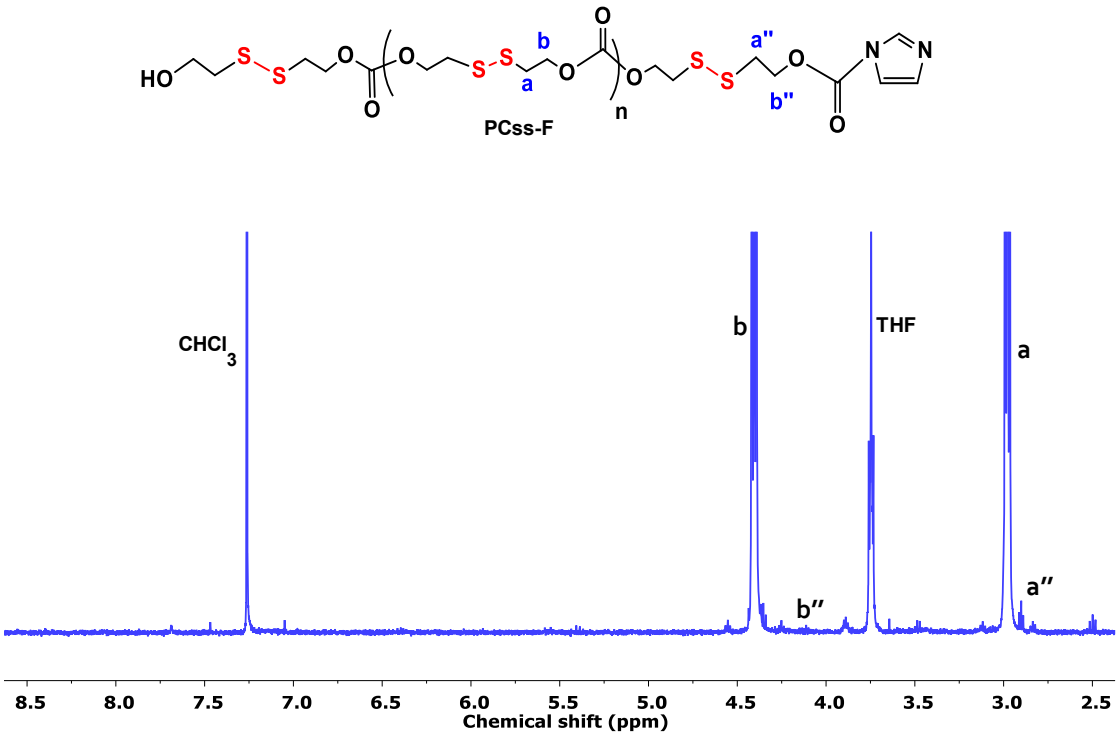

Figure A.6 GPC diagrams of PCss-E (under stoichiometric balance) and PCss-F (under stoichiometric imbalance) synthesized with ssDOH diol.

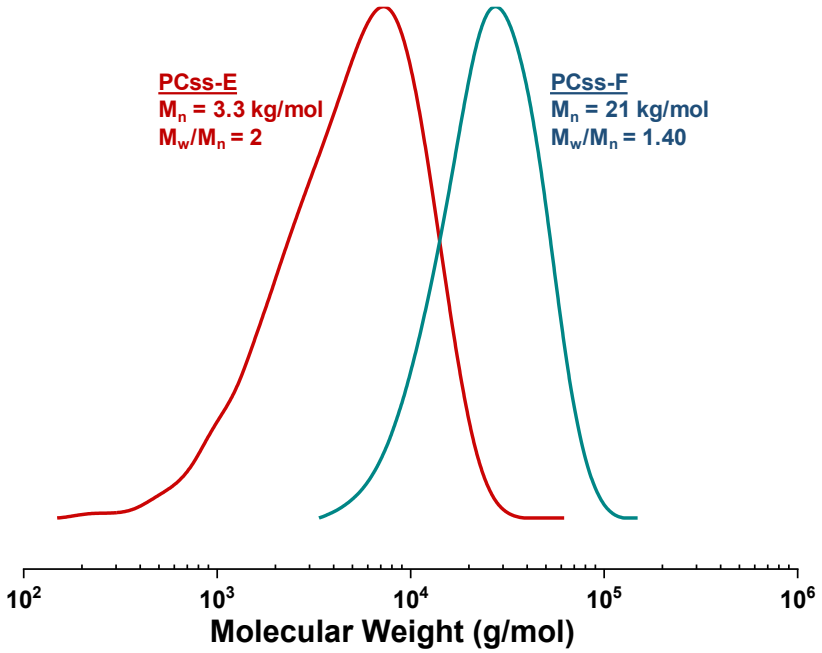

Figure A.7 ^{1}H-NMR spectrum in $CDCl_3$ of PCss-G.

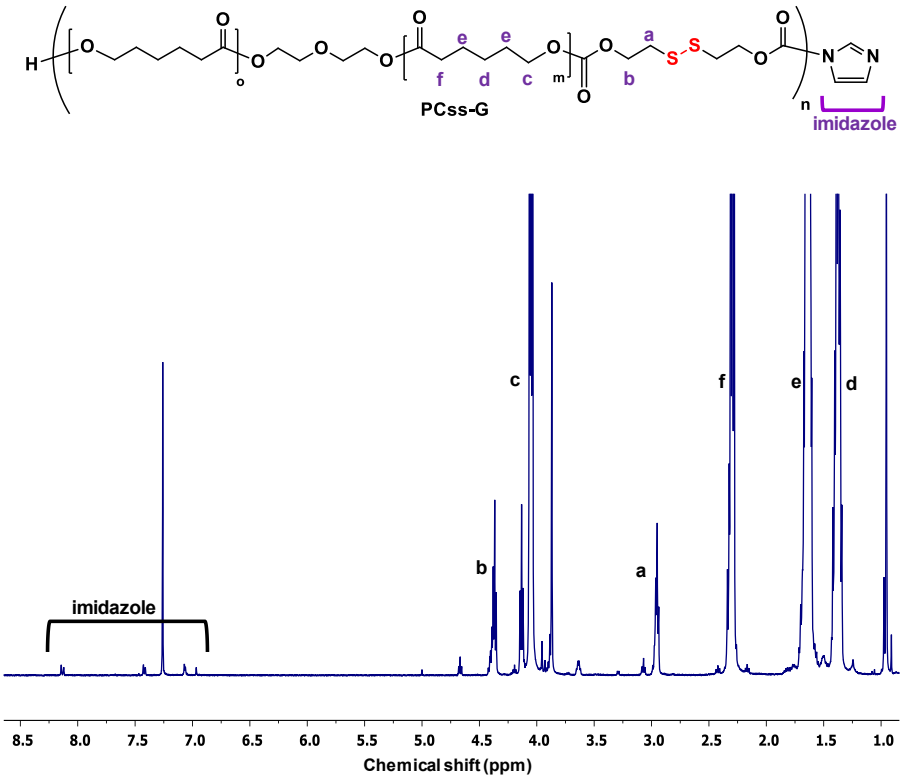

Figure A.8 ^{1}H-NMR spectrum in $CDCl_3$ of PCss-H.

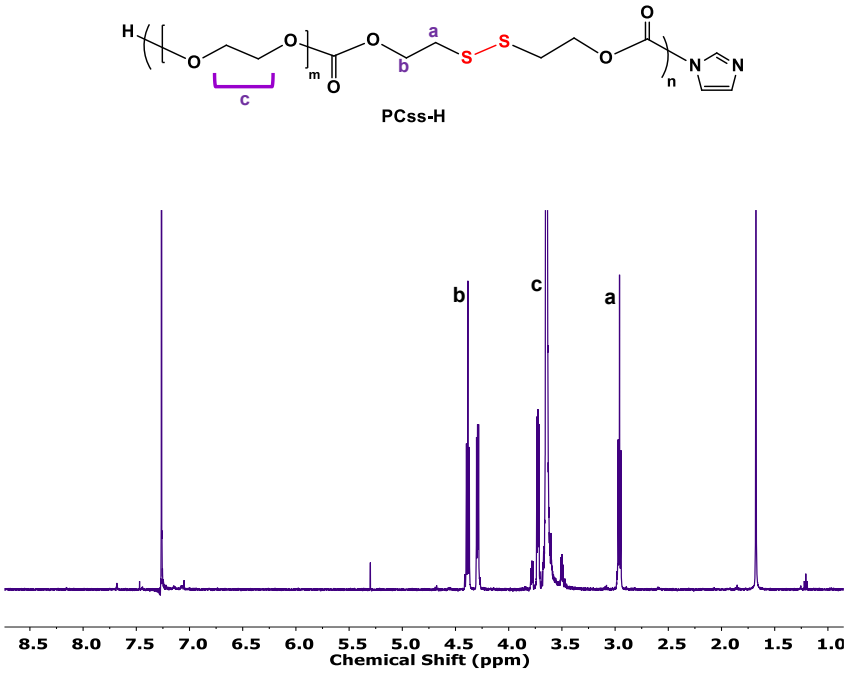

Figure A.9 ^{1}H-NMR spectrum in $CDCl_3$ of PCss-I.

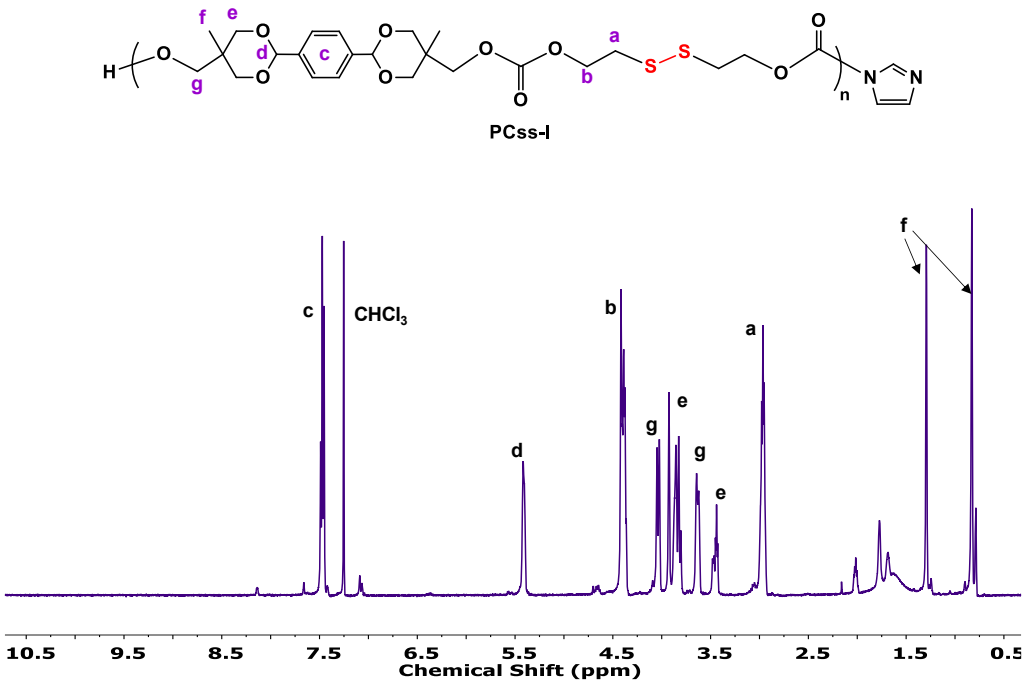

Figure A.10 GPC diagrams of PCss-G, PCss-H and PCss-I prepared by different diols.

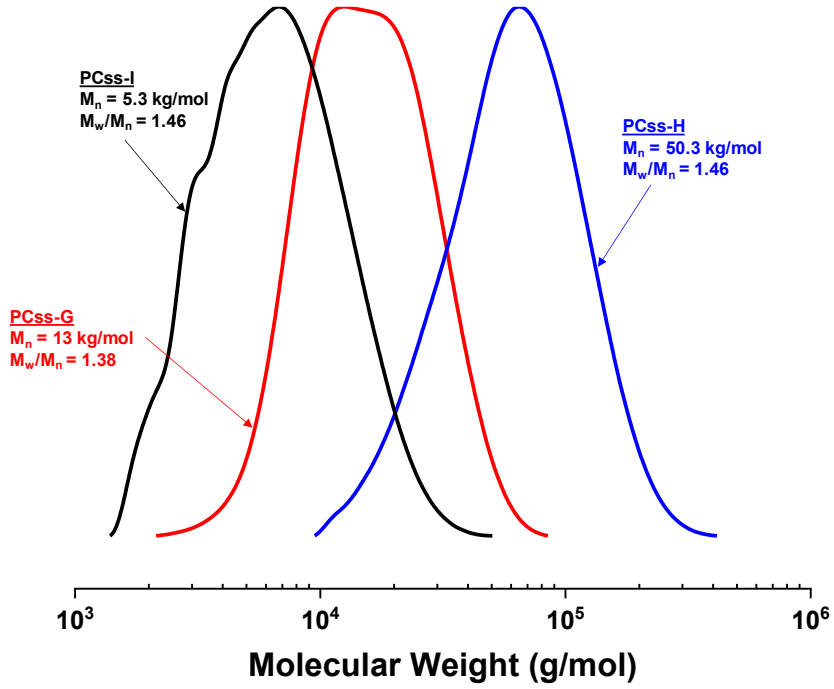

Figure A.11 DLS diagram of nanoassemblies self-assembled from PCss-H in aqueous solution.

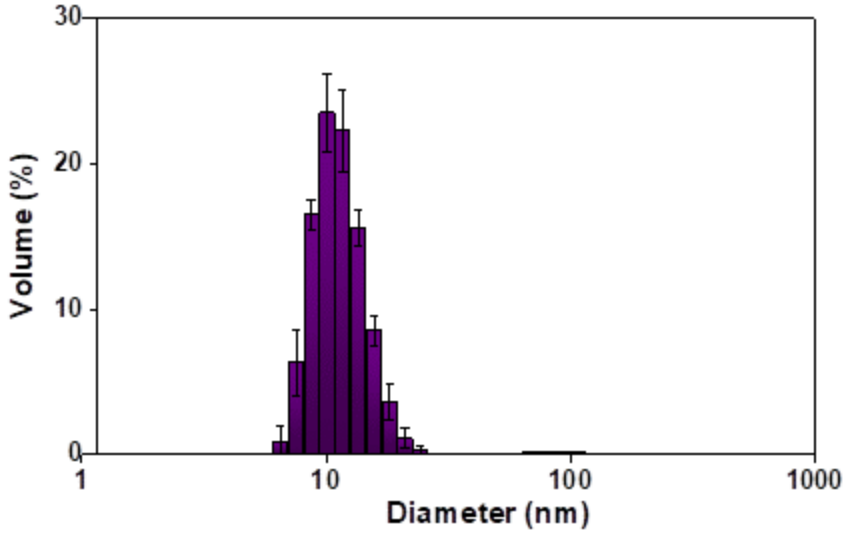

Figure A.12 Synthetic scheme for CAC-DOH (a); ^{1}H-NMR Spectrum of CAC-DOH in DMSO-d_6 (b).

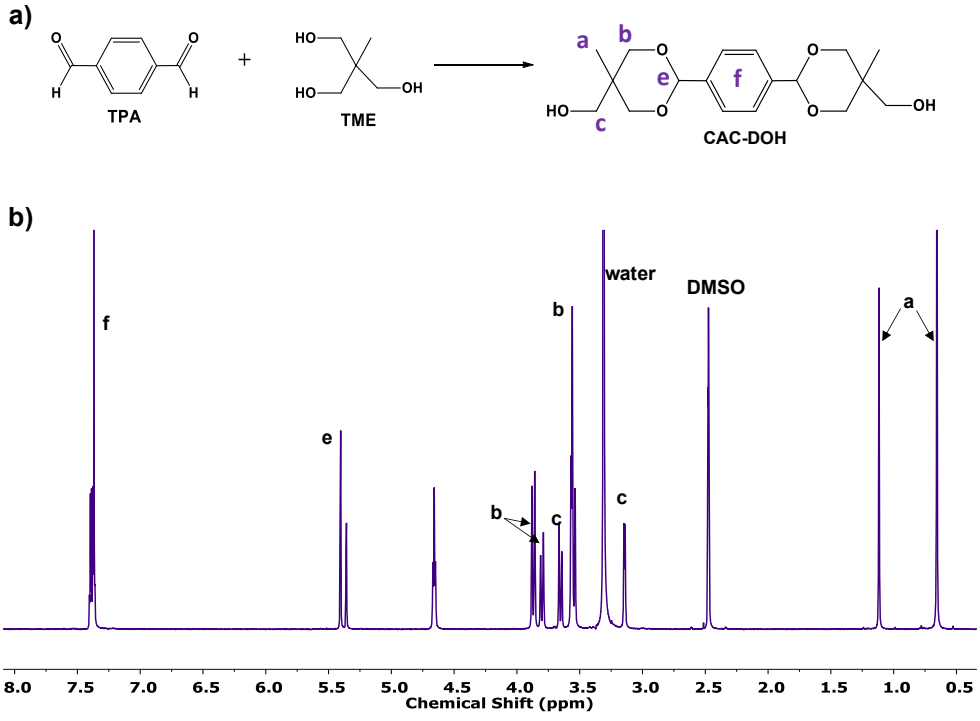

Figure A.13 ^{1}H-NMR of mPEG-COOH in $CDCl_3$.

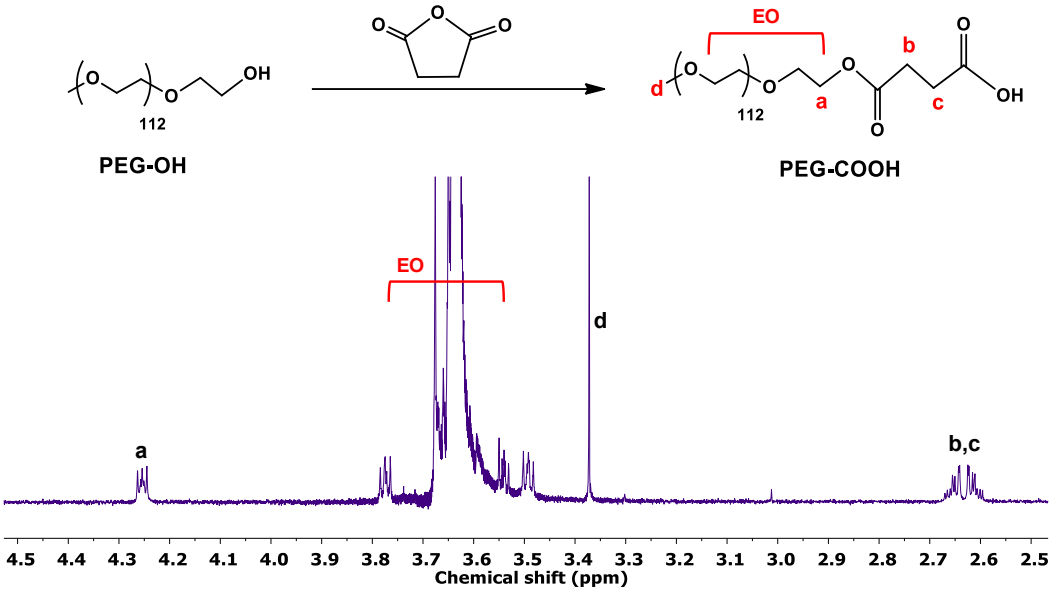

Figure A.14 Deconvolution analysis on GPC trace of mPEG-CAC-PCss-CAC-mPEG triblock polymer.

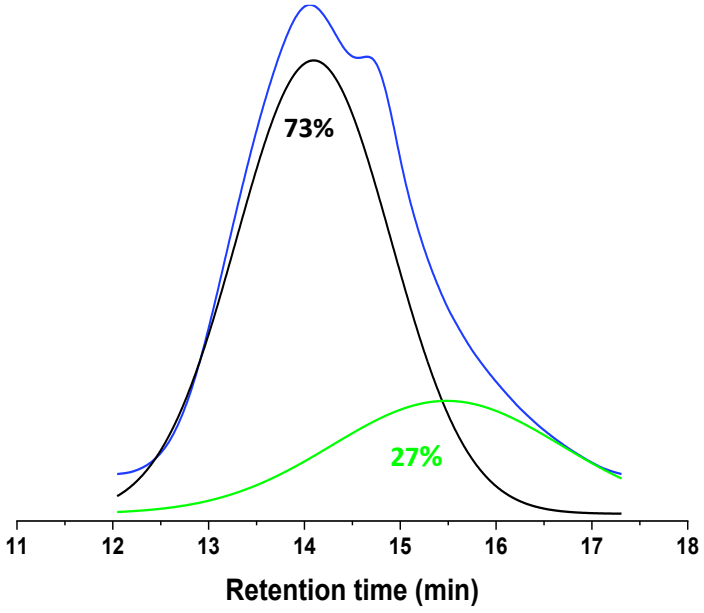

Appendix B

Supplementary Figures for Chapter 4

B1. Synthesis of mPEG-cyclic acetal-OH-Type 2

Three steps were involved as depicted in Figure B.1. Synthesis of PEG-COOH was described in section 3.2.7.

mPEG-benzaldehyde (mPEG-BA-T2): mPEG-COOH (0.3 g, 0.05 mmol) was mixed with 4-hydroxybenzaldehyde (0.07 g, 0.54 mmol), EDC (1.0 g, 0.54 mmol), and a catalytic amount of DMAP in a 1/1 DCM/THF v/v (20 mL in total) under stirring for 24 hrs. After the removal of solvent by rotary evaporation the product was dissolved in DCM (25 mL), washed with water twice and with aqueous brine solution once, and then dried over sodium sulfate. The product was precipitated from cold diethyl ether to remove impurities and dried in a vacuum oven at room temperature for 24 hrs: Yield 0.18 g, 64 %. (Figure B.2)

mPEG-CAC-OH-T2: The purified, dried PEG-BA (0.05 g, 0.01 mmol) was mixed with THME (0.82 g, 6.9 mmol) and HCl (1.0 µ) in THF (10 mL) under stirring at 60 ° C for 30 mins. The reaction mixture was quenched with Et_3N (2 µL). After the removal of solvent by rotary evaporation, the residue was dissolved in chloroform (10 mL) and passed through PTFE filter (0.25 µm) to remove excess and unreacted THME. The product was precipitated from cold diethyl ether to remove impurities and dried in a vacuum oven at room temperature for 24 hrs: Yield = 0.04 g, 71%. (Figure B.3)

B2. Degradation study of PEG-based cyclic acetal precursors.

mPEG-based precursor (10 mg) was dissolved in acetate buffer at pH = 4 (700 µl) and the degradation of the acetal linkage was followed by ^{1}H-NMR.

Figure B.1 Synthetic route to mPEG-CAC-OH-T2.

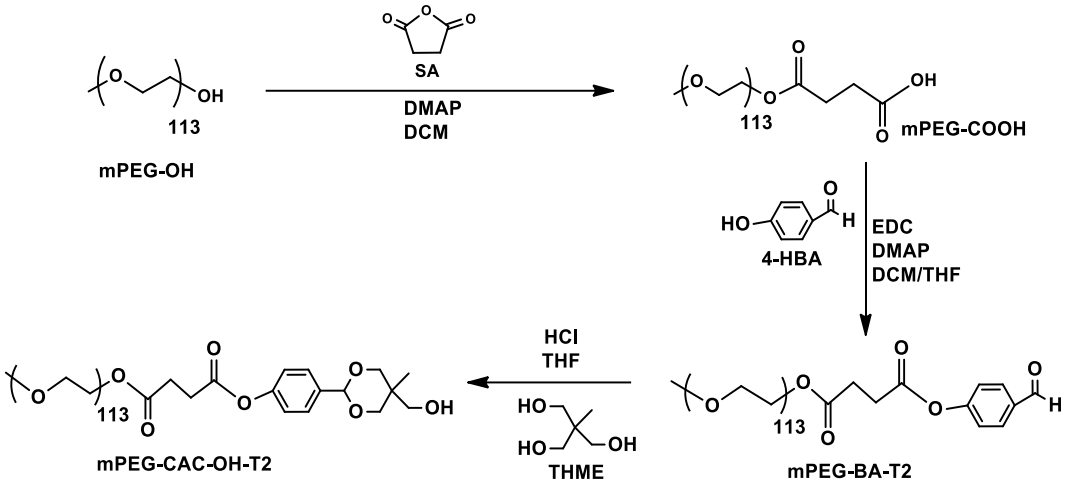

Figure B.2 ^{1}H-NMR spectra of and mPEG-BA-T2 in $CDCl_3$.

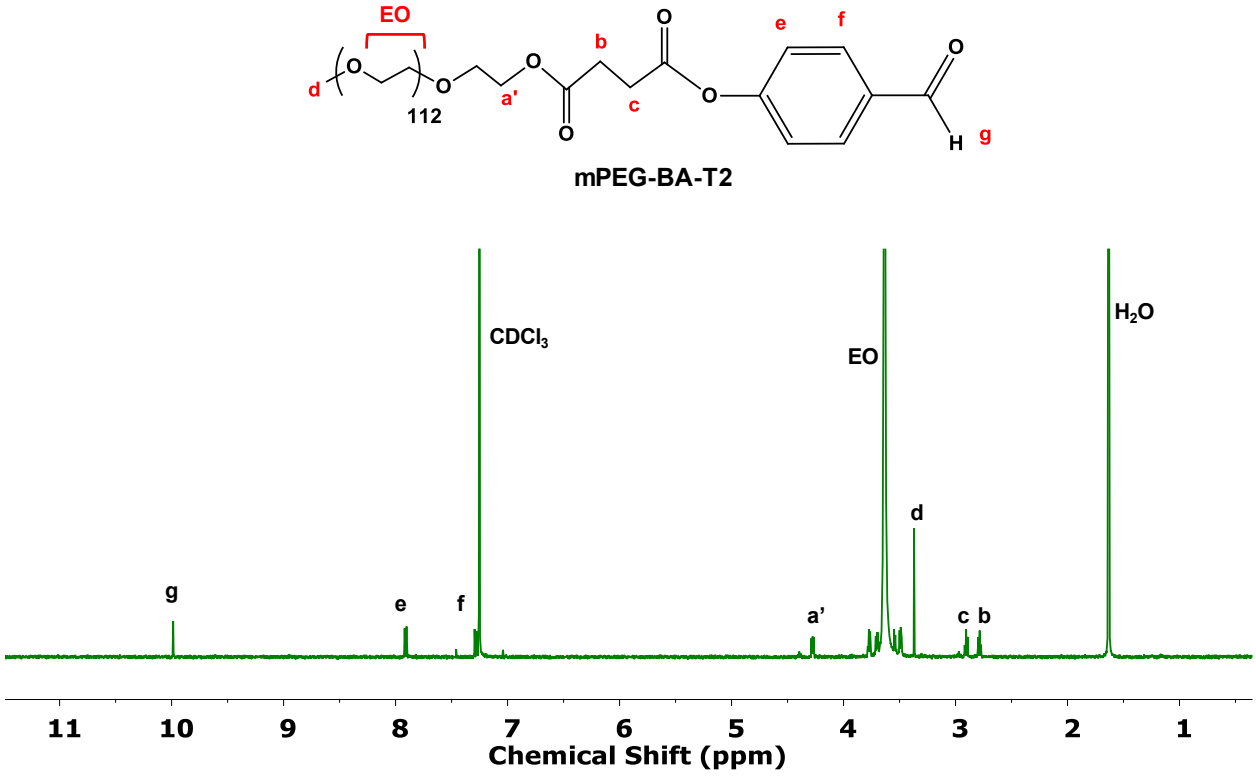

Figure B.3 ^{1}H-NMR spectra of and mPEG-CAC-OH-T2 in DMSO-d_6.